Hydrogen-bonded pigments for organic electronic applications

DISSERTATION

zur Erlangung des akademischen Grades

Doktor

im Doktoratsstudium der

TECHNISCHEN WISSENSCHAFTEN

Eingereicht von:
Eric Daniel Głowacki

Angefertigt am:
Institut für Physikalische Chemie

Beurteilung:
o. Univ. Prof. Mag. Dr. DDr. h.c. Niyazi Serdar Sariciftci (Betreuung)
Univ. Prof. Dr. Siegfried Bauer

Linz, Juli 2013

Sworn declaration

I hereby declare under oath that the submitted doctoral dissertation has been written solely by me without any outside assistance, information other than provided sources or aids have not been used and those used have been fully documented.

The dissertation here present is identical to the electronically transmitted text document.

German: Ich erkläre an Eides statt, dass ich die vorliegende Dissertation selbstständig und ohne fremde Hilfe verfasst, andere als die angegebenen Quellen und Hilfsmittel nicht benutzt bzw. die wörtlich oder sinngemäß entnommenen Stellen als solche kenntlich gemacht habe.

Die vorliegende Dissertation ist mit dem elektronisch übermittelten Textdokument identisch.

Eric Daniel Głowacki

Linz, July 13, 2013

Acknowledgements

Foremost I would like to thank Professor Serdar Sariciftci, who was in all respects a true *doktorvater* to me: for supervising and advising me during my doctoral dissertation work, and being a constant source of inspiration and support.

Special gratitude must be given to Professor Siegfried Bauer, for valuable advice and insights that made this work possible, and always being willing and open to discuss ideas – no matter how crazy!

A great deal of learning, especially concerning laboratory techniques, I obtained from older and more veteran colleagues in the lab. Their contribution to my learning cannot be underestimated and I owe much to the following people, in rough chronological order: Gebhard "Gebi" Matt, Philipp Stadler, Christoph Ulbricht, Matthew White, Martin Kaltenbrunner, Uwe Monkowius, Mihai Irimia-Vladu, Mateusz Bednorz, Marek Havliček, and Markus Scharber.

A very warm and special acknowledgement must be extended to Dr. Gundula Voss. Her lifelong synthetic achievements in the rich field of indigo chemistry made much of this work possible. I thank her for her inspiration and bottomless energy.

I would like to specially thank colleagues with whom I have worked closely during my doctoral studies. Mihai Irimia-Vladu – we made a very good team and thanks to your enthusiasm we were able to be so productive. I thank Lucia Leonat for patience and resilience during many long nights of preparing and measuring samples, and the many toasts we raised "to good results" – indeed this came true somehow. I thank Jacek Gąsiorowski for his critical eye and measurements we have done together, such as our studies on doped polymers. I warmly thank Mateusz Bednorz, for our exciting collaboration on inorganic/organic hybrid devices, and the camaraderie. Marek Havliček I thank for expert support on electron-spin resonance techniques. I thank Doğukan Apaydin for our fruitful collaboration on indigo interaction with CO_2. I thank again Martin Kaltenbrunner, Markus Scharber, Philipp Stadler, and Matthew White for many helpful and productive discussions, and fruitful experiments done together. I thank also Markus for help with technical German language translation.

I would like to thank the students I have supervised (or co-supervised) and mentored, for their patience with me, and likewise acknowledge their contributions to this work: Hava Akpinar, Zeynep Bozkurt, Halime Coskun, Kadir Demirak, Sandra Enengl, Dominik Farka, Artur Galiński, Mesut Inac, Barbara Małkowska, Aysu Okur, Nevsal Sünger, Melanie Weichselbaumer.

Much valuable work that became part of my thesis was done in collaboration with partners in other institutes and universities. I would like to thank foremost Dr. Uwe Monkowius, from the Inorganic Chemistry department at JKU for extremely valuable collaboration in the field of X-ray crystallography and DFT calculations, and all the fun and good ideas that we had along the way. Dr. Giuseppe Romanazzi and Prof. Gian Paolo Suranna, from the University of Bari, Italy, for synthetic chemistry concerning the fascinating epindolidione family of compounds. I thank Prof. Helmut Sitter for expert advice about vacuum processing techniques. I thank Prof. Wolfgang Heiss and Misha Sytnyk for our exciting collaboration on H-bonded nanoparticles and help with SEM measurements. I thank Prof. Johannes Pedarnig from the Applied Physics Institute at JKU for training on the XRD instrument. I likewise thank Dominik Kriegner and Prof. Julian Stangl for XRD support.

Last but not least I thank my family: my grandparents, my mother, father, and sister Sylvia, for the great efforts and life-long hard work which gave me wonderful possibilities and choices in my life that I am truly grateful for.

Abstract

The field of organic electronics is driven by the motivation of mass-producing cheap electronics with novel functionality and form factors inaccessible for traditional inorganic semiconductor-based electronics. The starting point for the work in this dissertation is the question: What can we learn from natural-origin molecular materials to design organic electronics that are not only cheap but also sustainable, and also have direct potential for bioelectronic functionality? The most common interaction governing supramolecular ordering in biology is hydrogen-bonding. Hydrogen-bonding is the dominant mechanism governing protein secondary and tertiary structure, DNA base-pair interaction, structural properties of polysaccharides, among many other examples. In this work, the concept of hydrogen-bonding is applied to organic semiconducting materials.

The work begins with evaluation of conduction in crystalline films of a representative class of hydrogen-bonded natural pigments: indigos. Indigo and its derivatives, dyes and pigments of natural origin are explored for their semiconducting properties. Fully bio-compatible organic electronics operating at the state-of-the-art level are realized using indigo semiconductors, in combination with other biomaterials functioning as dielectric and substrate. In indigos, intermolecular hydrogen-bonding enforces a crystalline ordering favorable to charge transport. The principle of intermolecular hydrogen-bonding was then put to the test as a viable design technique for obtaining organic semiconducting materials with good performance of stability: A range of hydrogen-bonded materials were successfully tested. An isomer of indigo, epindolidione, was shown to be one of the best reported organic transistor materials in terms of mobility (~2 cm^2/Vs) and operational stability. The photophysical properties of these hydrogen-bonded pigments were also evaluated, and have been applied to fabricate single-layer organic photovoltaic devices and light-emitting diodes. The work in this dissertation presents the novel principle of hydrogen-bonded pigment semiconductors, introduces some molecular structure vs. crystalline structure vs. charge transport relationships in these materials, and outlines various organic electronic and optoelectronic devices fabricated with them.

Zusammenfassung

Der Bereich der organischen Elektronik ist durch die Idee der Massenproduktion billiger elektronischer Bauteile mit neuartigen Funktionen und Formfaktoren, die für die traditionelle anorganische Halbleiter-Elektronik derzeit unzugänglich sind, motiviert. Der Ausgangspunkt dieser Dissertation war die Frage: Was können wir von nachhaltigen und billigen molekularen Materialien natürlichen Ursprungs, die auch das Potential für bioelektronische Anwendungen haben könnten, lernen? Die häufigste Wechselwirkung die zu einer supramolekulare Ordnung in der Biologie führt ist die Wasserstoffbrückenbindung. Wasserstoffbrücken sind die vorherrschenden Bindungen in Protein Sekundär-und Tertiärstrukturen, DNA-Basenpaar-Wechselwirkung und bestimmen die strukturellen Eigenschaften von Polysacchariden. In dieser Arbeit wird das Konzept der Wasserstoff-Bindung auf organische Halbleitermaterialien angewendet.

Die Arbeit beginnt mit der Evaluierung der elektrischen Leitfähigkeiten von verschiedenen, kristallinen, Indigo-basierten Naturfarbstoffen mit Wasserstoffbrückenbindung. Indigo und Indigo-Derivate, Farbstoffmoleküle und Pigmente natürlichen Ursprunges wurden auf ihre halbleitenden Eigenschaften untersucht. Elektronische Bauteile basierend auf Indigo, biokompatiblen Substraten und Dielektrika mit ausgezeichneter elektrischer Charakteristik wurden realisiert. Die intermolekularen Wasserstoffbrücken führen zu einer kristallinen Struktur in Indigo welche den Ladungstransport unterstützt. Das Prinzip der intermolekularen Wasserstoffbrücken wurde danach an anderen Molekülen getestet und einige Materialien mit sehr guten elektrischen Eigenschaften und Langzeitstabilität wurden identifiziert. Ein Isomer des Indigos Epindolidione zeigte in Feldeffekt-Transistoren sehr hohe Ladungsträger-Beweglichkeit (~2 cm^2/Vs) für Löcher und ausgezeichnete Langzeitstabilitäten. Weiters wurden die foto-physikalischen Eigenschaften der Materialien untersucht und organische Solarzellen und Leuchtdioden hergestellt. Diese Dissertation beschreibt das neue Konzept halbleitender, Wasserstoff-gebrückter Pigmente. Zusammenhänge zwischen molekularen Struktur, kristalliner Struktur und Ladungstransport in diesen Materialien werden detailliert beschrieben. Die Herstellung und Untersuchung verschiedener opto-elektronische Bauteile wird dargestellt.

Table of Contents

1. Introduction and motivation

In the modern science and technology of nanomaterials, interest in biological and bio-inspired materials is motivated by their potential for biomedical integration and sustainable development.[1] Research in the field of organic semiconductor-based technologies has grown tremendously in the past decades. The success of organic photoconductors in xerography in the 1960s-1990s [2,3] and the recent evolution of organic light emitting diodes[4,5] into a multi-billion dollar industry demonstrate relatively mature applications of organic semiconductors. Organic photovoltaics (OPVs), "plastic solar cells" have improved in power conversion efficiency from ~1% in 2000 [6–8] to values above 10% in the past years[9–11], making OPV a serious player in the photovoltaic field. Printable "plastic electronics" based on organic thin-film transistors, synonymously-called organic field-effect transistors (OFETs), have likewise been the topic of intensive research and commercial interest.[12–15] With the growing commercial success of organic semiconductor based technologies, and their potential for application at the interface of biomedical applications, evaluating bio-inspired materials for organic electronics is crucial for producing sustainable and low-cost devices as well as enabling unique and biochemically-specific functionality. The search for such novel functional materials can lead us to reevaluate substances right under our noses, indeed things familiar since ancient times. The subject of this dissertation is research in the family of Hydrogen-bonded organic pigments for organic electronics applications. This topic emerged from an ongoing study on biocompatible organic electronics. The chapters in this dissertation cover the use of H-bonded pigments as organic semiconductors, understanding their solid-state crystalline packing, their photophysics, and their use as functional synthetic building block for novel synthetic materials.

1.1 Biocompatible electronics and the inspiration for using bio-origin dyes and pigments

In the past few years, a growing body of scientific work has focused on utilizing the unique bio-integration and bio-functionality of organic conducting and semiconducting materials to fabricate devices for biomedical applications as well as various use-and-throw applications. A few examples of biocompatible organic electronic devices are shown in Figure 1. Some review articles have covered this recent work.[16–19] A series of papers in the years 2010-2013, reported efforts at the JKU to fabricate organic field effect transistors and circuits using exclusively bio-compatible materials.[18,20–22] Substrate materials used in these studies included cellulose-based polymers, gelatin, and caramelized glucose. Efforts at JKU showed that the natural resin shellac had superior properties, and could be processed into robust substrates and could additionally be cast into thin films with excellent insulating properties to function as the gate dielectric in the transistors, as well as an encapsulant.[23] The applicability of this resin in drug delivery applications made it particularly promising. A number of natural materials proved to function as gate insulators, including sugars like glucose and sucrose, as well as nucleobases guanine, adenine, cytosine, and thymine. Other groups have reported successful and creative demonstrations of natural materials for organic electronics. Paper is particularly attractive as a cheap and eco-friendly substrate material for OFETs[24–26] and OPVs.[27,28] Silk has been demonstrated to be a bio-resorbable material for implantable electronic devices,[29–31] and also can function as a gate dielectric for OFETs.[32] However, what was lacking in this work was natural-origin semiconductors with good performance. We initially explored β-carotene as a semiconductor, however the mobility remained low (μ_h~5×10^{-4}cm^2/Vs) and the material readily oxidizes and is thus unstable. This

early work is not included in this dissertation and information on these studies can be found in several papers [20,33] Upon surveying many conjugated molecules present in nature, we found that most natural chromophores are not dyes with large π-systems (with the carotenoids and porphyrins as the notable exceptions) but instead relatively small molecules that form pigments, *i.e.* they adopt their characteristic colors in the aggregated state. Examples include alizarin (madder root dye), napthoquinones, such as lawsone (Henna pigment), juglone (black walnut pigment), and indigos. Representatives of these classes of molecules are shown in Figure 2. These examples are representative of the major categories of such dyes – in fact many derivatives of each of these molecules are found in different places throughout nature. Several expansive reviews of natural pigments exist.[34,35] These molecules contain carbonyl and amine groups in conjugated segments. Since under neutral pH conditions mesomeric forms featuring enol or imine character are unfavorable, carbonyl and amine groups are seen as interrupting π-conjugation. The prevailing notion among synthetic chemists is that when designing organic semiconducting small molecules or polymers, maximizing π-conjugation is crucial, and thus amine or carbonyl functional groups are avoided.[36–39] Thus the limited π-conjugation of such molecules led them to be overlooked by the organic electronics community, which sought molecules with extensive π-conjugation. Nevertheless, the large bathochromic shifts (50-100 nm) that occur when these natural dyes aggregate into their pigment forms indicate that electronic coupling between molecules must be substantial. Indeed, a survey of the known crystal structures of indigo and alizarin, for example, reveals that these molecules pack with close and remarkably cofacial π-π stacking and therefore are arranged in a way that is considered favorable for charge transport. The subject of this dissertation is how these molecules can be applied to organic electronic applications.
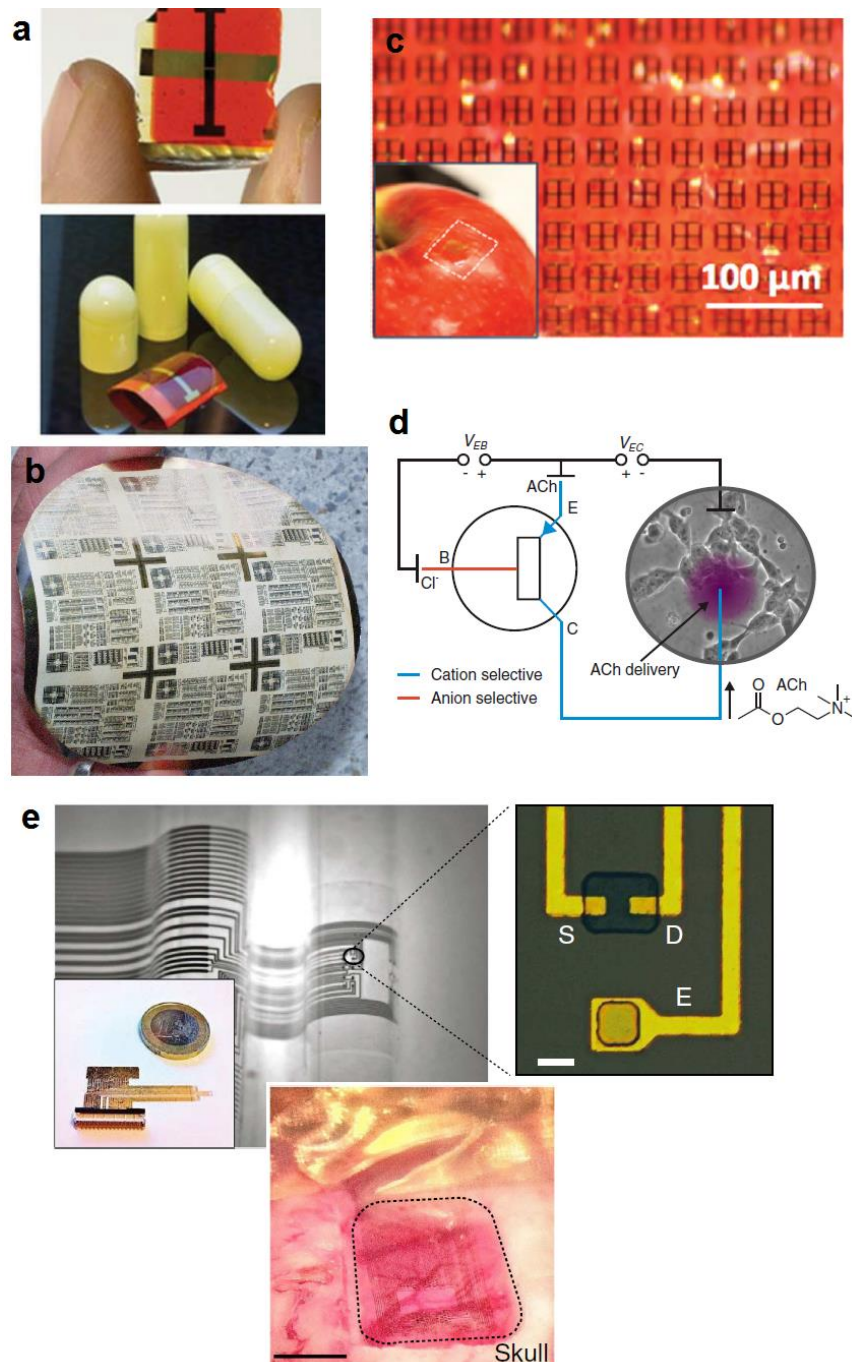
Figure 1. Some examples of biocompatible organic electronic devices. a) An example of OFETs fabricated using biodegradable and nontoxic materials, on caramelized glucose, and a gelatin drug carrier capsule – these are edible electronics. b) An array of OFETs fabricated on paper. Image courtesy of Hagen Klauk [24]. c) An electronic sensing element fabricated on natural bioresorbable silk, for food quality sensing. Reproduced from [30]. d) An example of a microfabricated electrochemical transistor functioning as an ion pump to deliver neurotransmitters directly into neural tissues. Reproduced from [40]. e) *In vivo* studies using organic conducting-polymer based transistors can be used for high-quality recordings of brain activity. Reproduced with permission from [41].
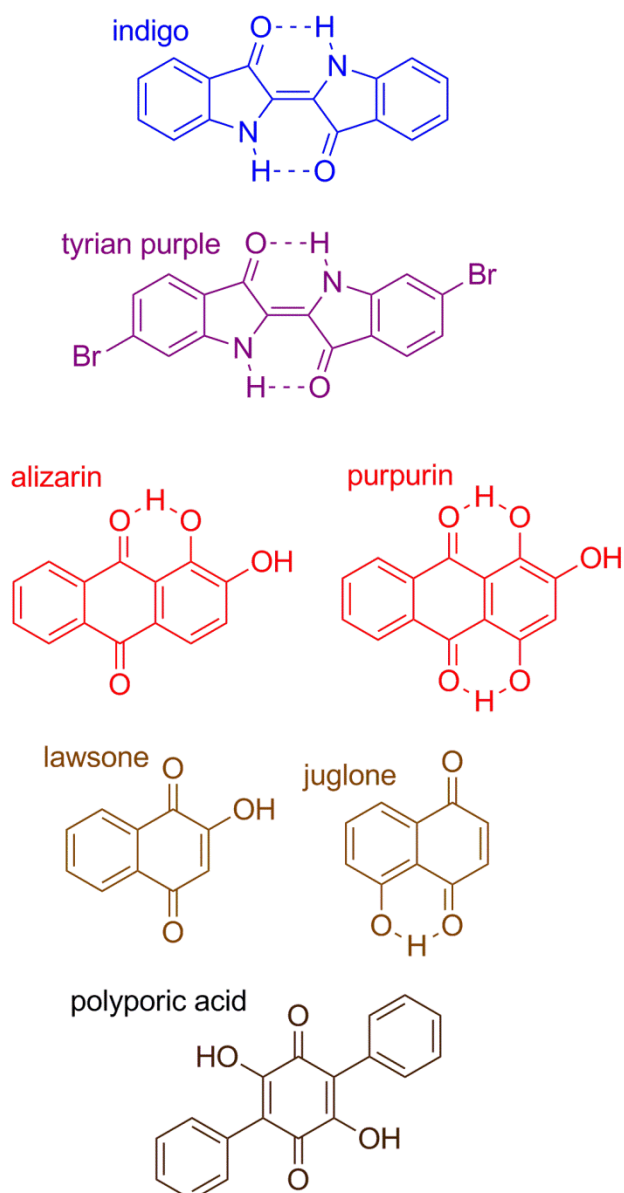
9

Figure 2. Structures of representative natural-origin pigment-forming dyes used throughout history. In fact, very numerous derivatives of each of these compounds are found throughout nature in plants, animals, and fungi.

1.2 Hydrogen Bonds and their role in biochemistry and materials science

Linus Pauling wrote in 1940: "It has been recognized in recent years that under certain conditions an atom of hydrogen is attracted by rather strong forces to two atoms, instead of only one, so that it may be considered to be acting as a bond between them."[42] In the 70 years since Pauling, many noncovalent interactions in structural organic chemistry have been classified as H-bonds, creating a difficulty in furnishing a satisfying all-encompassing definition of what constitutes an H-bond. A useful explanation is perhaps provided by Peter Atkins, in 1989: "A hydrogen bond is a link formed by a hydrogen atom lying between two strongly electronegative atoms". Many types of H-bonds exist, spanning a wide range of bond energies and geometries. A hydrogen atom can be shared between an "H-bond donor" and an "H-bond acceptor", a molecule with electron lone pairs. H-bond donor character increases with acidity while H-bond acceptor character increases with basicity. Such an interaction can involve interplay of multiple H-bond acceptors interacting with a single donor. A schematic with the common types of H-bond geometries is shown in the centre of Figure 3, together

10

with examples where H-bonds play an important role - in biomolecules, dyes and pigments, as well as in ionic conductors and organic semiconductors. The work in this dissertation aims at elucidating the role of H-bonds in these material classes, providing links between the seemingly unrelated dyes and pigments to organic semiconductors, and suggesting new research avenues to merge ionic and electronic devices.

Though H-bonds are typically weaker than most covalent bonds, with bond energies on the order of 5-65 kcal/mol, they are usually significantly stronger than van der Waals interactions, which are less than ~ 5 kcal/mol. In biological systems the role of H-bonds is ubiquitous. Biochemistry exists in an aqueous environment, where H-bonding interactions are responsible for many of the properties of water, such as high boiling point, dielectric constant, and surface tension. Perhaps the most familiar H-bonded biomolecule in biology is DNA – where base pairs are held together by highly-specific H-bonding between amine proton donors (-NH_2 or -NH) and carbonyl group (=O) acceptors. H-bonding is the most significant noncovalent interaction in most polypeptides, *i.e.* proteins. The two most common protein secondary structures − alpha helices and beta pleated sheets − are both held together by H-bonding between amino acids on adjacent chains, likewise caused by an amine hydrogen/carbonyl interaction of the type (-NH··O=). The antiparallel beta sheet, one of the biologically-important structures that this type of bonding leads to, is illustrated schematically in Figure 3. Amine/carbonyl bonds are the most frequently-encountered but not the only important category of H-bonding in biomolecules: H-bonds between –OH groups comprise the interchain interactions between polysaccharides such as cellulose and chitin and are thus responsible for the robust mechanical properties of these structural biopolymers.

Since H-bonding interactions are so common in the natural world it is worthwhile to consider what role they may play in organic conducting and semiconducting materials. At present, the field of organic electronics has evolved from the scientific laboratory into several mature commercial technologies, such as xerography and organic light-emitting diodes; with organic photovoltaics and organic transistor-based circuits poised to enter the market in the near future. Since early work in the 1960s where it was discovered that conjugated aromatic compounds exhibited semiconducting properties, research in organic materials for electronics focused on materials with extensive π-conjugation as well as π-π stacking between adjacent molecules. The first approach of using an extensive π-conjugated system yielded conducting conjugated polymers like polyaniline and polyacetylene – 1D metallic conducting systems for which the Nobel Prize in chemistry was awarded in 2000. The ultimate materials science realization of conduction through a 2D π-conjugated system is graphene, an achievement likewise recognized with a Nobel Prize in 2007. Difficulties in fabricating useful devices based on quasi 1D and 2D systems have led to the overall predominance of the second approach: involving conduction through the π-π stacking of adjacent overlapping conjugated molecules. It is exactly on this second concept that organic semiconductor devices like light-emitting diodes and solar cells are based.

Since H-bonding interactions are so prevalent in nature, and have been exploited extensively in the field of organic crystal engineering for commercial colorant applications, it is surprising that exploiting H-bonding as a molecular design tool for obtaining organic semiconducting and conducing materials has remained largely unexplored.
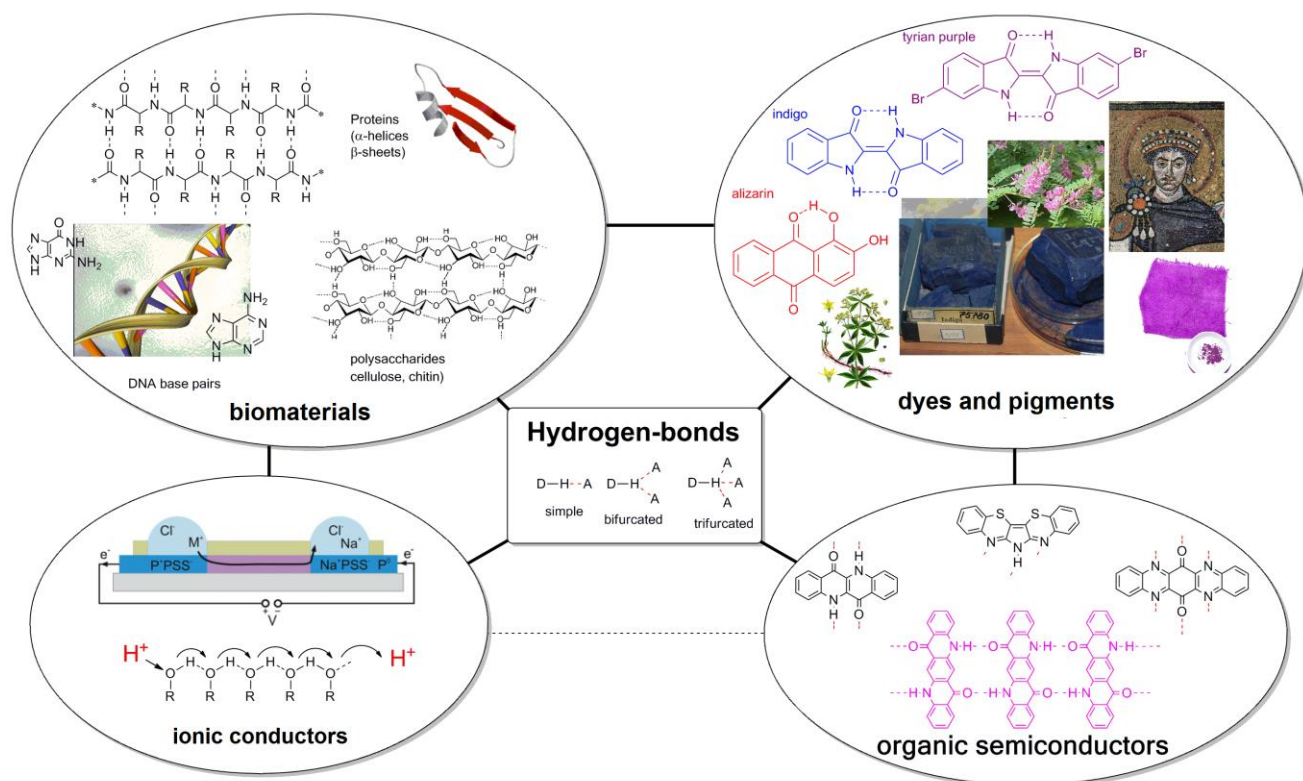
Figure 3. Summary of the role of Hydrogen-bonding in biomaterials, dyes and pigments, ionic conductors, and organic semiconductors. The central box shows a schematic summary of the H-bond: an interaction between a proton donor and a proton acceptor. H-bonding is an extremely important aspect in the structural organic chemistry of biomaterials such as proteins, DNA, and sugars, as well as in dyes and pigments of natural origin. Connections between the four categories, representing overlap of applicability of materials, are shown with black lines. The image of an electronic ion pump in the ionic conductors portion is reproduced courtesy of [43].

1.3 Indigos – history and chemistry

Along with the production of alcohol, bread, and cheese, the oldest 'biotechnology' known in human history is indigo dyeing. Archeological evidence shows that the practice of coloring fabrics with indigo dyes existed since at least 2000 BC and was practiced in different forms by civilizations in Asia, Europe, and the Americas.[44] The name originates from the Indus River, where the ancient Indus Valley civilization is thought to have first mastered the dying process. The name "indigo" comes down to us from the ancient Greeks, who named indigo based on its origin. The ancient trade of Indigo and Tyrian Purple (primary constituent: 6,6'-dibromoindigo) production was perfected by Egyptian, Phoenician, Greek, and Roman craftsmen, whose techniques were often carefully guarded secrets passed down from generation to generation.[44,45] Understanding the chemistry utilized by ancient indigo dyers is a major subject of interest for archeological chemists.[35,46] Indigo throughout history was the only available blue dye that could be used to color textiles, thus throughout ancient cultures garments colored with indigo and tyrian purple were extremely valuable and a symbol of wealth and power. The blue of indigo, mentioned in the Old Testament as "tekhelet" was the color of the Judaic priesthood. The underlying chemistry behind the Biblical indigo dying procedure has been a subject of much study and debate and only recently satisfying explanations have been proposed.[34,47] In all cases of plant-origin indigo, indigo was produced from glycosidic precursors featuring an indole ring attached to a sugar molecule (Figure 4). The biochemical origin of such molecules is from the amino acid tryptophan. In Europe, the plant *isatis tinctoria*, or Dyers' Woad, was cultivated for its indigo-precursors. The 'true' indigo plant, *Indigofera tinctoria*, originating in India, contained 30-

12

times more indigo precursor and was cultivated in tropical climates (Figure 4a). The precursor compound is known is indican, and the synthetic pathway to indigo from indicant is shown in Figure 4. Key steps involve the enzymatic cleavage of the glycosidic precursor, which was accomplished by fermenting the raw indigo plant matter. The resulting molecule, Indoxyl, would then oxidatively dimerize in the presence of oxygen, yielding a highly-insoluble blue indigo mass. Dying with the indigo was accomplished by reducing the indigo to produce the dianion salt, known as leucoindigo, which is water-soluble. This process is called Vat dying, and is shown schematically in Figure 4c. The negatively-charged leucoindigo readily would penetrate textile fibers dipped into the vat. Removing the textile would cause reoxidation in air of the leucoindigo to produce insoluble blue indigo – now trapped within the fibers. The chemical reduction of indigo in pre-modern times is thought to have been accomplished by several means, including further fermentation producing NADH as a reducing agent, or use of metals like zinc as reducing agents. In modern times, the vat process used to make indigo blue jeans (which are the reason that indigo is the most-produced dyestuff worldwide today) is conceptually identical to the ancient vat dying procedure. Nowadays, reducing agents like sodium dithionite are used in alkaline water to produce vats of leucoindigo. The photo in Figure 4c shows the author along with colleagues visiting an indigo dyeing "*blaufärberei*" in Bad Leonfelden, Austria – one of the last surviving dying facilities doing traditional indigo dying as it had been done for centuries in central Europe. Tyrian Purple, the dibrominated derivative of indigo, originates not from plants but from animals. Several species of marine snails in the Mediterrenean Sea produce the purple 6,6'-dibromoindigo in their hypobrachial gland (Figure 5b).[44,48,49] The biosynthesis of tyrian purple is likewise shown in Figure 4. Squeezing the glands of the snail releases the purple dye in tiny amounts. Thus thousands of snails need to be harvested to yield enough dye even to dye a small piece of textile, leading to the high value of the substance. Throughout the ancient world, purple became the symbol of power and wealth. The purple stripe on the toga was reserved in ancient Rome only for senators and high-ranking officials. Indigo and its derivatives hold a special place in the history of modern organic chemistry. The pursuit of economically-competitive dyestuffs was one of the primary motivating factors for development of the field in the 19th century and the commercial *raison d'être* for industry giants such as BASF, AGFA, Ciba, and Hoechst. Many of the great founders and innovators of synthetic organic chemistry, such as William Perkin, Adolf von Baeyer, Emil Fischer, Heinrich Caro, and Carl Lieberman – were all associated with indigo chemistry.[44,50] For his work on elucidating the structure of indigo, and its first synthetic preparation, Adolf von Baeyer received the Nobel prize in chemistry in 1905. The Baeyer-Drewsen indigo synthesis, first published in 1882, is one of the simplest ways for obtaining indigos synthetically. The reaction involves a base-catalyzed aldol condensation of *o*-nitrobenzaldehyde with acetone, followed by cyclization to 3-indolone and dimerization to indigo.[51] Substituted indigo derivatives can be obtained by using the corresponding substituted *o*-nitrobenzaldehydes. This synthesis is shown in Figure 4. Other useful syntheses for substituted indigos include the Heumann-Pfleger route, involving condensation of anilines with chloroacetic acid followed by cyclization in alkali conditions to yield indoxyl, which dimerizes to indigo[45], and the method of Clark and Cooksey for preparing asymmetrically-substituted indigos from substituted isatins and O-acetylindoxyl.[52]
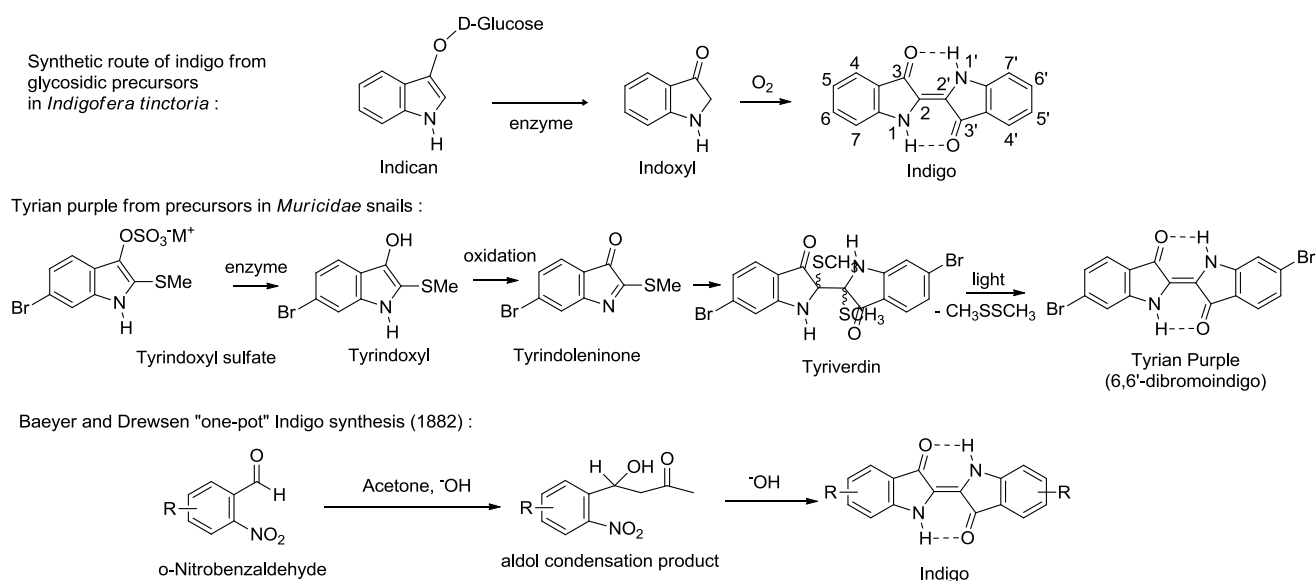
Figure 4. Synthetic pathways for indigo and tyrian purple from natural precursors. The upper-right figure shows the indigo numbering scheme accepted in most literature on indigos and used in this work. The bottom scheme shows the Baeyer-Drewsen indigo synthesis – a facile synthetic route to a wide variety of derivatized indigos.
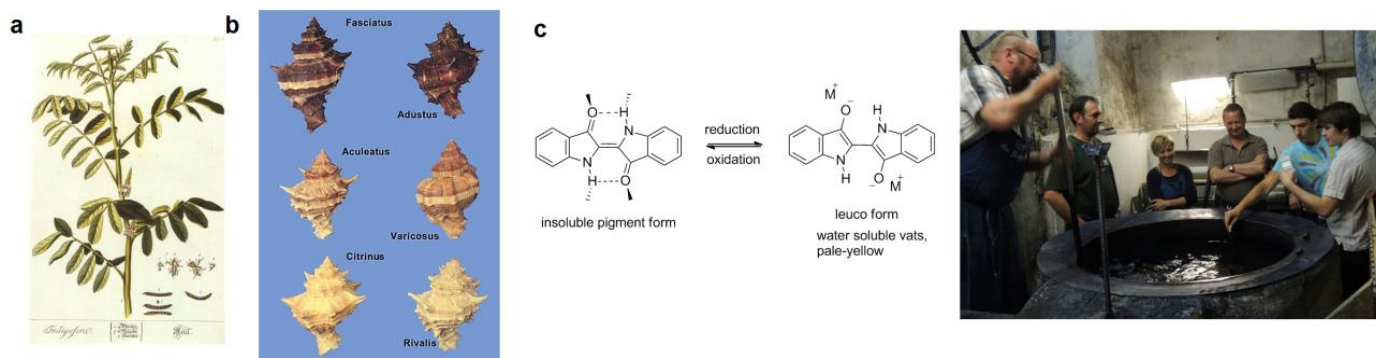

Figure 5. a) *Indigofera tinctoria*, the tropical source of indigo. b) Snails from the *Muricidae* and *Thaisidae* families are the source for tyrian purple dyes. c) The chemistry of vat dyeing. Indigos are reduced to produce an aqueous solution of the indigo^{2-} (known as *leuco* or "white" indigo) with K$^+$, Na$^+$, or other metal counterions. The photo shows the author visiting a traditional indigo vat dying facility in Bad Leonfelden, Austria. Stone indigo vats like this one were used for centuries in very much the same way in many parts of the world.

1.4 Chemistry and applications of synthetic Hydrogen-bonded pigments

Indigo and alizarin are two well-known H-bonded pigments of natural origin, however many modern synthetic pigments feature the same H-bonded schemes. Organic pigments are colorants that by definition are insoluble in the media that they are applied in. Modern paints and inks consist of pigment particles with size ranging from nanometers to several microns mixed with dispersing agents. In all cases, industrial organic pigments owe their poor solubility to strong intermolecular interactions, which are often an interplay of strong π-stacking and H-bonding.[53] Diketopyrrolopyrroles (DPPs), quinacridones, perylene diimides (PDIs), and indigos are four of the major classes of industrial colorants today. Dioxazine and isoindoline, as well as many azo compounds, are other industrially-important H-bonded

pigments.[54] All of these pigment classes feature H-bonding between –NH hydrogens (donor) and carbonyl groups (acceptor), reminiscent of the same type of H-bonding interactions present in proteins and DNA base pairs.

The interplay of H-bonding and π-stacking results in high lattice energies. This fact is reflected in the remarkable thermal stability of these pigments; they are known to sublime at very high temperatures (e.g. >500 °C for quinacridone). H-bonded pigments are remarkable for their photochemical and thermal stability, and are used in applications where long-term durability is necessary. Special nanoparticle dispersions of H-bonded pigments stabilized with surfactant ligand groups are used for ink formulations, especially in the case of inkjet printing inks, where magenta and yellow inks consist of H-bonded pigments.

Two industrial H-bonded pigments are discussed extensively in this work: Quinacridone and Epindolidione. They were chosen for study as the H-bonded analogs of the well-established acene molecular semiconducting materials: tetracene and pentacene (Figure 6).

Linear-*trans* Quinacridone (Figure 6) and its derivatives represent one of the most prolific commercial pigments, worldwide sales are estimated to be around 4000 tons per annum. Quinacridones owe their success to their simple chemical synthesis and excellent photochemical and thermal stability. Though highly-stable, they are considered safe and nontoxic, and are approved for use in children's toys and cosmetics.[54–56] The name Quinacridone was coined by Niementowski in 1896 for a bent-core derivative similar to linear-*trans* quinacridone.[57] Quinacridones gained little attention until the 1950s, when chemists working at Du Pont found a simple high-yield synthesis that yielded pigment-grade quinacridones.[56,58,59] Synthesis of quinacridones involves condensation of aniline with dimethyl succinoylsuccinate. Many derivatives can easily be obtained by starting with substituted anilines. The condensation product 2,5-diarylamino-3,6-dihydroterephthalates can then be oxidized and undergo cyclization at elevated temperatures, yielding quinacridone. The entire procedure can be carried out as a one-pot reaction. Quinacridones are remarkable for their polymorphism, with the violet β form and red γ form being commercially-important. Quinacridones form a high lattice-energy crystalline pigment with excellent thermal stability, featuring interplay between π-π stacking and intermolecular H-bonding.
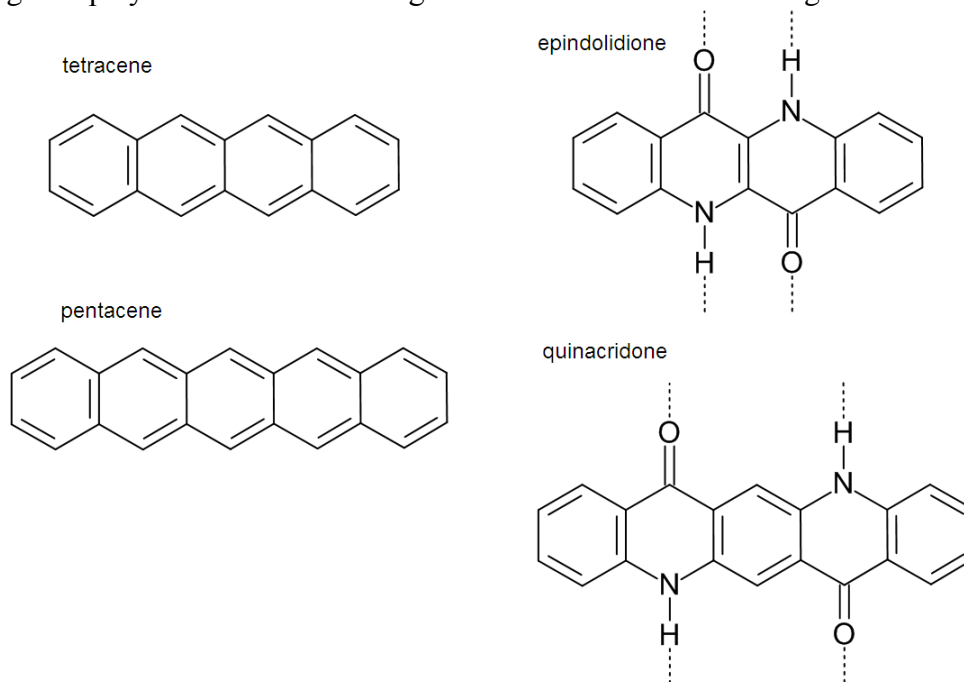

Figure 6. Epindolidione and quinacridone : industrial hydrogen-bonded pigments and analogs to the acene semiconductors: tetracene and pentacene, respectively.

15

Epindolidione is a structural isomer of indigo, featuring a four six-membered ring fused system analogous to tetracene (Figure 7). Epindolidione was first reported in 1934, and was synthesized with the intention of comparing it to indigo.[60] After arriving at the target compound via a complex multi-step synthesis, the researchers were surprised that epindolidione was a yellow and highly-fluorescent compound and thus did not resemble indigo at all. Interest in epindolidione reemerged in the 1960s following the commercial success of the structurally-related quinacridone pigments. In 1967, Jaffe and Matrick reported essentially the same synthetic methodology of their successful quinacridone synthesis to produce epindolidione (Figure 7b). The compound was the subject of several patents: for electrophotographic processes,[61] a 1984 patent for Kodak disclosing the use of epindolidione among a long list of suitable organic light-emitting diode materials,[62] and inkjet and other pigment formulations[63]. A 1989 paper from the Kodak labs likewise reported that evaporated epindolidione thin-films demonstrated photoconductivity response and an estimated hole mobility of approx. 0.01 cm^2/Vs.[64] Interestingly, it was found in 1995 that epindolidione can be produced from the direct thermal isomerization of indigo in vacuum at 460 °C (Figure 7a).[65]

This thermal rearrangement to form epindolidione was found to proceed with 80% yield. The authors also noted the remarkable stability of the epindolidione pigment at temperatures up to 1000 °C.
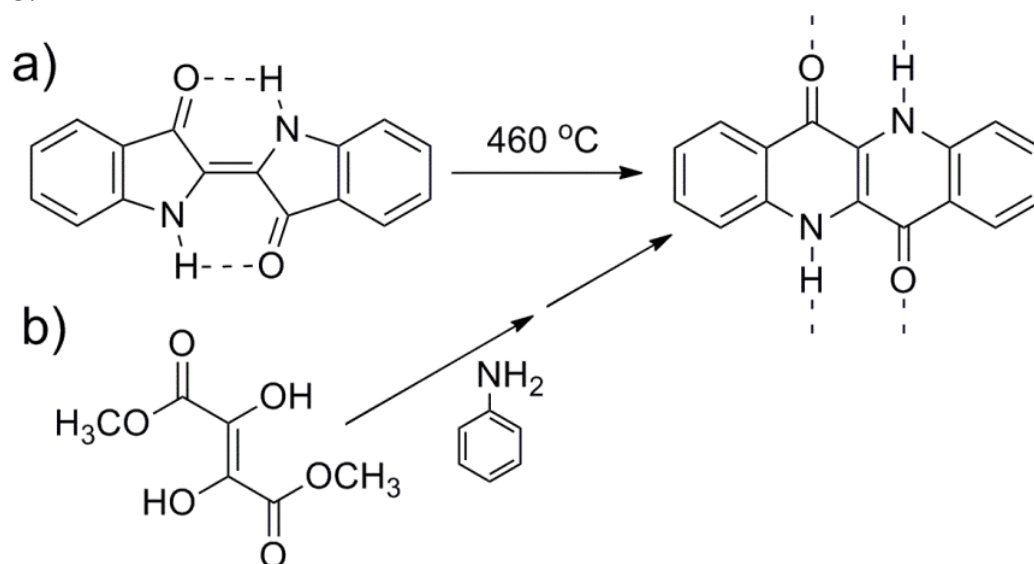

Figure 7. a) Direct synthesis of epindolidione via the thermal rearrangement of indigo. b) Synthesis from dihydroxy fumaric dimethylester condensation with aniline, followed by cyclization.

2.Experimental Techniques

2.1 Materials – synthesis and preparation

Indigo and thioindigo were purchased from Aldrich or Fluka, quinacridone was purchased from TCI. Epindolidione was synthesized by collaborators in Bari, Italy (G. Romanazzi and G.P. Suranna) according to the original procedure published by Du Pont. All indigo derivatives were synthesized according to the Baeyer-Drewsen technique[51], starting from an appropriately-substituted *o*-nitrobenzaldehyde (Figure 4). All benzaldehyde derivatives were purchased from Aldrich or Fluka with the exception of 4-bromo-2-nitrobenzaldehyde, the precursor for Tyrian purple, which was synthesized according to the procedure of Voss and Gerlach [66]. 5-bromoindigo was synthesized from 5-bromoisatin (Alfa Aesar) and O-acetylindoxyl (Alfa Aesar) via the procedure described by Clark and Cooksey [52], a variation on the original 2-chloroindolone route to indigo published originally by Baeyer.
Chemical composition was verified by ^{1}H and ^{13}C NMR measured in D_6-DMSO as a solvent or, in the case of insolubility, by first reducing the indigos to their *leuco* form and measuring in D_2O, according to the methods described by Voss.[67] In the case of nearly all indigo derivatives, single crystal X-ray diffraction was carried out as an absolute verification of structure (Section 3.3).

All H-bonded pigments used throughout this work were purified prior to use using well-established temperature gradient vacuum sublimation techniques [68,69]. Sublimation purification was carried out using a quartz vacuum tube at a pressure of $< 1 \times 10^{-6}$ mbar. A series of two or three flame-joined borosilicate glass tubes with a diameter ~1mm smaller than the quartz vacuum tube were inserted into the quartz tube and served to hold the source material and facilitate collection of the sublimed purified fractions following breaking of the glass tubes. Indigo, for example, sublimed effectively at 235 °C and was purified by triple temperature gradient sublimation. All other indigo derivatives were purified the same way, however dichloro and dibromo derivatives required higher temperatures of up to 285°C. Epindolidione and Quinacridone were purified by double temperature gradient sublimation at 290°C and 340°C, respectively.

2.2 Growth and measurement of single crystals – X-ray crystal structure determination

In order to determine the solid state crystalline structure of organic H-bonded pigments used throughout this study, single-crystals were grown and structure was determined using single-crystal X-ray diffraction methods.[70] For pigment-forming small molecules such as indigos, single crystals can be grown from the vapor phase using a temperature gradient furnace under the flow of an inert carrier gas, N_2 or Ar. The apparatus shown in Figure 8 was constructed for the purpose of optimizing growth conditions to obtain diffraction-quality single crystals. The procedure used was as follows: A quartz tube with a sealed gas inlet and outlet is mounted into a one-zone tube furnace. Borosilicate glass tubes are flame-joined to create a longer tube consisting of a total of three tubes. This tube is placed within the larger quartz tube and the sublimation and condensation/crystallization processes happen here. A purified sample (usually purified by temperature gradient sublimation) is placed in a ceramic crucible at one end of the flame-joined tube, such that it is located in the heating zone of the tube furnace. An inert gas flow is controlled via a gas flow meter (range 0.1 – 5 L min^{-1}). The gas used is nitrogen or argon, and prior to being regulated using a flow meter, the gas is passed through a series of glass wool filters to remove hydrocarbon residues and a column of KOH to dry the gas. A thermocouple was placed near the zone where crystals would begin to form in order to

record the temperature of the crystallization zone. Crystal growth from the vapor would be carried out for 1-7 days depending on the material.
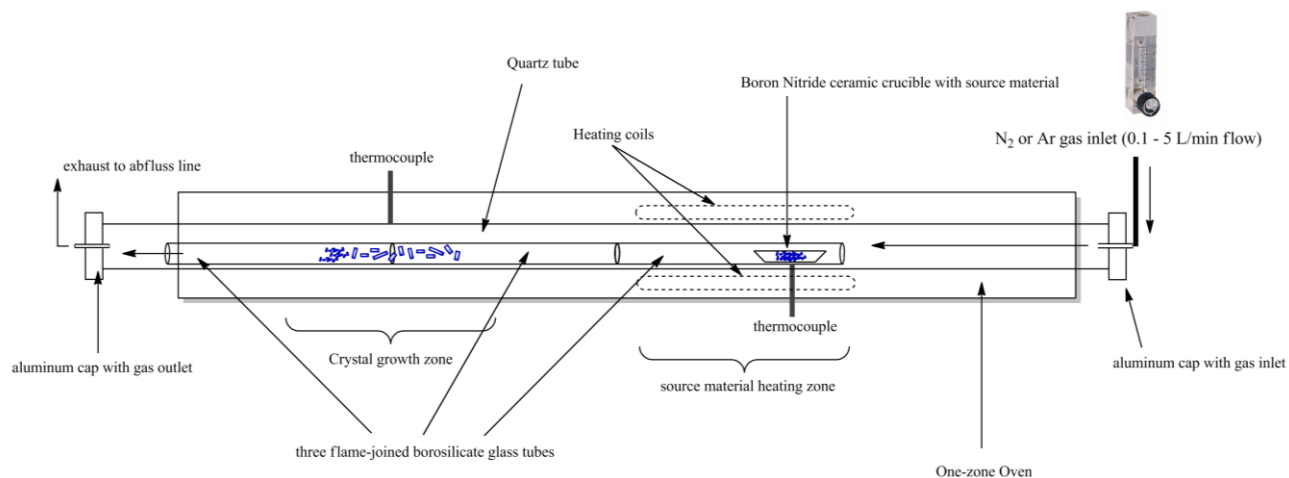

Figure 8. Tube furnace for the growth of H-bonded pigment single crystals for X-ray structure determination.

Single-crystal X-ray structure determination was carried out using a Bruker Smart X2S using a Molybdenum source with a wavelength of 0.71073 Å. Structures were solved using direct methods (SHELXS-97 software package) and refined by full-matrix least-squares F^2 (SHELXL-97). The H atoms were calculated geometrically, and a riding model was applied in the refinement process. Crystal structural data was evaluated using the Mercury software package. Mercury was also used to predict powder spectra. Structural data was uploaded to the Cambridge crystallographic database where appropriate.

2.3 Thin film deposition and characterization techniques

Organic thin films used throughout this work were prepared using thermal evaporation in a high vacuum or processing from solution via drop-casting or spin-coating. The primary method for obtaining high-quality films of H-bonded pigments was hot-wall epitaxy (HWE) physical vapor deposition. HWE is a variation on standard resistive thermal evaporation of organic small molecules, featuring the use of a large "hot wall" source tube that is uniformly heated to a desired temperature and substrates that essentially seal off the top of this tube, forming a semi-closed system. The substrates can be heated to a given temperature as well, allowing growth of organic films close to the thermodynamic equilibrium of molecules adsorbing and desorbing from the substrate surface. This allows the growth of high-quality films with tight control of deposition rate.[71,72] A significant benefit of the method is that materials usage is highly efficient, due to the fact that the organic material only condenses on the substrate/substrate holder. Thus experimental materials available in limited quantities can be used with minimal waste. During the course of this doctoral study, two separate HWE systems were used. One system, original built up by Prof. Helmut Sitter, was modified with a new substrate mounting and heating system. The second set-up was constructed by the author along with Dr. Alberto Montaigne-Ramil and Thomas Istok with two parallel HWE sources and a rotating sample carousel. The source and substrate arrangement common to both systems is shown in Figure 9. The new two-source HWE system built up during this study is shown in Figure 10.
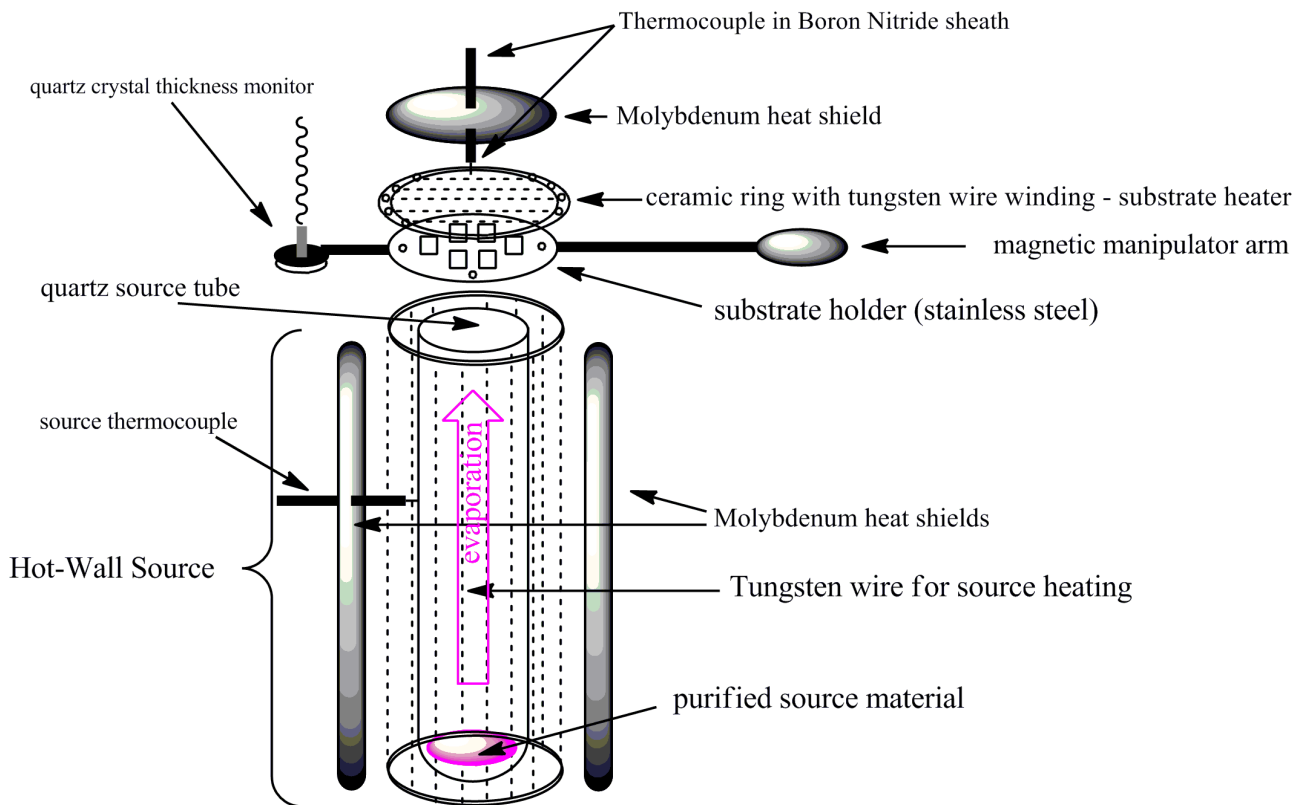
Figure 9. Hot-wall epitaxy (HWE) source and substrate mounting set-up.

Figure 10. Two-source HWE system with rotating sample carousel. The source shutters are both open.

2.3.1 Optical Spectroscopy methods

Routine UV-Vis absorption and photoluminescence measurements were carried out on all H-bonded pigment forming molecules, both in various solutions as well as in solid state. UV-Vis spectra were obtained using a Cary 100 spectrophotometer or a Perkin Elmer Lambda 1050. Photoluminescence spectra were obtained using a Horiba Jobin Yvon Fluorolog 3 integrated steady-state modular fluorometer.

Light-induced electron spin resonance (L-ESR) is a useful technique for establishing the presence of photoinduced electron-transfer reactions.[73–75] L-ESR spectra were obtained using a Bruker EMX X-band spectrometer at 9.45 GHz with a rectangular TE_{102} cavity allowing illumination of the sample through a 50% transmittance metal grid. Experiments were conducted using an Oxford ESR continuous-flow Helium cryostat between 300K and 4K. The experimental set-up and method is described in detail in the dissertation of Dr. Markus Scharber.[76] Various laser diodes were used as excitation sources.

Electroluminescence spectra were collected using a Photo Research Spectrascan PR-655.
Optical Microscopy was conducted using a Nikon polarization-enabled microscope with digital camera accessory.

2.3.2 Electrochemical measurements

All the semiconducting H-bonded pigment molecules used throughout this work were characterized by cyclic voltammetry (CV) according to established methods[77] in order to provide an estimate of the HOMO and LUMO energy values as well as predict the feasibility/stability of electron or hole transport processes. CV measurements were carried out using thin films of the organic material under test processed onto indium tin oxide-coated glass, functioning as the working electrode. Ag/AgCl was used as a quasi-reference electrode. Ag/AgCl electrodes were prepared before each set of measurements starting with clean silver wires using potentiostatic (4 V) growth method in 0.1M HCl. Platinum was used as a counter electrode. The electrolyte solution used for all experiments was tetrabutylammonium hexafluorophosphate 0.1 M in acetonitrile. CV measurements were always carried out in a N_2-filled glove box. The CV experimental set-up is shown in Figure 11. The ferrocene/ferrocenium redox couple was used as an external standard prior to every measurement on a new compound. The values of the Fc/Fc$^+$ vs. NHE and NHE vs. vacuum level used in this work were 0.64 and −4.75 V, respectively.[77]
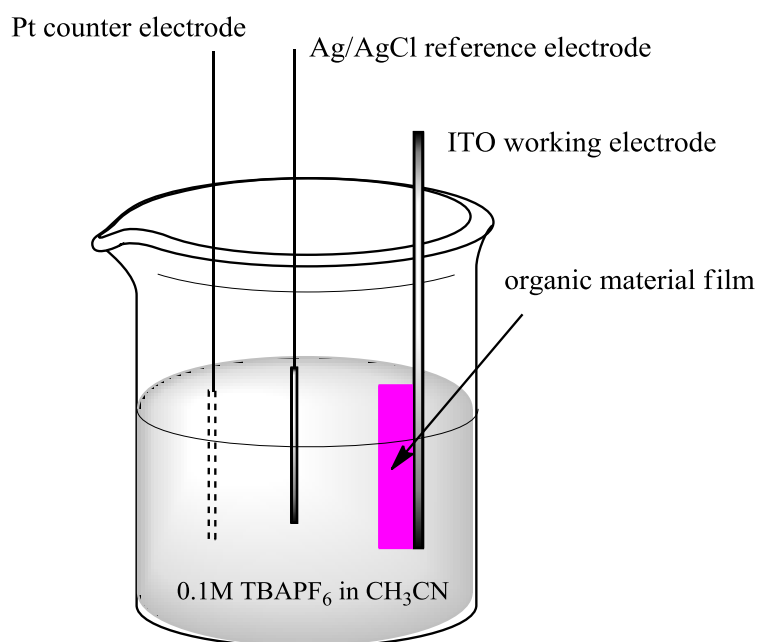
Pt counter electrode

Ag/AgCl reference electrode

ITO working electrode

organic material film

0.1M TBAPF$_6$ in CH$_3$CN

Figure 11. Experimental set-up for cyclic voltammetry measurements on organic thin films.

2.3.3 X-ray diffraction techniques

Out-of-plane X-ray diffraction is critical to understanding how organic small molecules grow on surfaces. Reciprocal space maps from ω/2θ diffraction scans of films were obtained for all the H-bonded semiconducting molecules.[70] The diffraction peaks of thin films of organic molecules can be correlated to known crystal structures obtained as described in 2.2 with the help of the Mercury software package for powder spectrum prediction. Thus, the orientation molecules adopt relative to the film growth direction, *i.e.* normal to the substrate, can be established. For these studies, a Bruker AXS diffractometer (Cu K$_\alpha$ source) at the Applied Physics Institute of JKU was used. The experimental set-up for measuring X-ray diffraction on thin films (ω/2θ) is shown in Figure 12.

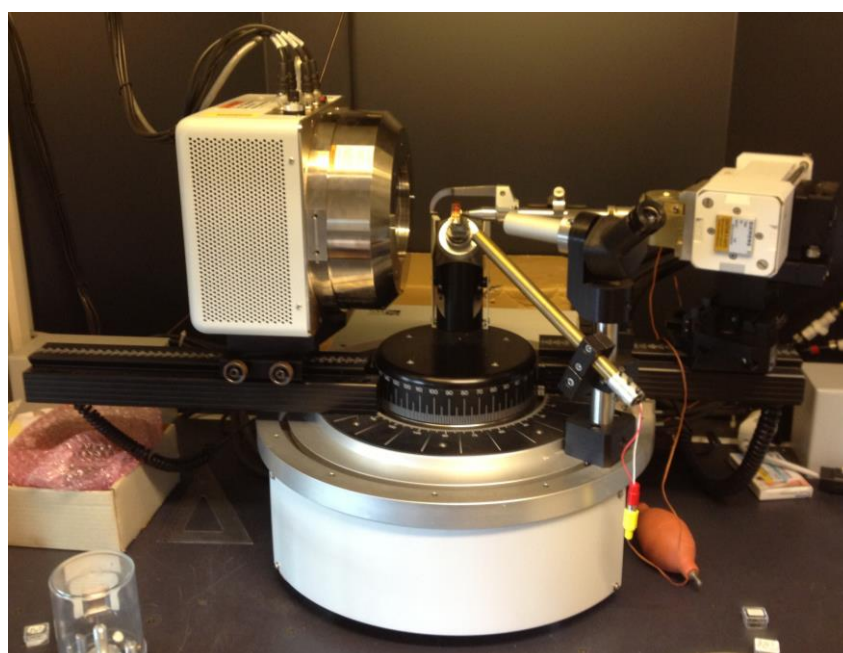**Figure 12.** Bruker AXS X-ray diffractometer for measuring ω/2θ scans of thin films. A film is mounted on the goniometer.

21

2.4 Preparation and measurement of organic field-effect transistors (OFETs)

The organic field-effect transistors (OFETs) used throughout this work for measuring the mobility of H-bonded pigments consisted of bottom gate-top contact geometry (Figure 13). Like many organic semiconducting materials, the H-bonded pigments used in this study proved to be intrinsic semiconductors, and OFETs were operated in accumulation mode, with the application of a given gate voltage causing the accumulation of carriers in the conducting channel of the OFET.[12,13,15] Horowitz et al. reviewed that the traditional expressions for inorganic semiconductor transistors can be applied to OFETs as well.[14,78] Charge carrier mobility, µ, was calculated from the saturated I-V regime according to Equation 1.

$$I_{SD} = \frac{W}{2L} \mu C_{0d} \left(V_G - V_T\right)^2$$
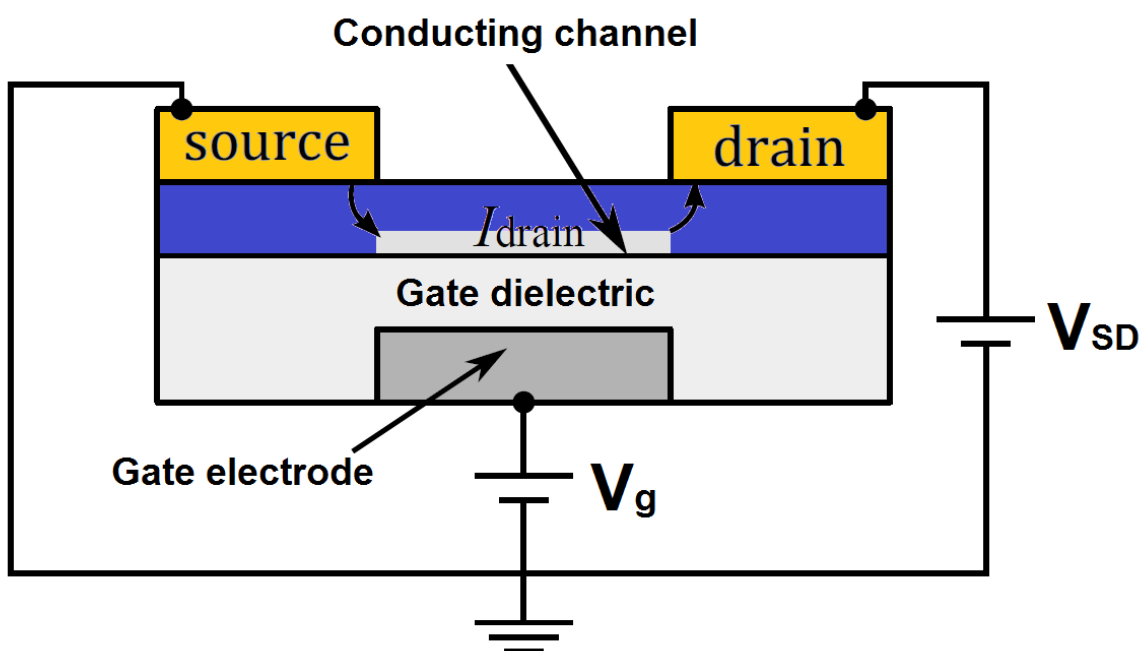
Equation 1

Figure 13. A schematic of a top-contact/bottom gate organic thin-film transistor. This architecture was used throughout this study to establish the charge carrier mobility in H-bonded pigments.

As a gate electrode, vacuum-evaporated aluminum was used, which was conveniently patterned using a shadow mask. A thin (10-40 nm) aluminum oxide layer was then grown electrochemically to provide a low-leakage and relatively high-ε dielectric layer (ε ~ 9).[79,80] The aluminum oxide layer was grown according to the well-known potentiostatic method, where a positive potential is applied to the aluminum gate electrode, which is dipped into a 0.1M solution of citric acid/trisodium citrate buffered electrolyte solution, with a stainless steel counter electrode. The high-field oxide growth process is self-limiting, with a formation factor of ~1.6 nm V^{-1}.[79] Thus applying 20V should produce an oxide with a thickness of about 32 nm. After electrochemical oxide growth, the OFET samples were dried at 120 °C for 20 minutes and then loaded into an organic materials evaporation system for deposition of a thin organic passivation layer. This step is necessary because the surface of aluminum oxide has a high density of trap states for electrons, impeding n-type operation mode of OFETs or even eliminating it completely. Also, applying an aliphatic organic

passivation layer is critical to obtain a low surface energy and promote the growth of large crystallites of organic small molecule semiconductors.[81] In the case of the H-bonded pigments, low surface energy is also critical to obtain a crystallographic orientation that is necessary for supporting transport in OFETs. Two organic passivation layers were used throughout the studies of H-bonded semiconductors: the oligoethylene tetratetracontane, $C_{44}H_{90}$ (TTC); and low-density polyethylene (LD-PE). Both are long-chain hydrocarbons that can be readily vacuum-processed onto aluminum oxide and can be heated above their melting points in order to form very smooth and conformal coatings with a low surface energy. TTC was introduced as a vacuum-processable dielectric for effectively passivating trap states of silica and alumina to obtain trap-free ambipolar operation of a wide variety of organic semiconductors by the group of Brütting.[82–84] Typically, between 10-20 nm of TTC or LD-PE were evaporated onto the oxide, followed by heating above the melting point of the material (70°C for TTC, 110°C for LD-PE). This second step is critical to obtain a conformal ultrathin coating without pinholes and with excellent smoothness. The use of LD-PE as a gate dielectric for OFETs was done during the course of this study and was published in [85]. Thus an inorganic/organic hybrid gate dielectric was used throughout this work – an architecture that combines the excellent dielectric properties of aluminum oxide with the desirable surface characteristics of a simple hydrocarbon.

The organic semiconducting layer was then processed on top of the gate dielectric by vacuum-evaporation in an HWE system. For OFETs, a thickness between 25-80 nm was used. Optimal thickness must balance two considerations: 1) The thicker the film, the higher the effective contact resistance will be (*i.e.* resistance that is independent of the transistor channel). 2) Since the film of organic small molecules consists of grains on the lateral size order of between tens of nanometers up to a few micrometers, the film must be thick enough to consist of continuous grains that are interconnected.

Finally, source and drain contacts are evaporated through a shadow mask. Different designs were used, with channel width ranging from 500 μm to 5 mm, and length ranging from 20 μm to 100 μm. The complete device schematic, as well as a picture of an example device placed for measurement on a probe station are shown in Figure 14.
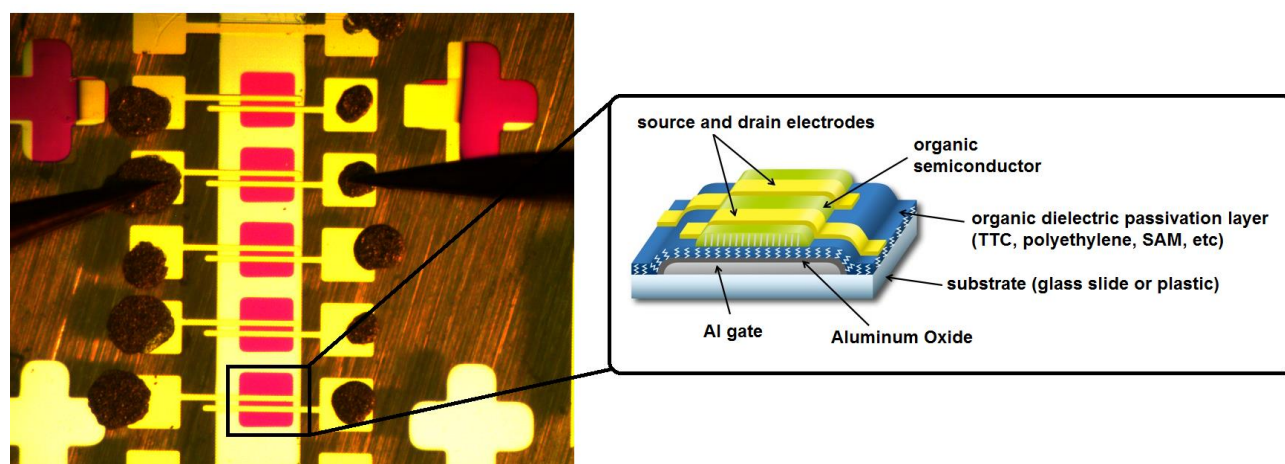

Figure 14. A sample with OFET devices photographed on the probe station, with a schematic illustrating the different layers of an individual OFET device. The uppermost device in the photograph is a capacitor for verifying gate dielectric capacitance.

One of the important building blocks of modern microelectronics is the CMOS logic gate, or CMOS inverter. CMOS stands for "complementary metal oxide semiconductor". This refers to the use of a pair of metal-oxide-semiconductor (typically Silicon with SiO_2 as the gate dielectric) field-effect transistors, where one is p-type and the other n-type. In a CMOS

inverter, the gates of both transistors are connected together, so the application of a low voltage on the gates will turn on the p-type transistor and the n-type off.[86] This is speaking in terms of an accumulation mode of operation, in the case of inversion regime as is commonly used in real Silicon-based CMOS technology, this behavior is opposite. A CMOS element "inverts" the input – a low input voltage yields as high output voltage, while a high input voltage yields a low output voltage. The ratio of input/output is the gain. Since one of the transistors is always in the off state the noise level of CMOS based circuits is very low, and the power consumption is low because the device only consumes power during switching. Complementary logic inverters that are analogous to inorganic-based CMOS based on ambipolar organic transistors have been reported by several groups.[87–90] Such devices are inherently different than traditional CMOS devices because the active material is intrinsic and both transistors are identical. A circuit schematic is shown in Figure 15. In order to achieve high noise margin and low power consumption, combined with high gains, ambipolar OFET-based complementary inverters must feature OFETs that can be truly turned off; as well as balanced hole and electron mobilities. In this work, a combination of true "off" state and balanced mobilities in some H-bonded pigment semiconductors in this work leads to high gains.
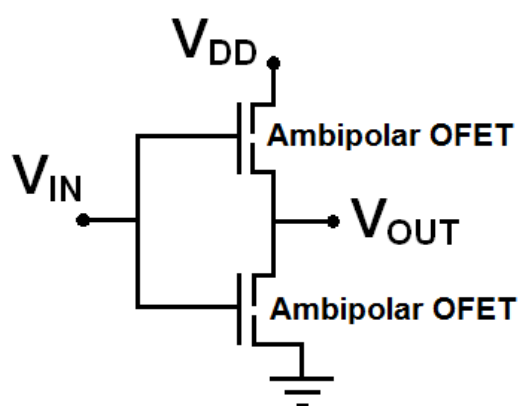

Figure 15. Circuit diagram for a voltage inverter based on two ambipolar OFETs.

2.5 Preparation and measurement organic diodes

The organic diodes used in this work feature an organic layer sandwiched between two metallic electrodes. All diodes were processed on top of indium tin oxide-coated glass (ITO), a standard transparent conducting electrode.[91,92] The ITO was cleaned by ultrasonication sequentially in acetone, isopropanol, detergent, and DI water, and finally treated with oxygen plasma at a power of 50W. The ITO was in most cases modified with a layer of PEDOT:PSS, poly(3,4-ethylenedioxythiophene) doped with poly(styrenesulfonate), a commercial conducting polymer formulation processable from water. The PEDOT:PSS layer serves to increase the work function of the ITO, thereby making a more hole-selective contact, and to smooth the surface of the ITO to prevent shunts. Alternatively, PEIE (ethoxylated polyethylenimine) is spin-cast on the ITO to form a low work-function contact for "inverted" type diodes.[93] The ITO bottom contact functions as the transparent side through which the sample is illuminated, or light emission is observed. The reflective top contact consists of an evaporated metal contact. For electron-selective contacts relatively low work-function metals like aluminum, silver, samarium, or ytterbium are used. In the case of inverted diodes, a high work function 8-10 nm layer of MoO_x was thermally deposited[94] followed by silver. Diodes with such a structure used in this work (Figure 16a) were thus metal/semiconductor/metal diodes, where the organic semiconductor is intrinsic, *i.e.* there is no doping in the semiconductor layer and no band bending at the metal/semiconductor contacts (Figure 16b).
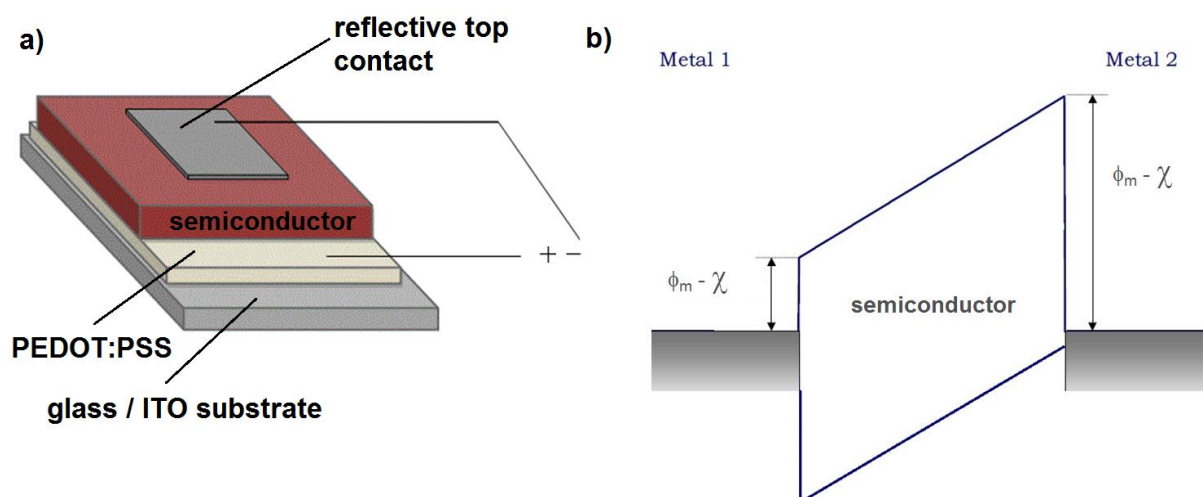
24

Figure 16. Metal-insulator-Metal diodes (MIM) diodes a) diagram of the devices used in this study. b) metal/semiconductor/metal diode energy diagram, assuming that the semiconductor is intrinsic.

Bulk heterojunction devices, consisting of a mixture of an electron donor and electron acceptor material, were also prepared for the experimental studies described in section 6.3. Bulk heterojunction films were prepared via spin-coating according to well-known procedures.[7,95]

3.Indigos in OFETs

3.1 Indigo OFETs

Initial measurements of electrical transport properties of indigo were motivated by the goal of finding truly natural-origin organic semiconductors. Indigo has an extremely low solubility in water and organic solvents and is thermally stable, subliming before melting. Its thermal stability and low solubility are explained by stabilization from inter- and intramolecular hydrogen bonding. Intermolecular interactions of π domains also strongly influence the electronic and vibrational spectra of indigo in solutions and dispersions. It is also likely that strong intermolecular interactions are responsible for the good charge transport we observed in thin indigo films. The results contained in this section were published in *Advanced Materials* in 2012.[96] In this work, indigo transistors are fabricated using only biocompatible materials: shellac resin is used as the substrate, the gate dielectric is Al_2O_3 passivated with tetratetracontane, a natural wax well-known from the *aloe vera* plant, and finally indigo as the semiconducting material (Figure 17). Source-drain contacts were made using biocompatible metals: silver or gold.
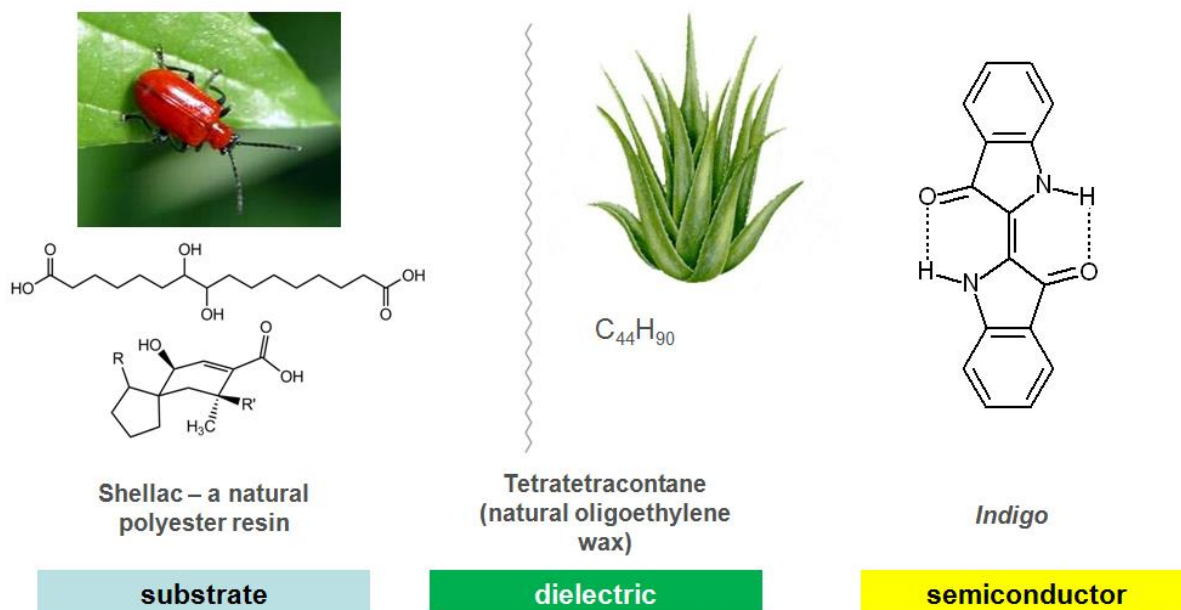
Figure 17. Components of indigo-based bio-transistors.

Before characterizing indigo-based OFETs (Figure 18a) and inverters, we studied the optical, morphological, and electrochemical properties of thin evaporated films of indigo. These films were prepared by means of evaporation, after purification of indigo by temperature gradient sublimation. Evaporated thin films of indigo show a broad (450-730 nm) absorption band, with an absorbance onset bathochromically shifted by about 80 nm with respect to dilute indigo in solution. In addition, indigo thin films show a broader and stronger absorption in the visible range than indigo in solution (Figure 18b). We found that indigo formed uniform and continuous thin films that were highly crystalline. X-ray diffraction (XRD) measurement of purified indigo powders afforded a diffraction pattern consistent with the literature. Based on single-crystal diffraction data, a powder spectrum was calculated (Figure 19). XRD of thin films of indigo evaporated on TTC or LD-PE yielded a single diffraction peak centered at ~ 11.06 degrees (Figure 18c), indicating a crystalline texture with a single preferential orientation in the growth direction of the film. This diffraction peak corresponds to the [100] plane of indigo (Figure 19) meaning that the indigo molecules are in the "Standing-up" orientation. This can be rationalized as the hydrophobic low surface-energy TTC or LD-PE interacts favorably with the outer edges of the phenyl rings of indigo which constitute the van der Waals contacts in the indigo crystal structure. XRD scans were conducted for indigo of different thicknesses and on different substrates (Figure 20).Weak and broad diffractions around 11 degrees were found for indigo on glass or quartz, but strong and narrow for hydrophobic substrates. We conclude that indigo deposited on hydrophobic substrates consistently grows with only the [100] prominently developed. We found that this was critical to measure charge transport in transistor geometry. Indigo π-π stacks along the b-axis (Figure 21). With the [100] planes parallel to the transistor gate dielectric (Figure 23), the stacking axis is oriented parallel to the dielectric and thus favorable for charge transport. The lack of this peak correlated to a lack of measurable transport. Thus, stacking parallel to the gate dielectric is absolutely critical for transport.

In the crystal structure, along the b-direction π-π stacking occurs, with an interplanar distance of ~3.3 Å and distance between equivalent atom positions of 5.77 Å. Along the c-axis intermolecular H-bonding is present, with each indigo molecule H-bonded to four of its neighbors with –NH―O= bond lengths of 2.11 Å. Along the a-axis there are only van der Waals contacts. The packing is relatively cofacial, especially when compared to the

herringbone pattern present in many organic molecular semiconductors. Packing motifs enhancing cofacial stacking are considered favorable for charge transport. Two modifications of indigo have been reported, based on single-crystal X-ray diffraction: The A form and B form. Both are very similar, consisting stacked molecules along the b-axis and the same intermolecular H-bonds, however with slightly different alignment between neighboring stacks of molecules. Atomic force microscopy (AFM) investigations of the indigo films of various thicknesses on glass show that indigo exhibits intensive island formation with grains in the range of 100 to 250 nm (Figure 24). AFM of indigo grown on TTC shows that a film of considerably large (250-600 nm) grains forms, with less-defined grain boundaries (Figure 25).

As part of our initial experiments, we also evaluated the material thioindigo, a structural derivative of indigo containing sulfurs in the place of the NH groups. Processed identically to indigo, thioindigo showed ambipolar charge transport, however with mobilities one to two orders of magnitude lower. Thioindigo has no hydrogen bonding, suggesting that strong hydrogen bonding-mediated intermolecular interactions could play the major part in the good performance of indigo as an ambipolar semiconductor.

Cyclic voltammetry (CV) scans of indigo films in acetonitrile using ITO | Indigo for the working and platinum for the counter electrode, respectively, were measured. A quasi-reversible two-electron reduction is observed, with an onset of approx. -0.9 V with respect to Ag/AgCl (Figure 18b). This is the well-known reduction to dianionic leucoindigo, utilized as the first step in textile dying. In the positive direction, a quasi-reversible two-electron oxidation was observed as well, with an oxidation onset at +0.8 V. Verifying reversibility is complicated in the case of indigo due to the solubility of the oxidized and reduced forms of indigo in the electrolyte solution. From CV one can estimate a band gap of 1.7 eV, corresponding closely with the band gap estimated from the onset of optical absorption, ~1.7 eV. The oxidation and reduction behavior of indigo suggests that hole and electron transport is possible, and with the low band gap of indigo injection of both carriers could be possible by selecting the appropriate source/drain contact metal.

OFET devices were fabricated with indigo on natural resin shellac substrates. The substrates were produced as described in [23]. We have found that drop-cast shellac resin forms smooth and uniform substrates (0.5 nm rms roughness for a 0.5 mm thick substrate. Shellac is a cross-linked resin that is completely insoluble in water and is unaffected by aqueous citric acid solution, recommending it as a substrate for the anodization of aluminum to form aluminum oxide gates. Tetratetracontane ($C_{44}H_{90}$, TTC), a long-chain alkane, was chosen as the passivation layer for the aluminum oxide. TTC occurs abundantly in nature, being found in plants, including medicinal plants, and is biodegradable. X-ray diffraction investigation of TTC (tetratetracontane) deposited on glass did not yield any diffraction peaks. It was found 10-30 nm tetratetracontane effectively passivates the electrochemically-grown oxide layer. Indigo only afforded semiconducting behavior on TTC and LD-PE, Indigo did not show any semiconductor behavior on other investigated dielectrics, *i.e.*, poly(vinyl alcohol), shellac, melamine, adenine and guanine as well as plain aluminum oxide. Possibly, the interaction of indigo with non-polar and/or aliphatic dielectrics is vital for charge transport.
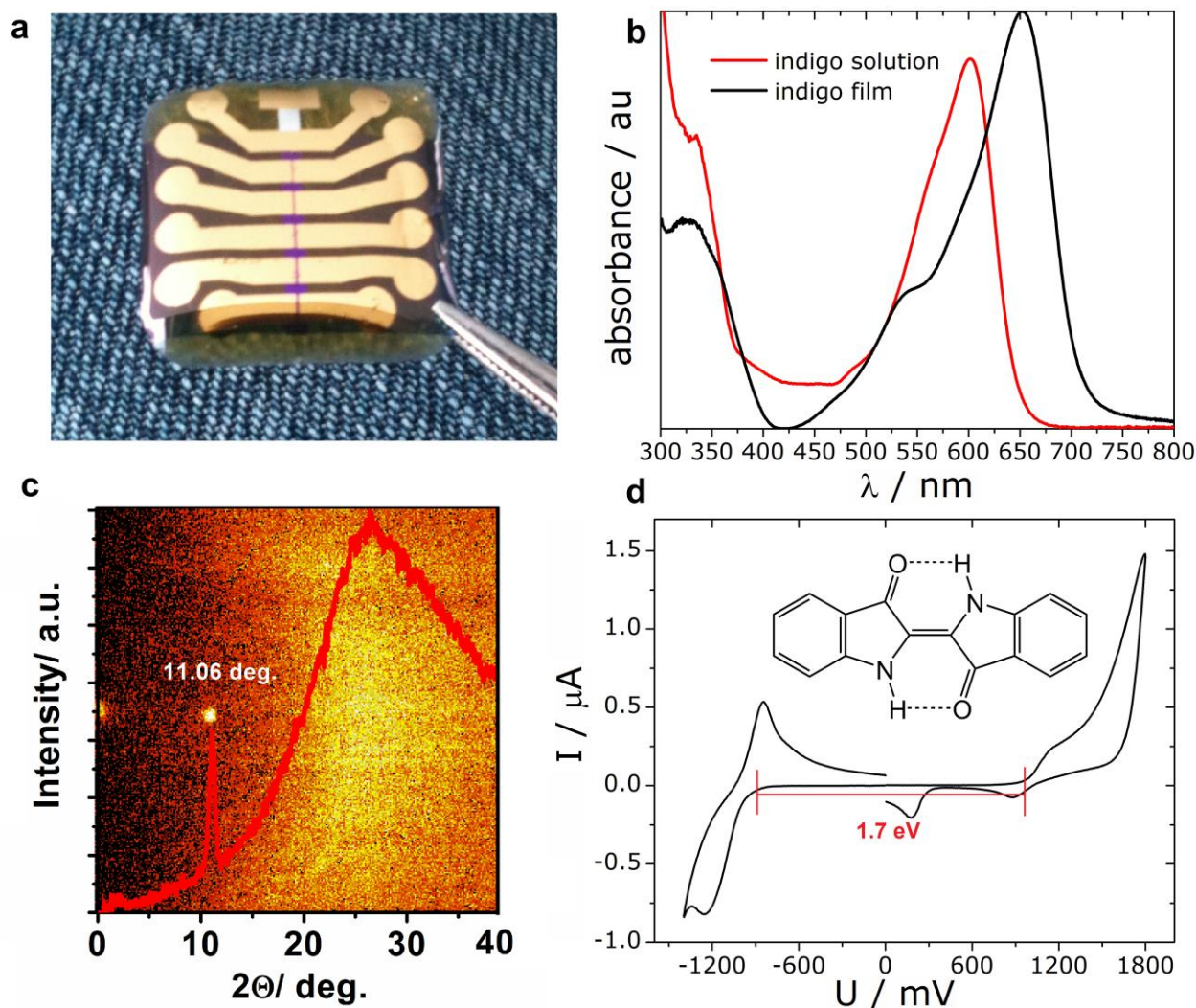
Figure 18. a) a photo of an indigo transistor fabricated using TTC/Al$_2$O$_3$ as the gate dielectric on top of a shellac resin substrate. b) UV-Vis spectra of indigo in CHCl$_3$ solution compared with an evaporated thin-film. c) X-ray diffraction taken normal to the substrate, ω/2θ scan. The broad amorphous peak originates from the glass substrate, only one indigo peak is visible at 2θ = 11.06°, corresponding to the indigo [100] plane meaning that the molecules grow in the "Standing" orientation with stacking parallel to the substrate. d) Cyclic voltammetry of an indigo thin film evaporated on ITO functioning as the working electrode.
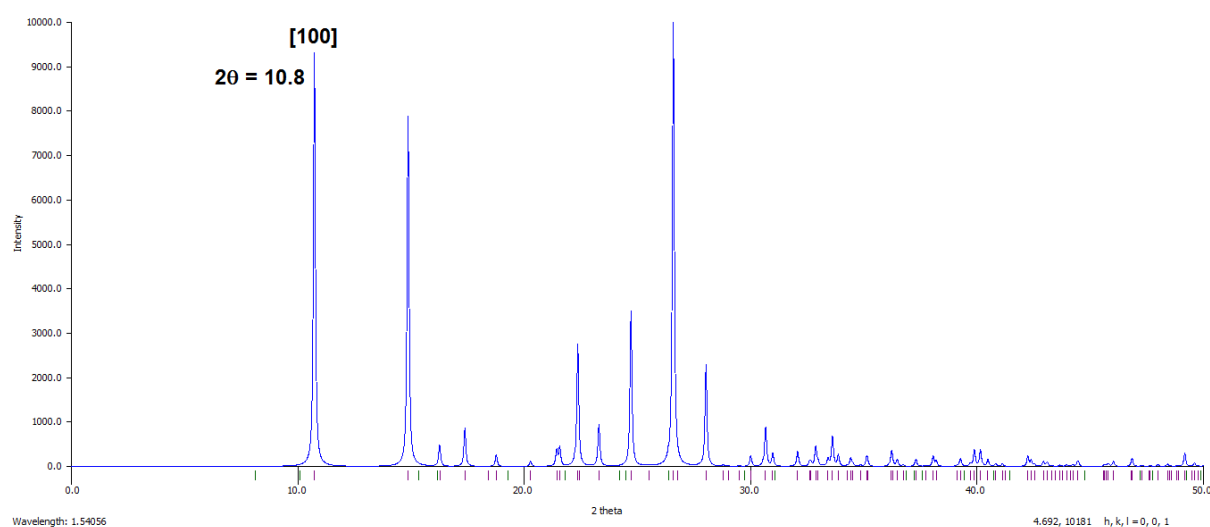
Figure 19. Powder X-ray diffraction pattern predicted using Mercury software from single-crystal diffraction data measured in [97].
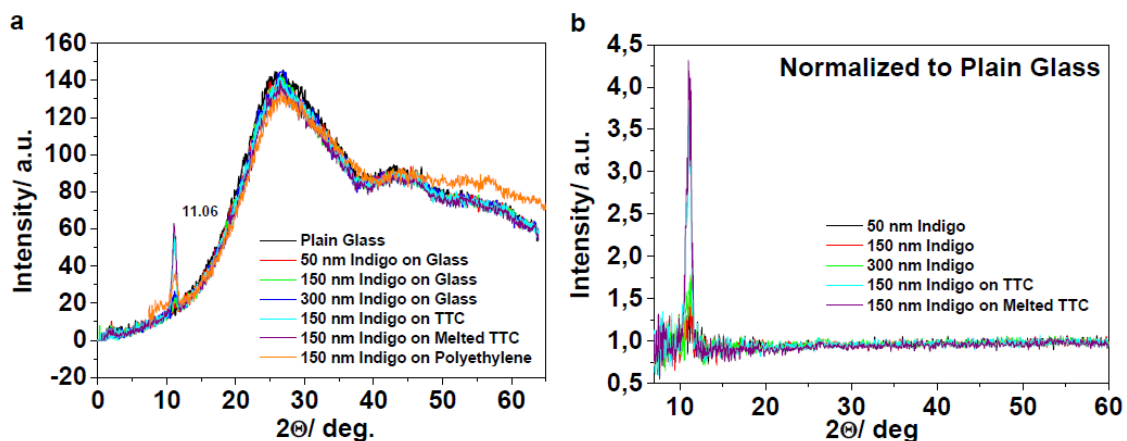
Figure 20. X-ray diffraction of indigo on different glass substrates. When deposited on low surface-energy substrates, such as in the case of TTC or polyethylene, the [100] peak corresponding to standing molecules is visible.
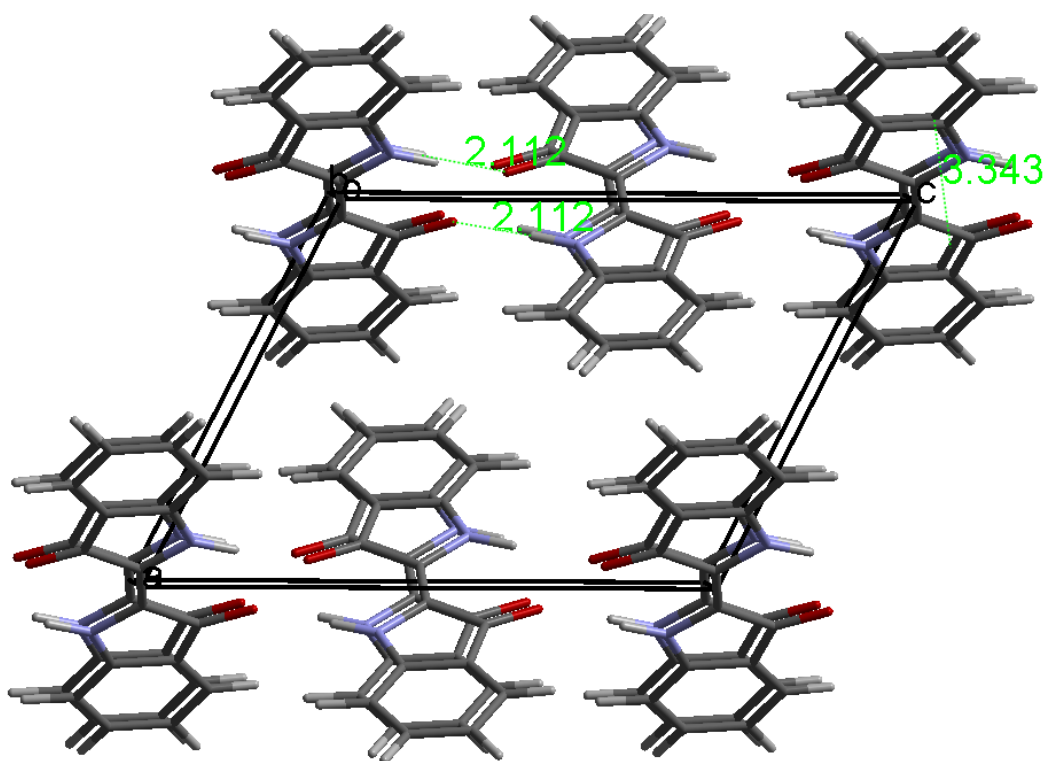

Figure 21. Indigo unit cell viewed down the b-axis showing the H-bonding (2.11 Å N-H—O=) along the c-axis and π-π interplanar spacing along the b-axis (3.34 Å).
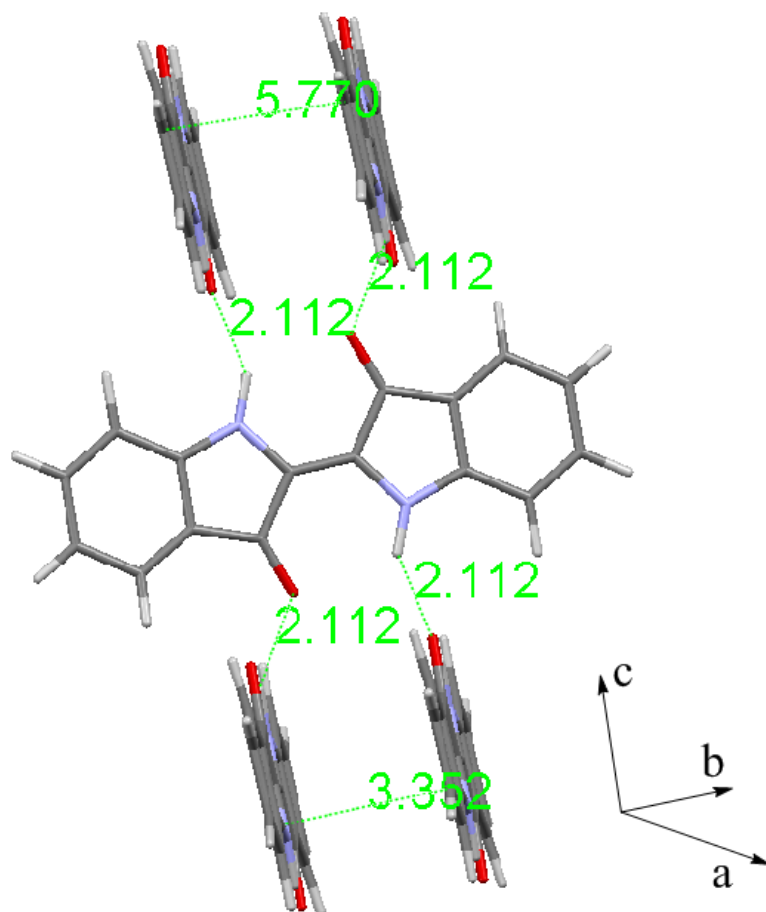
Figure 22. Indigo half unit cell showing each indigo molecule H-bonded to four neighbors, as well as the π-π stacking in the perpendicular direction.
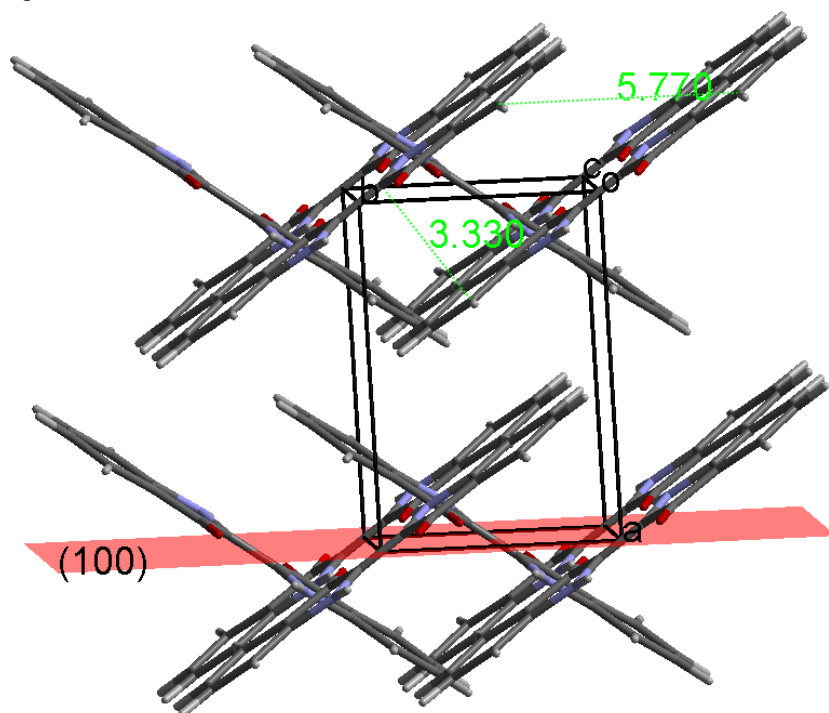

Figure 23. Indigo crystal structure viewed down a-axis. The [100] plane is prominently developed in the growth direction.
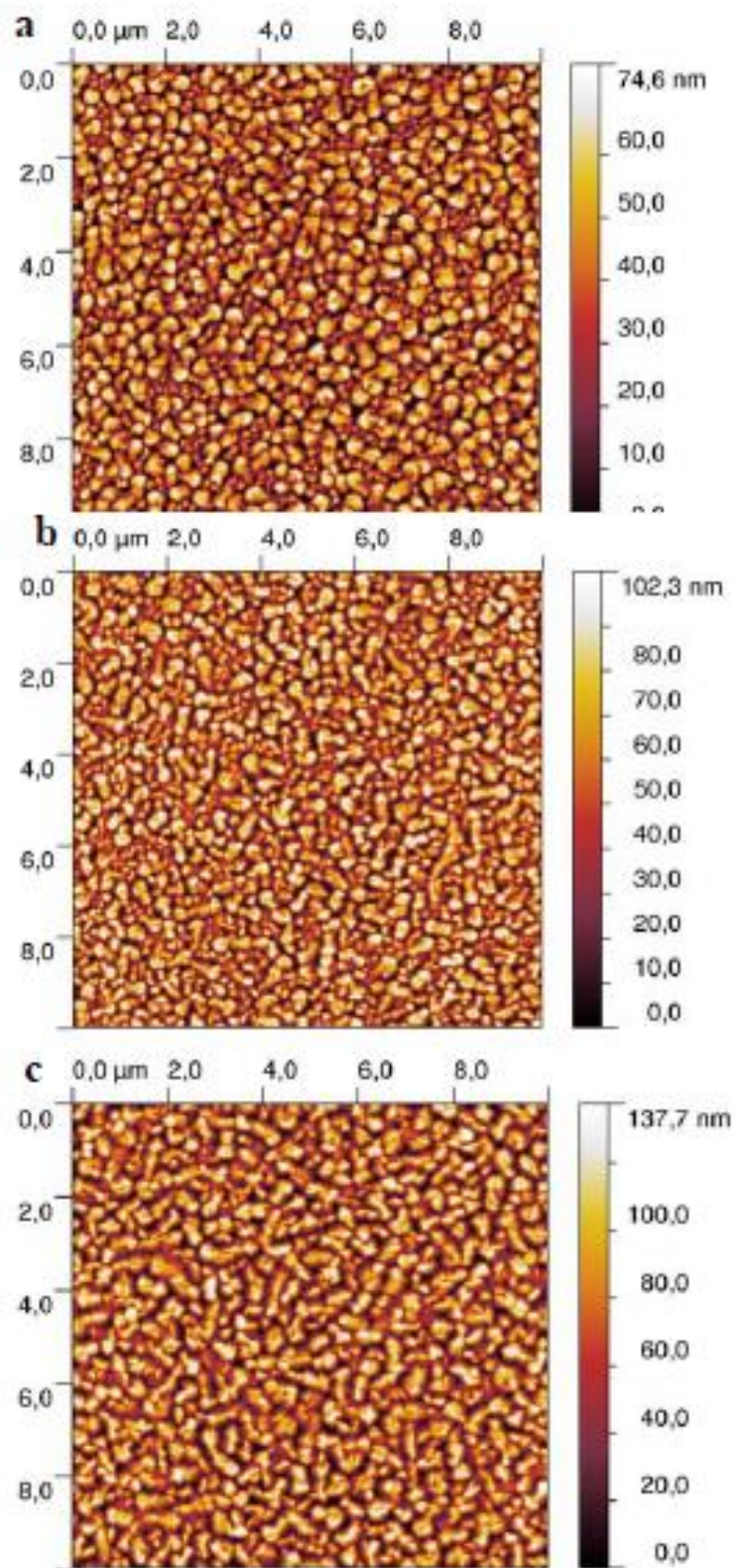
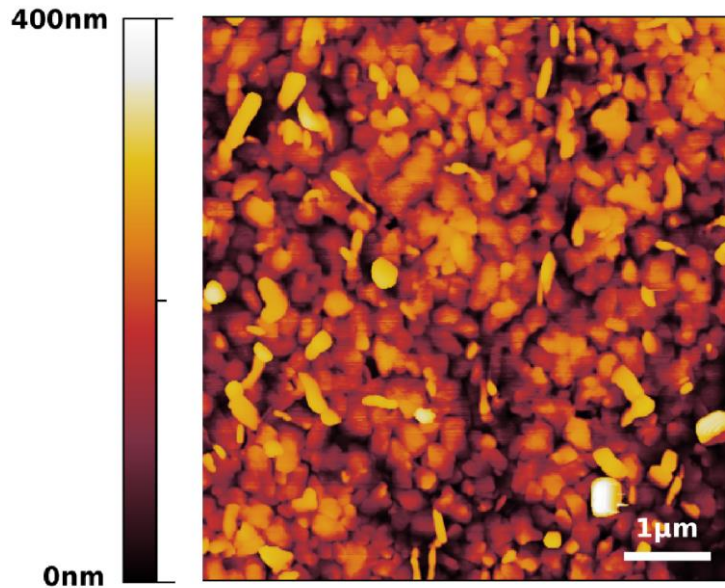**Figure 24.** AFM of indigo films on glass substrates a, 10 nm thick, b, 50 nm thick, c, 150 nm thick

Figure 25. AFM of indigo on TTC/Al$_2$O$_3$ substrate

Transfer characteristics of an indigo OFET are shown in Figure 26a, output characteristics are displayed in Figure 26b and Figure 26c. Both the output and transfer characteristics show ambipolar charge transport with low hysteresis. Measured with positive source-drain voltages, the threshold voltages of indigo-based OFETs are consistently in the range of -1.5 to -3V for holes and 4.5 to 7V for electrons. In the first quadrant, the output characteristics of indigo show a superlinear increase in the current at low gate voltages due to the injection of electrons in a channel dominated by holes. A similar effect is observed in the third quadrant for decreasingly negative gate voltages, as a result of the injection of holes. Because of the low band gap of indigo and its position of the HOMO and LUMO energy levels (-5.5 eV and -3.8 eV, respectively) with respect to the work function of gold (-5.2 eV), we conclude that the superlinear increase in current is not due to the contact resistance between the source and drain electrodes and the semiconductor layer. The electron and hole field-effect mobilities are calculated in the saturation regime. They are typically around 1×10^{-2} cm^2/Vs for electrons and 5×10^{-3} to 1×10^{-2} cm^2/Vs for holes.
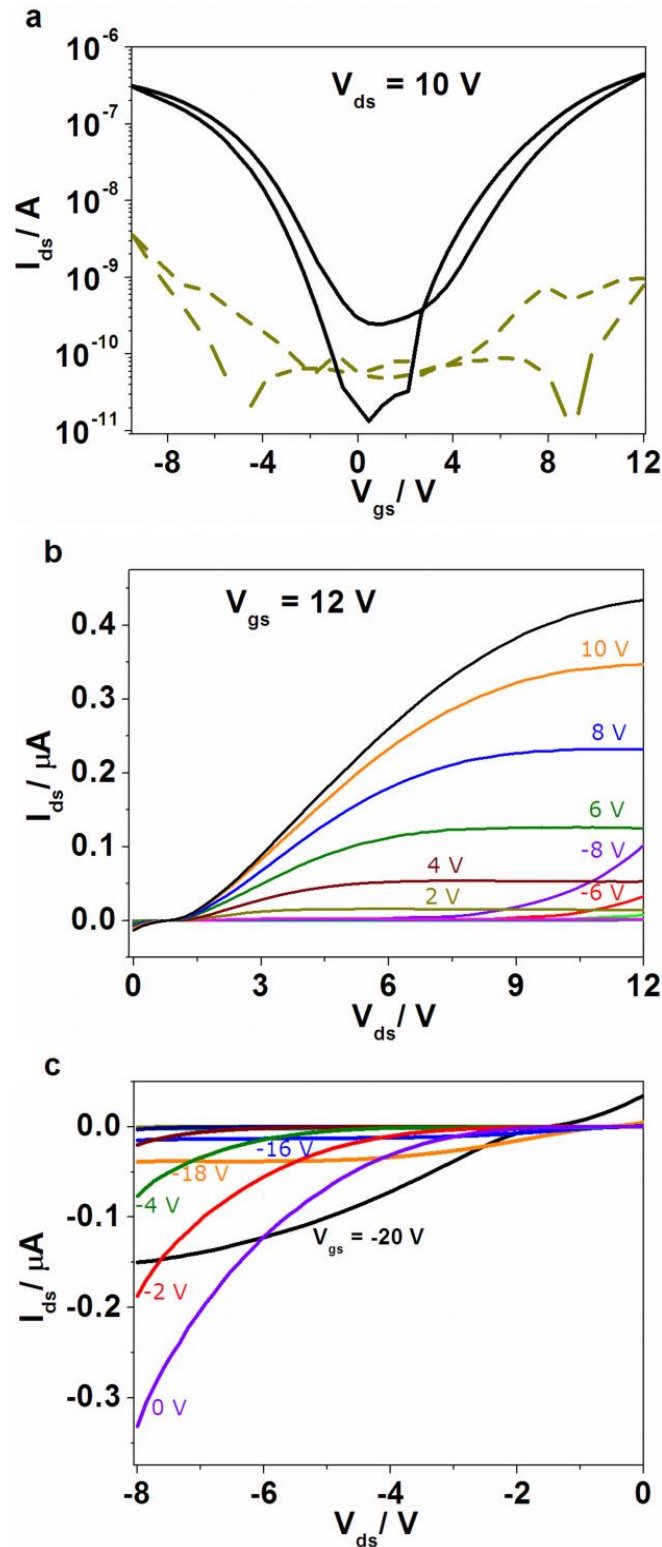
Figure 26. a, Transfer characteristics of an ambipolar indigo OFET. The black trace shows the forward and reverse V_{gs} scans, the dotted line shows the leakage current. b, Output characteristics for n-channel and c, p-channel. Channel dimensions: L = 75 μm, W = 2 mm. Gate dielectric C_{0d} = 80 nF/cm^2.

The operational stability of indigo-based OFETs was tested under various conditions, *i.e.* aging, dark-light exposure, cycling and exposure to ambient conditions. P-channel operation occurs stably in air and n-channel operation is stable in air only upon encapsulation using

polyimide tape. However, exposing the devices to air for several weeks does not produce irreversible degradation. The measurement in N_2 environment before and after extended exposure to air yielded comparable performance: the p-channel modulation remained unaffected by the oxygen exposure (field-effect mobility of 1×10^{-2} cm^2/Vs), whereas the n-channel mobility decreased only by a factor of 2.5, *i.e.* from 1×10^{-2} cm^2/Vs to 4.5×10^{-3} cm^2/Vs. The slight degradation of the n-channel after extensive exposure to air is a consequence of a shallow LUMO level of the indigo molecule that does not allow electron transport to occur in an oxygenated environment. The latter problem was effectively mitigated by a simple encapsulation with polyimide tape, which allowed stable operation in air of both channels. In conclusion, indigo devices are stable with respect to chemical degradation. Devices stored in N_2 showed no degradation even after seven months.

Measurements of a complementary-like voltage inverter built with two transistors on the same shellac substrate are presented in Figure 27a-b. The gain of the inverters fabricated, 105 in the first quadrant and 110 in the third quadrant, is remarkable for an ambipolar material with a single source and drain contact metal.
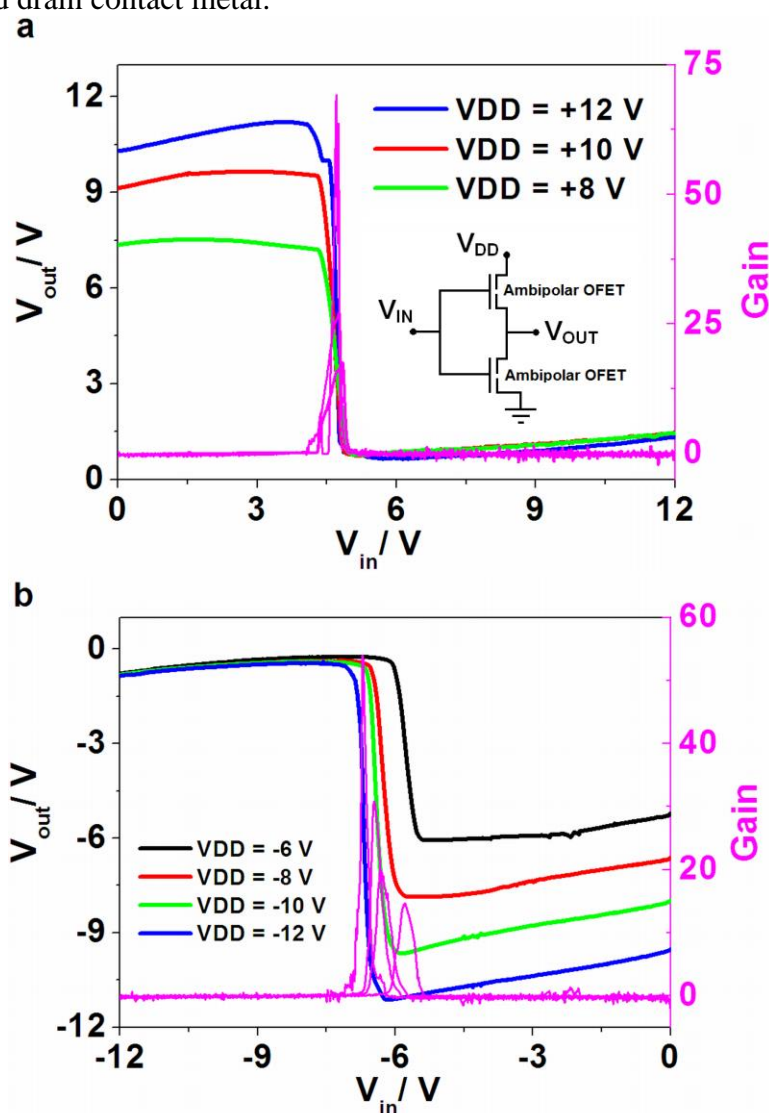

Figure 27. Quasi steady-state output characteristics of an indigo based voltage inverter in the first quadrant (a) and third quadrant (b). The inset schematic shows the voltage inverter circuit.

3.2 Tyrian Purple OFETs

With the promising results on OFETs based on indigo, the next point of attention was the dibromo derivative, Tyrian purple (Figure 28a). As described in section 1.2, tyrian purple is a natural product with an equally long history to that of indigo. Studying charge transport in the dibromo derivative of indigo was the first step in establishing first of all the generality of charge transport in H-bonded pigments, as well as understanding how derivatization of the indigo core effects physical properties. We prepared Tyrian purple synthetically via published procedures and purified it twice by temperature gradient sublimation, as described in section 2.1. OFETs were fabricated according to the procedures described in section 2.4, using Al_2O_3/TTC as a hybrid gate dielectric. The specific capacitance, C_{0d}, for OFETs fabricated during the Tyrian purple study was 43 nF·cm^{-2}. Devices with a W/L of 1 mm / 80 μm were used for initial OFET studies and inverter circuits published in [98], however performance was later optimized using Al_2O_3 passivated with LD-PE, reported in [85].

Similar to indigo, X-ray diffraction (XRD) of Tyrian Purple deposited on TTC showed only one diffraction peak (Figure 28b) in the reciprocal space map (ω/2θ) demonstrating a crystalline texture with a single preferential orientation. This peak corresponds to the [100] plane developed parallel to the substrate. Thus the molecules are, as in the case of indigo, in the "Standing" orientation favorable for charge transport in the transistors configuration. The X-ray crystal structure for Tyrian purple was first reported in 1979 by Süsse and Krampe.[99] We obtained a single crystal structure from vapor-phase grown single crystals with the same crystal structure as that reported earlier, however with higher resolution and hydrogen coordinates. Qualitatively, the crystal packing of tyrian purple is identical to indigo. The tyrian purple crystal structure viewed along the π-π stacking direction (b-axis) is shown in Figure 29. The crystal lattice view down the a-axis, perpendicular to the π-π stacking axis, is shown in Figure 30. As in the case of indigo, each tyrian purple molecule is H-bonded to four neighbors via single N-H—O= H-bonds (Figure 29). The H-bond length is identical to that of indigo, 2.122 Å. Like indigo, the tyrian purple molecule is remarkably planar, with an overall deviation from planarity less than 0.05 Å. The interplanar π-π stacking distance is 3.4 Å, however the distance between equivalent atom positions is shorter than that in indigo, with a value of 4.84 Å. The closer, more cofacial, stacking in tyrian purple may account for the higher charge carrier mobility observed in this material relative to indigo. As in the case of indigo, we surmise that the highly-ordered growth resulting in intermolecular π-stacking is integral for charge transport. UV-Vis measurement of Tyrian Purple thin films is shown in Figure 31, compared with the spectrum of indigo. The hypsochromic shift and thus purple color of tyrian purple can be rationalized according to the inductive effect of the weakly electron-donating bromine atoms in the 6,6'-positions according to the mesomeric models proposed by Sadler et al.[100,101] Electron-donating substituents in the 6,6'-positions push negative charge onto the carbonyl oxygen atoms, thus decreasing their electron-accepting power and shifting the H-chromophore absorption to higher energy. For more detailed discussion see section 5.1. On the basis of absorption edge one can estimate a band gap of ~1.8 eV. Cyclic voltammetry of tyrian purple thin films yielded the characteristic two-electron reduction and oxidation behavior observed for indigo (Figure 32). The reversibility of the oxidation and reduction processes is difficult to verify from CV due to the solubility of the charged anionic and cationic tyrian purple in the acetonitrile and thus rapid dissolution of the sample film. From CV, one can estimate a HOMO level of -5.8 eV, and a LUMO level of -4.0 eV. Atomic-force microscopy (AFM) measurements of Tyrian Purple on TTC/Al_2O_3 show the formation of crystalline needle-like grains with sizes in the 200-500 nm range (Figure 33). With the channel length used in these transistors, 80 μm, and grains of this size it is likely that overall mobility is limited by intergrain mobility.
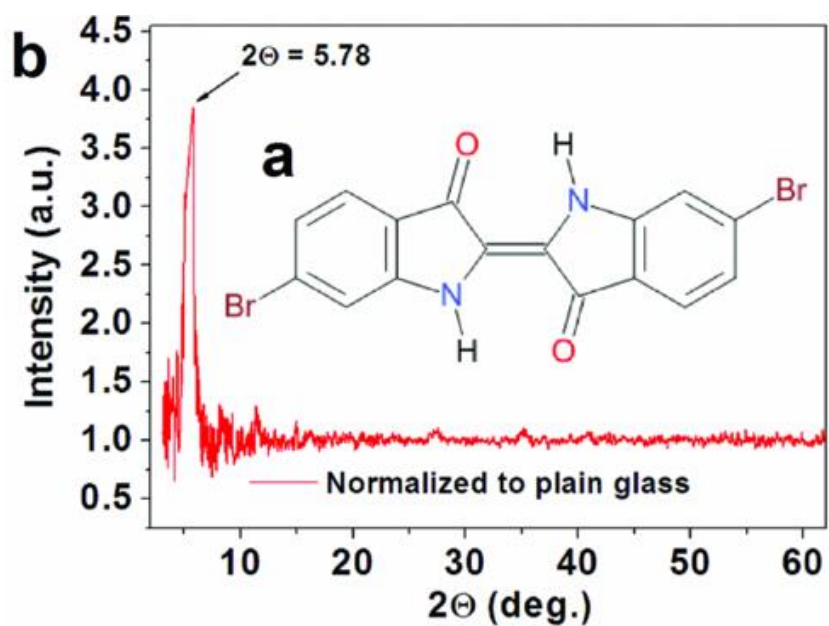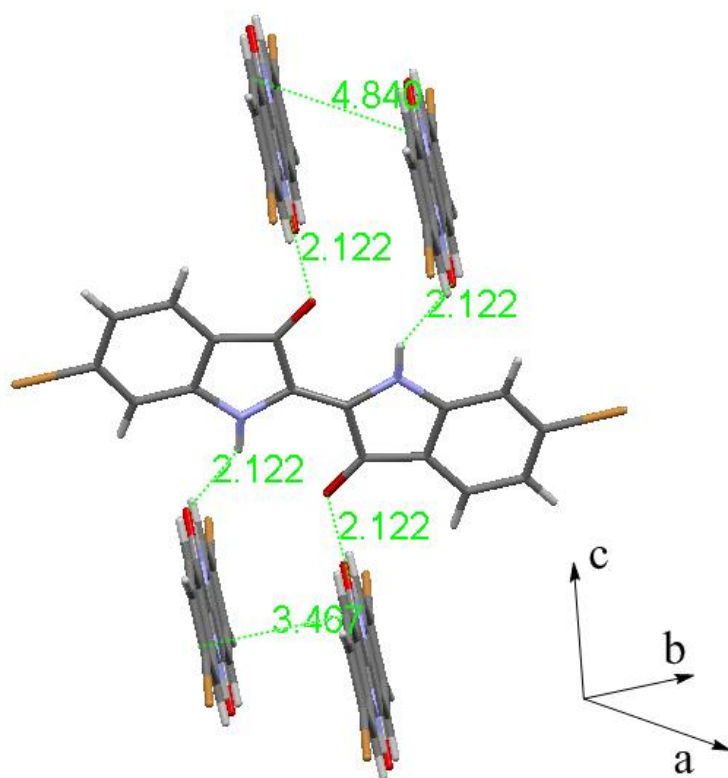
Figure 28. (a) Molecular structure of Tyrian Purple. (b) XRD of an 80 nm Tyrian Purple film deposited on TTC (40 nm)|glass. A single diffraction peak at 2θ = 5.78 is visible. TTC by itself showed no diffraction peaks in the measured range.
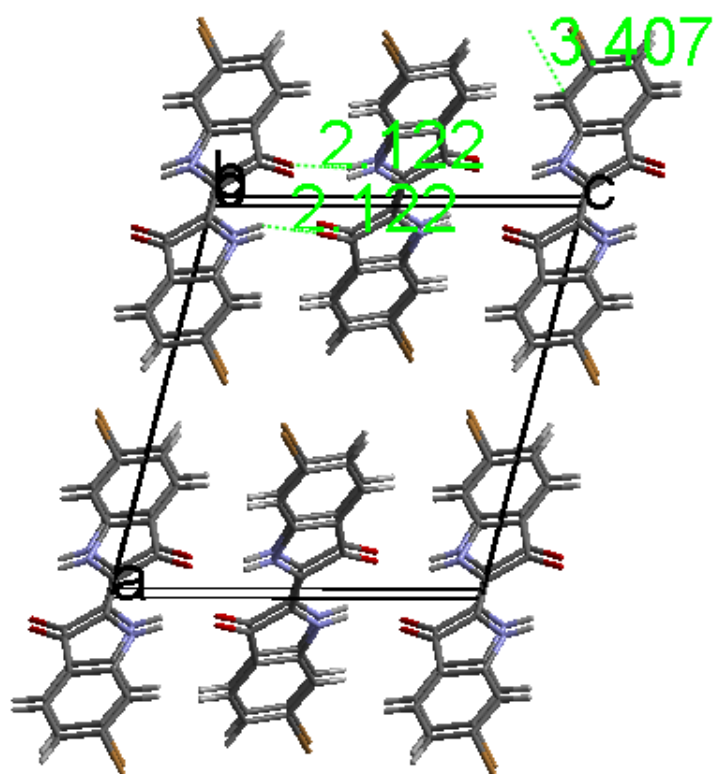
Figure 29. Tyrian Purple crystal structure, measured at JKU. (top) Half unit cell showing each tyrian purple molecule H-bonded to four neighbors, as well as the π-π stacking in the perpendicular direction. (bottom) View down b-axis (π-stacking axis)
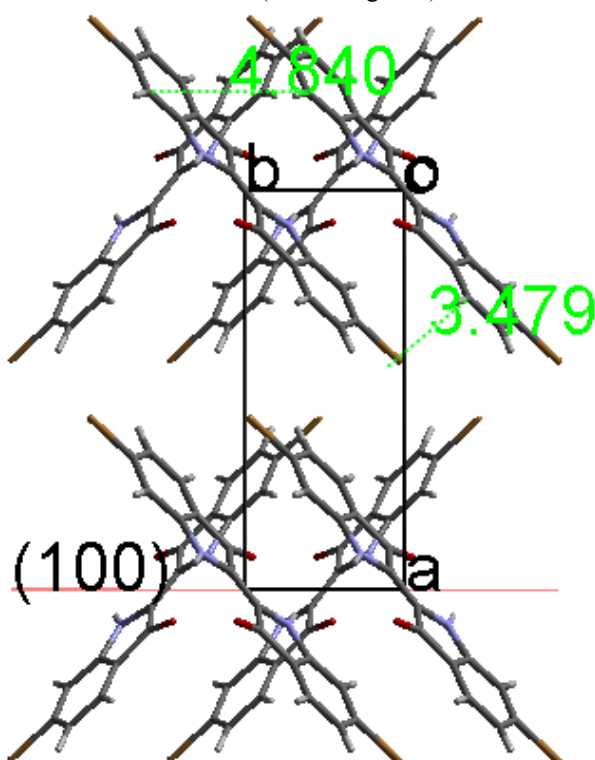

Figure 30. Tyrian purple crystal structure. View down a-axis, showing interplanar π- π distance of 3.479Å and distance between equivalent atom positions 4.84 Å. Tyrian purple grows on TTC and LD-PE with the [100] prominently developed, *i.e.* with the "standing" orientation.
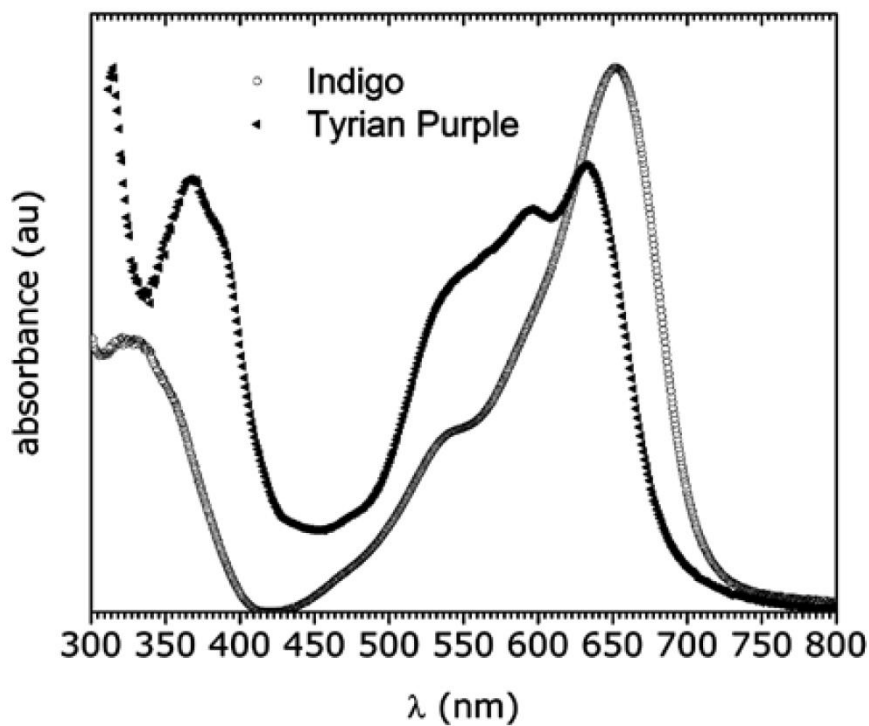
Figure 31. Comparison of the absorption of indigo and tyrian purple thin-films evaporated on glass.
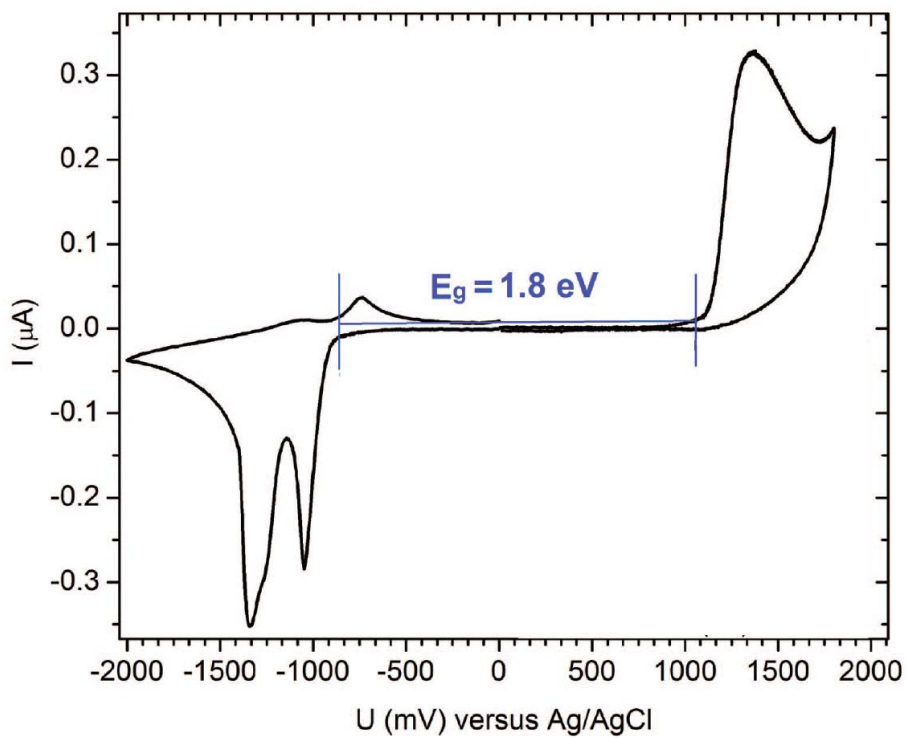

Figure 32. Cyclic voltammetry of a Tyrian Purple thin film on ITO measured with a scan rate of 20 mV/s.
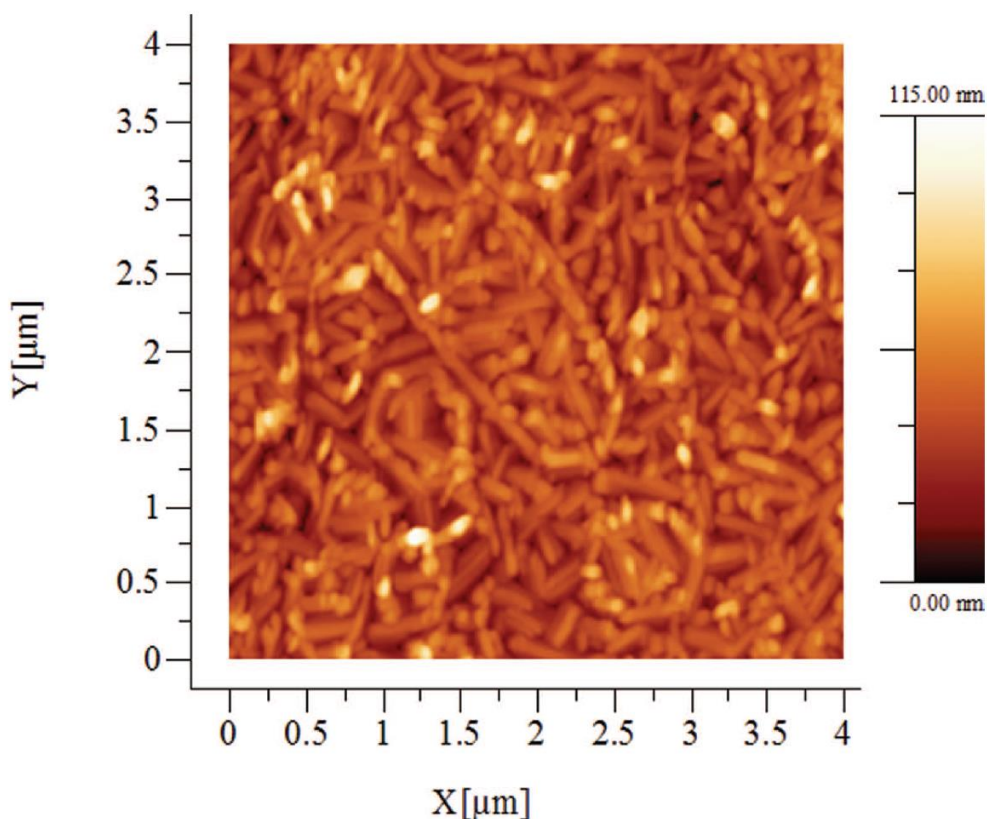
Figure 33. AFM image of Tyrian purple grown on TTC/Al$_2$O$_3$

Transfer and output characteristics of tyrian purple OFET devices are shown in Figure 34. In the first quadrant, the output characteristics of Tyrian Purple show a superlinear increase of current at low applied gate voltages due to the injection of electrons in a channel dominated by holes. Similarly, in the third quadrant the superlinear regime occurs for decreasingly negative gate voltages, due to the injection of holes. Typical values for field effect mobilities are typically around 0.2 cm^2/Vs for holes and 0.03 cm^2/Vs for electrons. With a positive source-drain voltage, threshold gate voltages for holes are in the 1.5 – 1.75 V range, while for electrons, 3V – 5V. On/Off ratios were 10^3 – 10^4 for both channels. The "off" state for such transistors was approx. 0.5 nA. Leakage current, I$_{gs}$, was in the picoamp range. We found that both hole and electron mobilities show little deterioration during measurement in air, even after repeated cycles (Figure 34d). This can be attributed to the relatively low-lying LUMO value of -4.0 eV, as electron transport at energy levels higher than about -3.7 eV is prone to trapping by atmospheric oxygen. The value of -4.0 eV is considered to be the threshold for true air stability.[38,102]

Quasi-static transfer curves and corresponding voltage gains of CMOS-like complementary inverter circuits are shown at various V$_{DD}$ voltages in Figure 35a-d. Gains of 255 in the first and 285 in the third quadrants are among the highest reported to-date for ambipolar OFET-based inverters. These devices showed little hysteresis upon cycling and were stable to cycling over 6+ hours in a N$_2$ environment. Stability studies in air were not carried out.

39
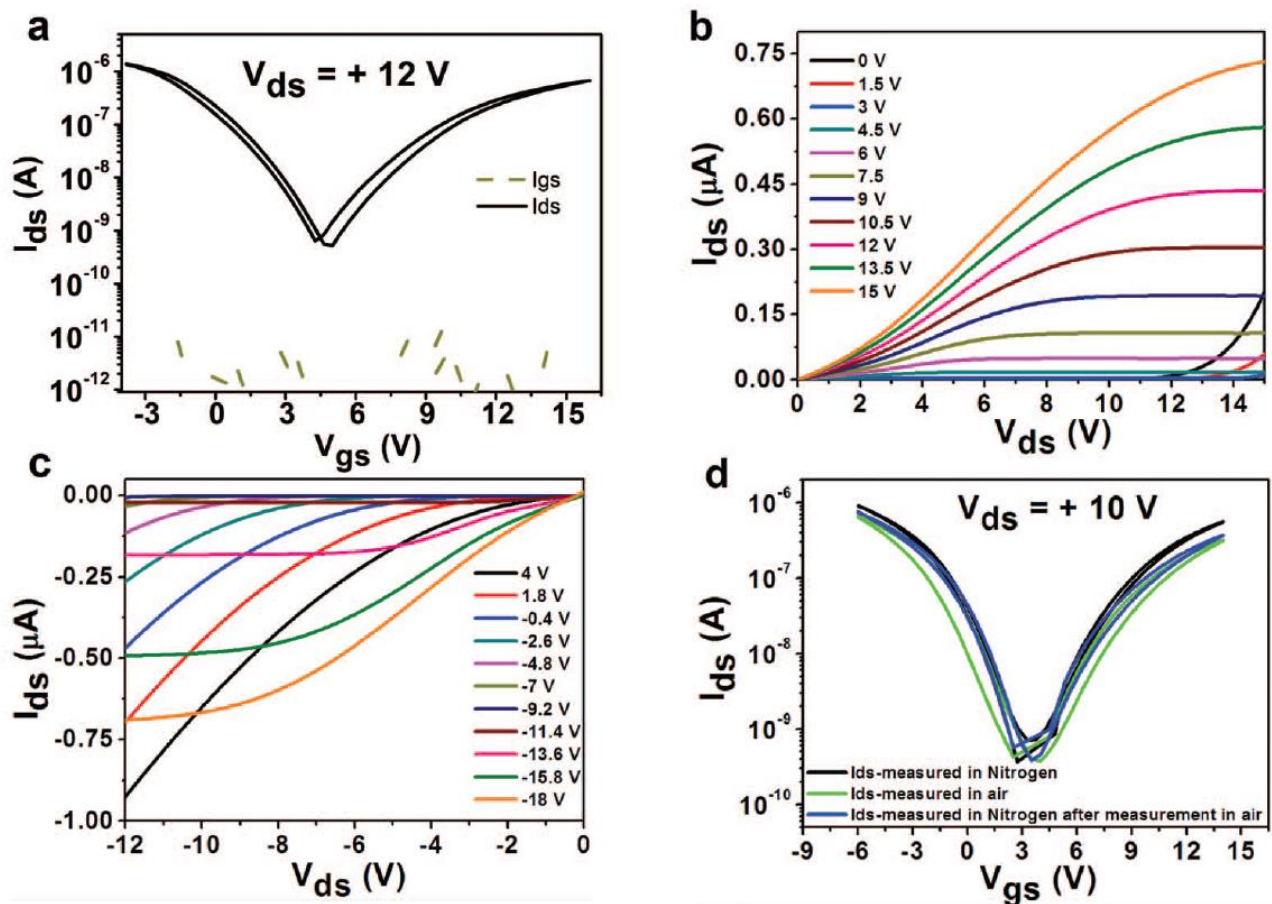
Figure 34. (a) Transfer characteristics of a Tyrian Purple transistor showing source-drain current (Ids) in black type, leakage current (I$_{gs}$) in olive **(b)** Output characteristics in the first quadrant. **(c)** Output characteristics in the third quadrant. **(d)** Comparison of transfer characteristics during measurement inN$_2$ atmosphere and air. Mobility for electrons drops by a factor of 2, but after this initial drop remains stable during cycling. Originally published in [98].

Figure 35. (a) Quasi steady-state transfer characteristics of complementary-like voltage inverters in the first quadrant, with (c) showing the corresponding voltage gain. (b) Quasi steady-state transfer characteristics of complementary-like voltage inverters in the third quadrant, with voltage g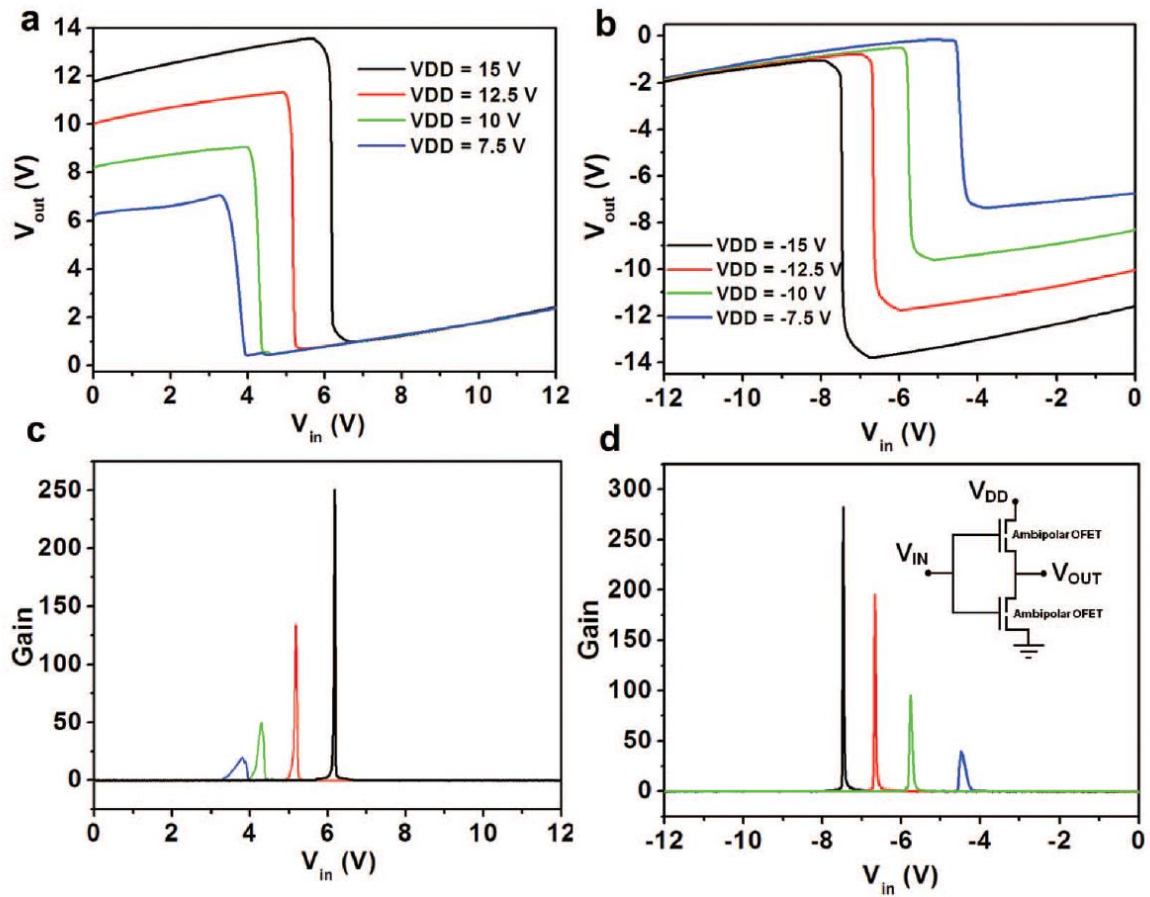ain shown in (d). Each measurement is performed through 1000 points with hold time, step delay and delay time of 1 second each. Originally published in [98].
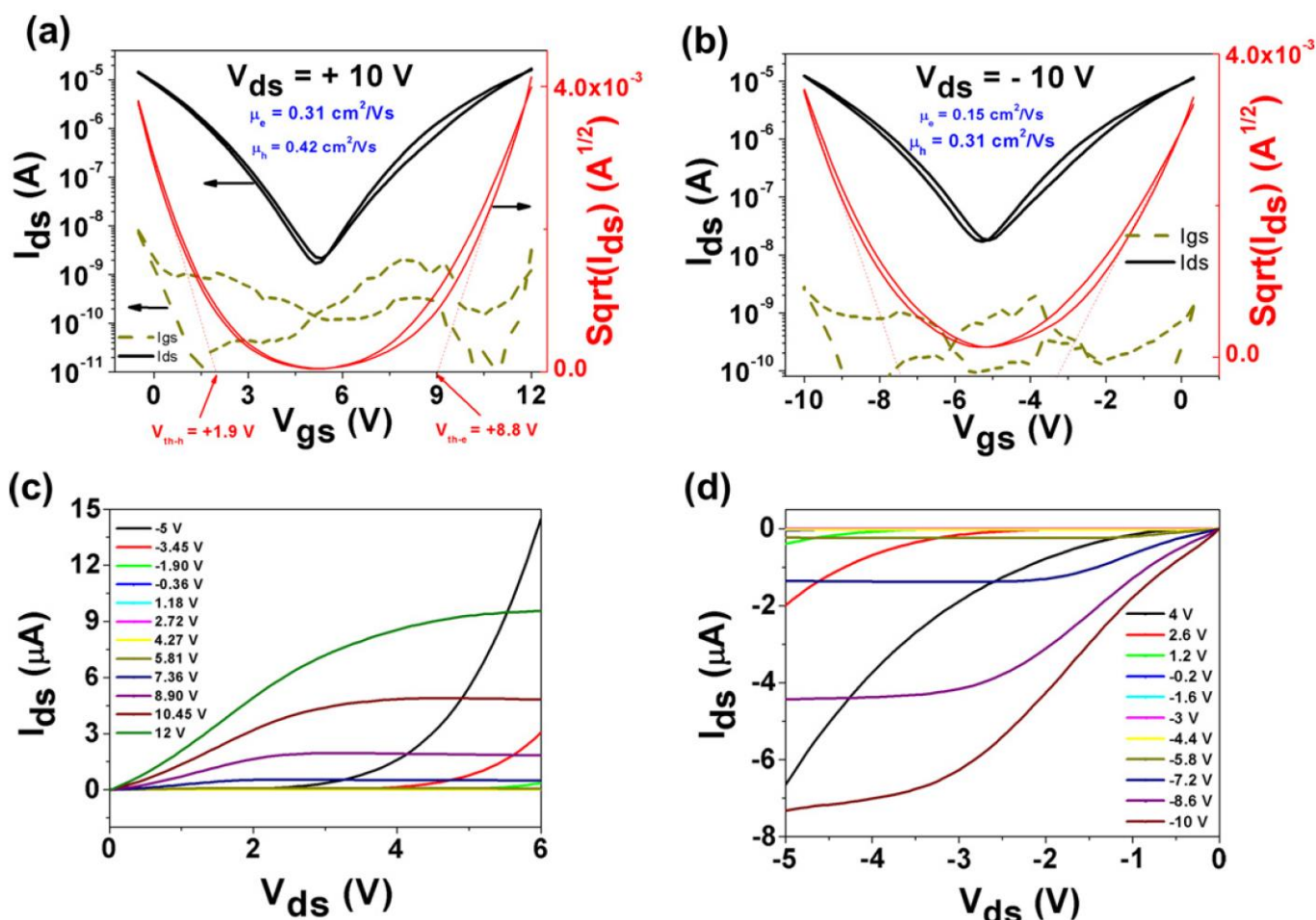
Figure 36. (a and b) Transfer and (c and d) output characteristics of a tyrian purple based OFET on evaporated polyethylene-passivated aluminum oxide dielectric. Thicknesses: aluminum oxide 30 nm, polyethylene 15 nm, tyrian purple 50 nm, gold source and drain electrodes 100 nm. Channel dimensions: L =35 µm, W= 5 mm. Originally published in [85].

As part of a study [85] evaluating the applicability of vacuum-processing low-density polyethylene (LD-PE) as a hydrophobic passivation layer for Al_2O_3 gate dielectrics, we used tyrian purple as well. The results demonstrated that tyrian purple grown on LD-PE layers afforded higher charge carrier mobility, with $\mu_e=\mu_h = 0.4$ cm^2/Vs. Transfer and output characteristics of tyrian purple on LD-PE OFETs are shown in Figure 36. AFM studies showed that the morphology of tyrian purple appeared the same as in the case of TTC. In summary, tyrian purple performed similarly to indigo, however with overall higher mobility and impressive electron-transport air stability. This significant improvement in performance of tyrian purple over indigo ultimately originated from the substitution of two bromine atoms onto the molecular structure. This led us to question what could be learned from the relationship between indigo molecular and supramolecular structure and the semiconductor performance parameters, and led us to study the molecular library described in the next section.

3.3 Indigo derivatives

In order to understand the structure/function relationships for charge transport in indigo materials, several indigo derivatives were synthesized along with Dr. Gundula Voss using substituted *o*-nitrobenzaldehydes as described in section 2.1. Nine indigo derivatives were prepared in total, and single-crystal X-ray structures were determined for eight of them. The

structures are shown in Figure 37. Additionally, two indigo structural derivatives lacking H-bonding were studied for comparison: thioindigo and cibalackrot.
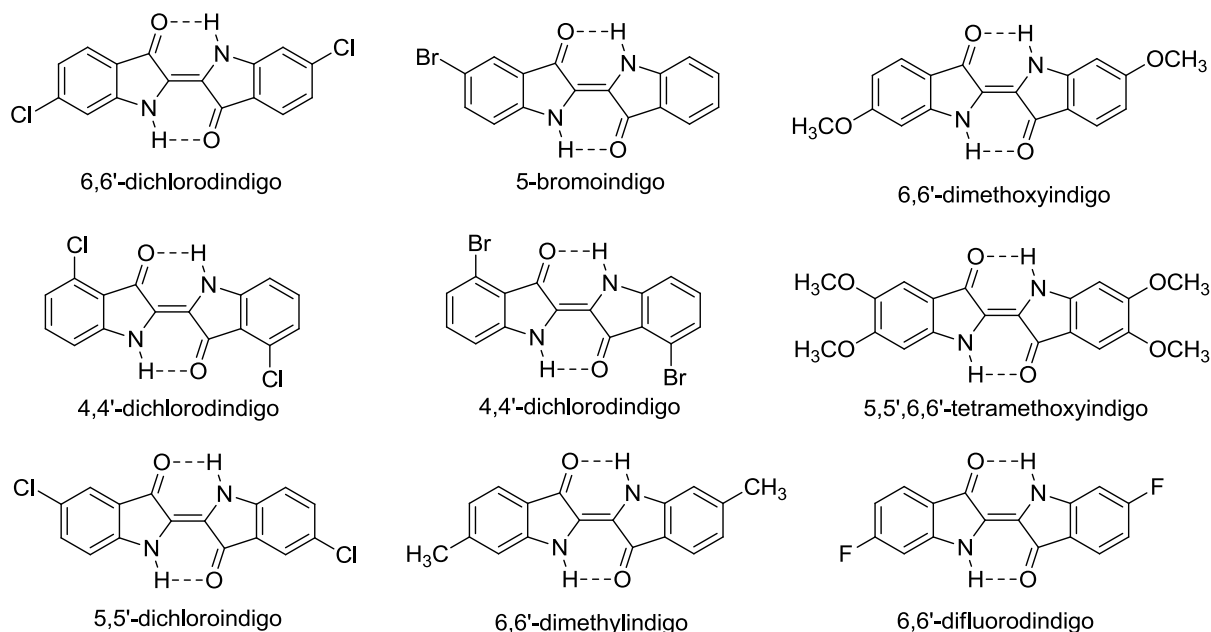

Figure 37. Indigo derivatives synthesized and with crystal structures determined by single-crystal X-ray diffraction

From the single-crystal structure determinations, several conclusions can be drawn about the influence of substituents on the indigo molecule and the resultant solid state structure. Key structural parameters are shown in Table 1: intermolecular N-H—O= H-bond length, interplanar π-π spacing, distance between equivalent atom positions, and space group. The largest group of compounds evaluated contain substituents in the 6,6' positions. All 4,4'-, 5,5'-, and 6,6'- disubstituted derivatives form single intermolecular H-bonds to 4 neighbors, with the interesting exception of 6,6'-dichloroindigo. 6,6'-dichloroindigo adopts a "linear chain" crystal packing, involving the intermolecular H-bonding of each indigo molecule to two neighbors in-plane, as opposed to four. The H-bonding length in these compounds was very similar throughout, between 2.1 – 2.3 Å, and thus similar to unsubstituted indigo. 5,5'-dichloroindigo demonstrated a longer H-bonding distance of 2.39 Å, and thus weaker bond. The 4,4'-substituted compounds, 4,4'-dichloro- and dibromoindigo displayed longer H-bond lengths of 2.82 Å and 3.24 Å, respectively. This is apparently caused by the steric hindrance of the 4,4'-substituents, which cause the parallel chains of stacked indigo molecules to adopt a longer distance between them and a sharper angle, and a longer H-bond length. This effect is predictably larger in the case of the dibromo versus the dichloro compound. In the case of the 5,5',6,6'-tetramethoxyindigo, apparently the steric bulk of the methoxy groups impedes the formation of intermolecular H-bonding completely. All derivatives studied, however, do show apparent π-π spacing, however in contrast to the effects of substituents on H-bonding, there is no obvious pattern for either interplanar π-π spacing distance or interatomic distance along the π-π stacking direction.

Table 1. Summary of results obtained from single crystal X-ray diffraction of different indigo derivatives. *X-ray structure without solution of hydrogen positions.

Compound	Space group	-NH―O= H-bond (Å)	Interplanar π-π spacing (Å)	Interatomic distance (Å)	Ref.
indigo	P21/c	2.12	3.41	5.77	[97]
6,6'-dibromoindigo	P21/c	2.12	3.48	4.84	This work
6,6'-difluoroindigo	P21/c	2.18	3.44	6.03	This work
6,6'-dichloroindigo	P-1	~2.2*	3.41	3.75	[103]
6,6'-dimethylindigo	P21/c	2.30	3.43	4.81	This work
6,6'-dimethoxyindigo	P21/c	2.18	4.41	6.25	This work
5,5'-dichloroindigo	P21/c	2.39	3.18	4.53	This work
4,4'-dichloroindigo	P21/n	2.82	3.46	6.52	This work
4,4'-dibromoindigo	P21/n	3.24	3.22	7.46	This work
5,5',6,6'-tetramethoxyindigo	P42/n	none	3.52	5.88	This work

OFET characterization for all the derivatives is a work in progress. Full characterization was carried out for 5-bromoindigo and 6,6'-dichloroindigo. The optical absorption coefficient of thin films of both compounds in the UV-Vis is shown in Figure 38. 5-bromoindigo forms deep blue films, while the 6,6'-dichloroindigo, consistent with the mesomeric model of Sadler[101], shows hypsochromic absorption relative to indigo, and films appear violet/red. Both compounds demonstrate electrochemical behavior similar to indigo, with two-electron reduction and oxidation Figure 39. In OFETs on TTC/Al$_2$O$_3$, both compounds supported ambipolar transport. Transfer characteristics for 6,6'-dibromoindigo are shown in Figure 40. Silver source/drain contacts were used to afford well-balanced electron and hole channels, where $\mu_e = \mu_h = 0.08$ cm^2/Vs. 6,6'-dibromoindigo demonstrated an 'off' state at ~10 pA that spanned 1-2 V along the V$_g$ axis. This 'off' state is superior to that observed for indigo and tyrian purple, where the channel depleted of one carrier polarity smoothly accumulated with the carriers of opposite polarity. This true 'off' state is advantageous for producing high performance complementary logic circuits. 5-bromoindigo demonstrated a hole mobility of 0.2 cm^2/Vs, while electron mobility remained lower, 0.02 cm^2/Vs (Figure 41). A summary of relevant semiconductor parameters for different indigo derivatives is shown in Table 2.

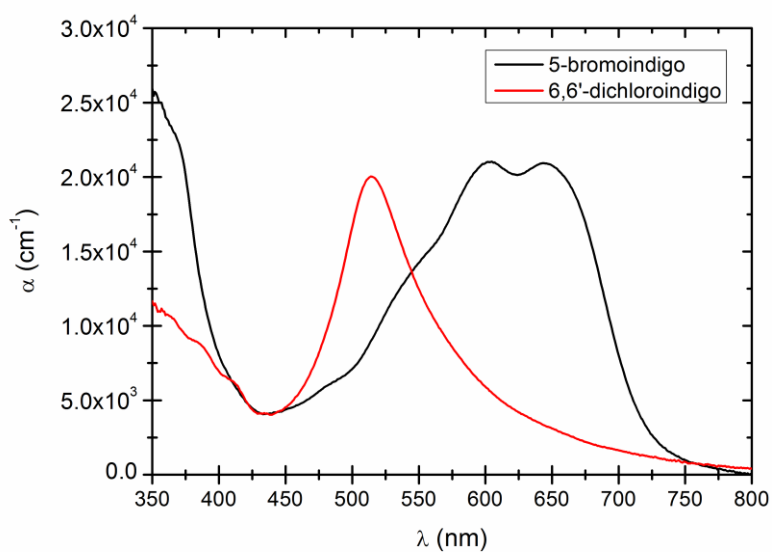**Figure 38.** UV-Vis absorbance spectra of 5-bromoindigo and 6,6'-dichloroindigo evaporated films on glass.
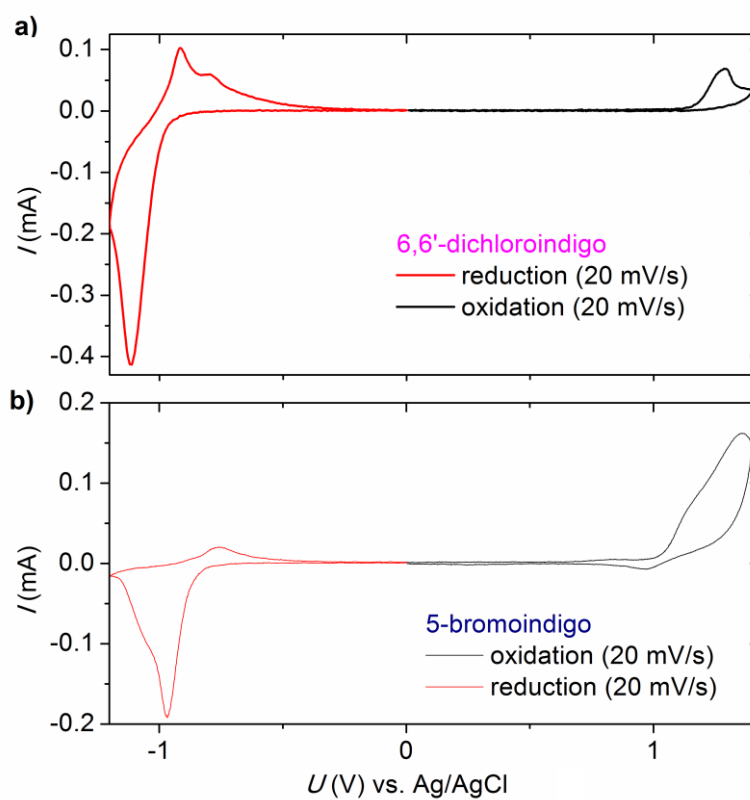

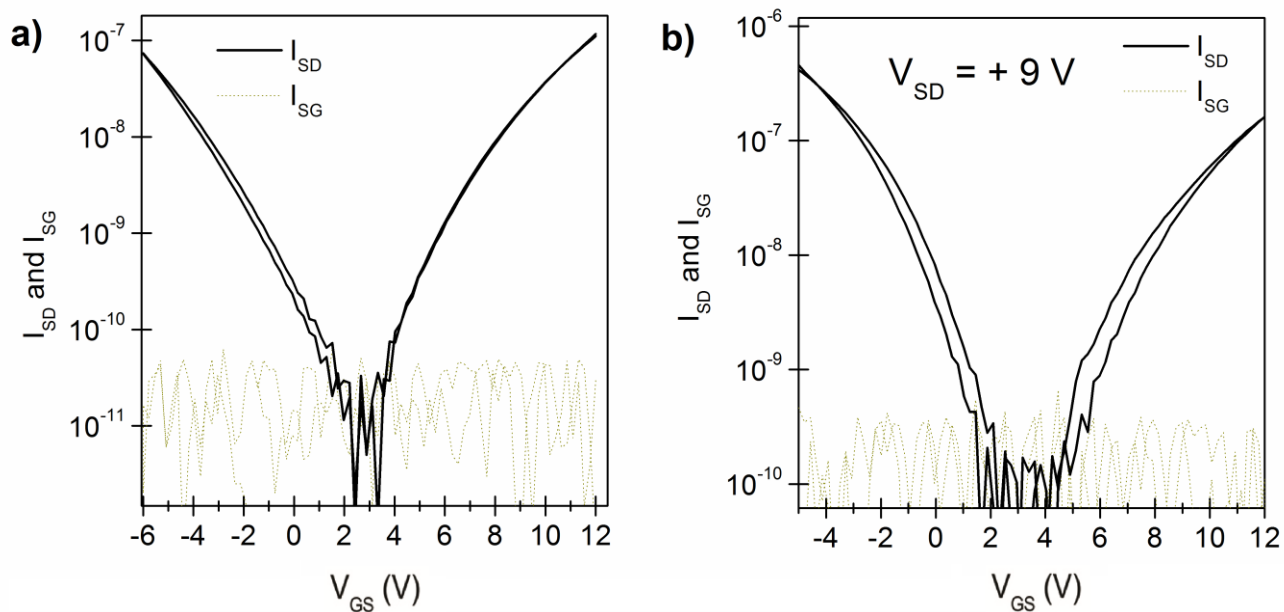**Figure 39.** CV of 6,6'-dichloroindigo and 5-bromoindigo on ITO.

45

Figure 40. a) Transfer characteristics of a 6,6'-dichloroindigo OFET with Ag source/drain contacts. W/L=500 µm / 50µm. b) with Au source/drain contacts.
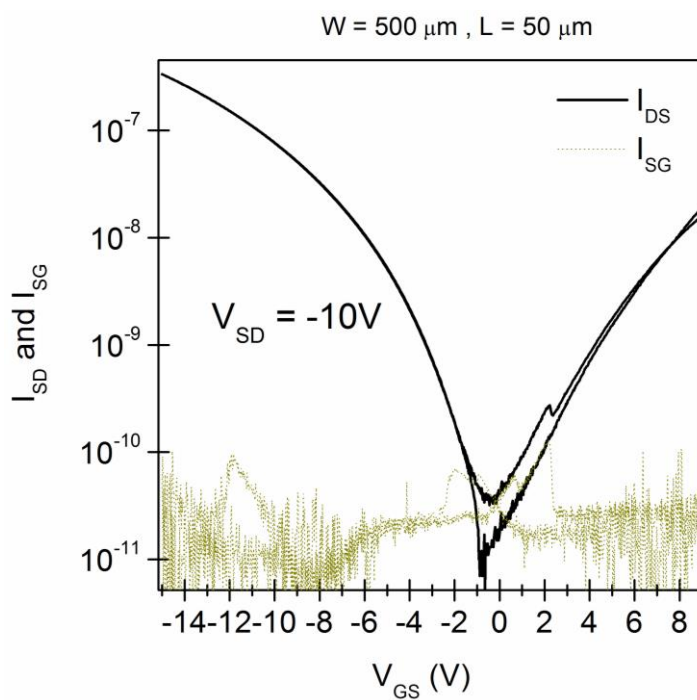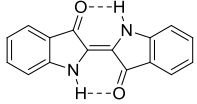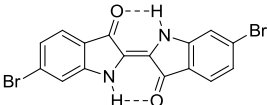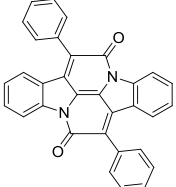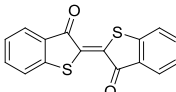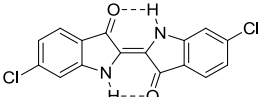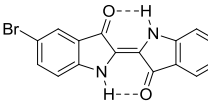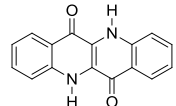
Figure 41. Transfer characteristics for a 5-bromoindigo OFET.

Table 2. Basic organic semiconductor benchmark data for indigo and some of its derivatives

Name	Structure	HOMO (eV)[a]	LUMO (eV)[a]	E_g (eV)[b]	μ_e (cm^2/Vs)	μ_h (cm^2/Vs)	Ref.
Indigo		-5.5	-3.8	1.7	.01	.01	[96]
Tyrian Purple		-5.8	-4.0	1.8	0.4	0.4	[98,104]
Cibalackrot		-5.6	-3.5	2.1	.009	.005	[33]
Thioindigo		-	-	1.9(opt.)	1×10^{-4}	6×10^{-4}	[96]
6,6'-dichlorodindigo		-5.4	-3.6	1.8	0.08	0.08	[105]
5-bromoindigo		-5.4	-3.8	1.6	.02	0.2	[105]
epindolidione		-5.6	-2.9	2.7	-	1.5	[106]

[a] Estimated based on cyclic voltammetry measurements of evaporated thin films [b] Electrochemical band gap, with the exception of thioindigo, where the optical band gap is given.

4. H-bonded acene analogs – Epindolidione and Quinacridone

The impressive charge carrier mobility in indigo and its derivatives was an observation which led me to question how general the "indigo model" of H-bonded molecules forming crystalline structures with a high degree of π-π overlap was. In order to evaluate this concept further, I chose to study the molecules epindolidione and quinacridone (Structures shown in Figure 42a). Epindolidione and quinacridone are H-bonded analogs to the well-known organic semiconductors tetracene and pentacene. A high degree of intramolecular π-conjugation and close intermolecular stacking are considered to be necessary for good charge transport. Epindolidione and Quinacridone low-cost hydrogen-bonded organic molecules primarily used as industrial colorants and widely as toners in inkjet printing (see section 1.4). Though these molecules have limited intramolecular conjugation from the perspective of mesomerism, in the aggregated pigment form they show high carrier mobility up to 1.5 cm^2/Vs in organic field-effect transistors; with on-off ratios up to 5×10^6. The transistors are stable under operation in air without significant degradation for at least 1 year. The work in this section suggests that the approach of maximizing intramolecular π-conjugation may not be requisite for high performance, and that intermolecular hydrogen-bonding may be utilized in the design of air-stable, low-cost organic semiconductors.

Ideally, organic electronic devices can be mass-produced with minimal cost and ecological impact. Synthesis of novel materials with desired properties is the most successful approach towards achieving this goal. In the quest for optimum organic semiconductors, molecular design focuses on planar molecules with sp^2 hybridized carbons to afford π-conjugated systems. Though organic materials are nearly unlimited in chemical design, this focus on maximizing π-conjugation significantly narrows the available molecular library. The pigments presented in this work represent one class of materials that would fall outside of this selection rule.

From the point of view of creating sustainable "green" electronics as outlined in section 1.1, quinacridone pigments are considered non-toxic and safe for cosmetic applications, and are available at low cost. The synthetic pathways used for epindolidione and quinacridone synthesis are simple and safe and do not utilize hazardous reagents. Pigments in the quinacridone class possess carbonyl or amine groups in conjugated segments, and form intermolecularly H-bonded organic solids with high lattice energies. As charge transporting materials, they received little attention. Amine/carbonyl pigment-forming molecules, including quinacridone, were reported to support only very low field-effect charge carrier mobilities in the $1\times10^{-7} - 5\times10^{-4}$ cm^2/Vs range. The devices fabricated in this work based on epindolidione and quinacridone show improved field-effect mobilities between 0.2 and 1.5 cm^2/Vs. These results may stimulate further experimental work to elucidate the potential of intermolecular H-bonding in the design of organic semiconductors and may motivate theoretical and experimental studies of the solid-state structure and charge carrier transport mechanism in such materials.
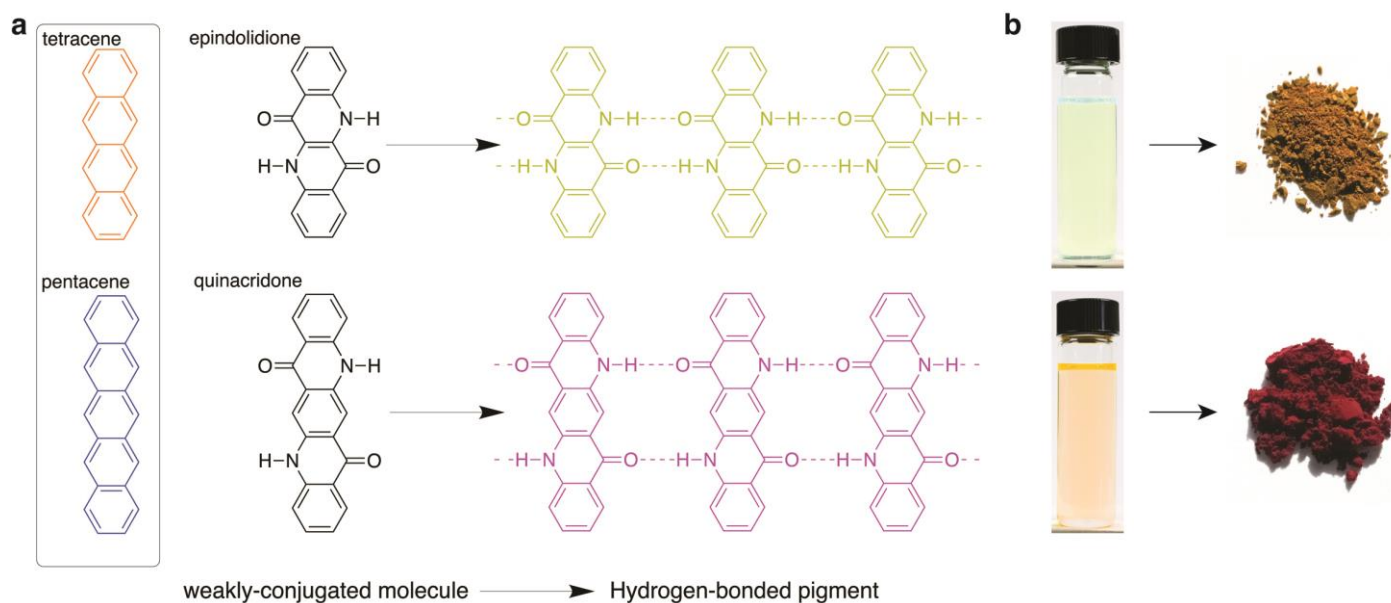
Figure 42. H-bonded pigment analogs of the acenes. a) Chemical structures of the acenes: tetracene and pentacene, and their H-bonded analogs: epindolidione and quinacridone. In the solid state, these molecules aggregate into H-bonded pigment particles, which have markedly different optical properties than the isolated dye molecules. Intermolecular hydrogen bonds between carbonyl groups and amine hydrogens are shown with dashed lines. b) 0.1 mM solutions of epindolidione and quinacridone in dimethylsulfoxide. At this concentration the molecules can be dissolved in some polar solvents. In the true molecularly-dispersed solution, the isolated chromophores are pale yellow. Upon aggregation in the solid state, a bathochromic shift in absorption occurs and they adopt their characteristic pigment colors.

4.1 Optical, electrochemical, and solid state properties of epindolidione and quinacridone

From the perspective of structural mesomerism, resonance structures of molecules like epindolidione and quinacridone containing enol/enolate or imine/imminium character are thermodynamically unfavorable under neutral pH conditions; therefore the carbonyl and amine groups essentially perturb conjugation. It is widely considered in the field of chemistry of organic semiconductors that such functional groups should be avoided. From such a perspective, molecules with carbonyl and amine groups can be regarded as being less conjugated than the acenes. However, these molecules have intermolecular H-bonding between carbonyl and amine groups on adjacent molecules. The molecules strongly aggregate and form pigment particles with markedly different optical properties in comparison to isolated molecules. This shift is illustrated in Figure 42, where solutions of the dyes are shown alongside aggregated solid pigment powders. For example, quinacridone is pale yellow in dilute solution, but adopts colors ranging from red to purple in the aggregated H-bonded pigment form. UV-Vis absorption spectra of epindolidione and quinacridone in dilute solution and thin films are shown in Figure 43a and b, respectively. This behavior of becoming highly-colored only in the aggregated state signals the involvement of strong intermolecular electronic coupling. In order to estimate HOMO and LUMO energies, cyclic voltammetry (CV) and UV-Vis absorption of vacuum-evaporated films of each material were measured. The absorption coefficients of thin films of epindolidione and quinacridone are plotted in Figure 43b. Figure 43c shows the CV scans of epindolidione and quinacridone. The CV measurements demonstrate that both materials support reversible two-electron oxidation and reduction, analogous to the indigo pigments. Such behavior can be rationalized from the presence of two amine groups, which are electron-donating and can be oxidized, and two electron-accepting carbonyl groups, which are electron-accepting. The estimates for energy levels are presented in Table 3.

49
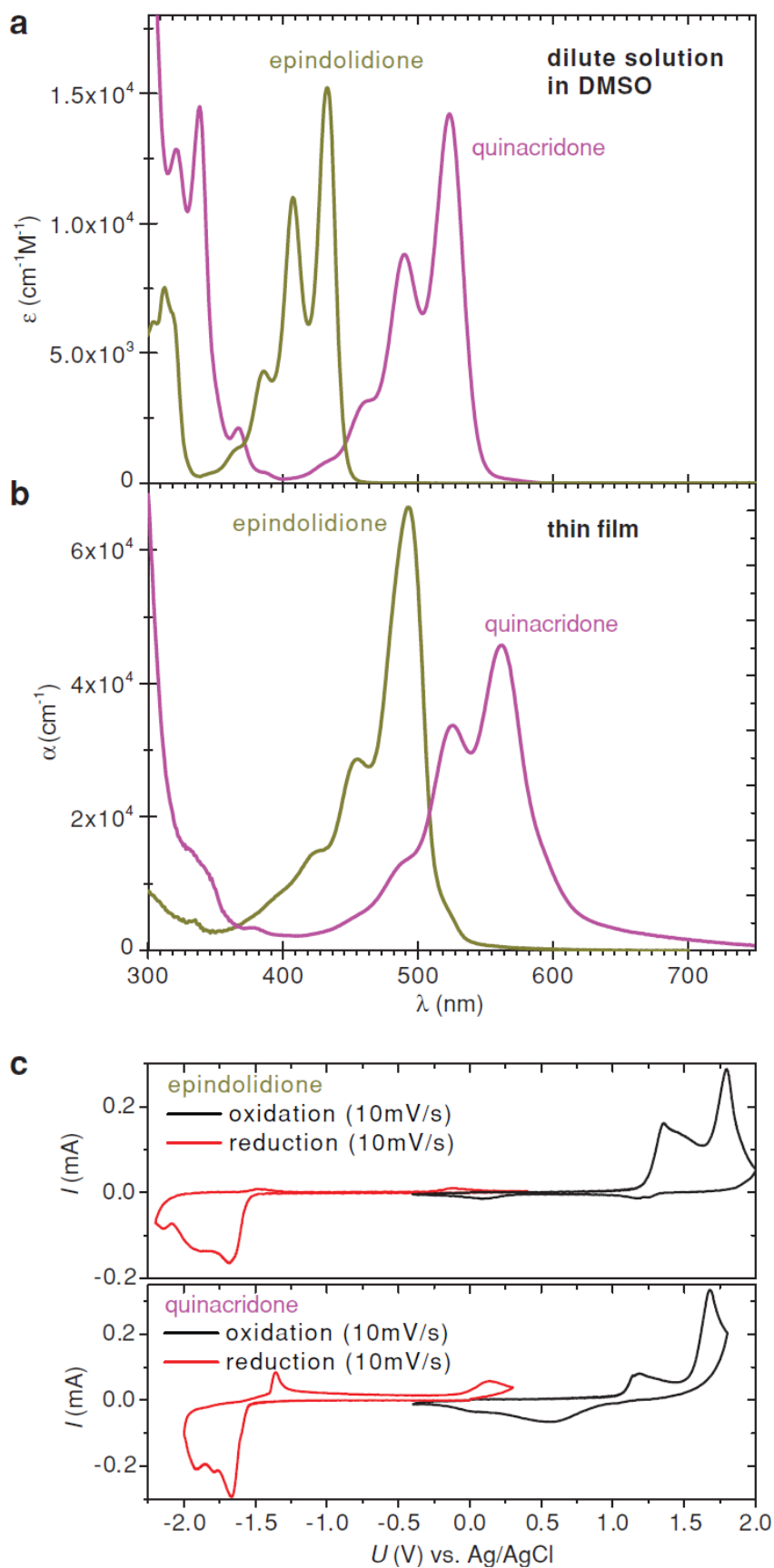
Figure 43. Optical and electrochemical properties of H-bonded pigment films. a) Extinction coefficient, ε, of epindolidione and quinacridone in DMSO solution. b) Absorption coefficient, α, of vacuum-evaporated films of epindolidione and quinacridone. c) Cyclic voltammetry scans for epindolidione and quinacridone thin-films evaporated on ITO functioning as the working electrode. Both materials can be reversibly oxidized and reduced.

50

Table 3. Estimated energy levels, mobilities, and sublimation temperatures of epindolidione and quinacridone and their acene analogs.

Material	HOMO (eV)	LUMO (eV)	E_g, from CV (eV)	E_g, optical (eV)	Hole mobility, μ_h (cm^2/Vs)	Electron mobility, μ_h (cm^2/Vs)	Sublimation temperature, from TGA (°C)
tetracene	- 5.3	- 2.8	2.5	2.3	0.1	N/A	280
epindolidione	- 5.5	- 2.9	2.6	2.4	1.5	N/A	404
pentacene	- 5.4	- 3.3	2.1	1.7	1	0.2	370
quinacridone	- 5.5	- 2.9	2.6	2	0.2	0.01	535

DFT calculations were carried out to better understand the observed properties of the molecules. Details of the DFT calculations are described in the supplementary information of [106]. Relative calculated energy levels are shown in Figure 44. The LUMO levels of the acenes and their H-bonded analogs do not differ significantly. The incorporation of the heteroatoms in the structures of epindolidione and quinacridone results in significantly more-stable HOMO levels relative to the acenes, however. This gives a larger HOMO-LUMO gap and helps to explain the blue-shifted absorption of the H-bonded molecules relative to the acenes; while the deeper HOMO levels correlate with the better air stability. These findings correspond well to the experimental CV data. Due to H-bonding in the solid state, epindolidione or quinacridone molecules can be regarded as mutually protonating and deprotonating one another, leading to a situation where the enol and imine mesomers are more favored. An interesting experimental observation is that quinacridone dissolved in concentrated H_2SO_4 becomes blue/violet, with an absorption spectrum very similar to that of pentacene, indicating that the protonated form indeed features an enol-imminium aromatic backbone. We conducted calculations on the protonated molecules, finding that in the case of epindolidione and quinacridone both HOMO and LUMO levels become more stable and the gap shrinks. This is shown in Figure 44. This suggests that intermolecular H-bonding interactions support mesomeric structures with increased conjugated character. A comparison of the solution spectra of quinacridone in DMSO, in thin film, and in its protonated, fully-aromatic form, is shown in Figure 45. To support charge transport in solid films, organic molecules must demonstrate π-π stacking. It is known that quinacridone and related H-bonded materials such as the indigos discussed in section 3 show relatively tight π-stacking along one crystallographic direction. In all four of the reported polymorphs of quinacridone, the π-stacking distance is found to be ~3.4 Å. Based on the evidence of film color,[54,55] growth temperature [107], and IR absorption [108] we conclude that quinacridone arranges in the β polymorph in the transistors discussed here (Figure 46). The structure of the β-polymorph is shown in Figure 46. In the α[I] and β-polymorphs [55,107], quinacridone molecules form linear H-bonded chains, where each molecule is H-bonded to two neighbors via two H-bonds. This is analogous to the linear chain structure of 6,6'-dichloroindigo (section 3.3). The α[II] [109] and γ-polymorphs [110], in contrast, form a "criss-cross" lattice with each quinacridone molecule H-bonded via single H-bonds to four neighbors, exactly as in the case of indigo and most of its derivatives (section 3). Since it is known that quinacridone adopts tight π-stacking along one crystallographic direction, controlling orientation of molecules in the film is crucial to obtain good transport in a device. For this reason we choose to use low surface energy

hydrophobic gate dielectric surfaces to achieve 'standing up' molecules and thus π-stacking parallel to the gate electrode, perpendicular to the source and drain contacts. From XRD of quinacridone thin films on TTC as well as on glass, we found consistently one peak at 2θ = 6.5°, in the cases of all polymorphs originating from the longest lattice parameter and thus corresponding to the "Standing up" orientation of molecules relative to the substrate (Figure 47). However, based on these out-of-plane XRD results it is impossible to determine which polymorph quinacridone crystallized in on the surface. For the case of epindolidione, the problem is lack of an existing X-ray crystal structure. We were not able to, despite extensive efforts, obtain single crystal X-ray diffraction data for epindolidione. The difficulties in establishing crystal structure in this class of materials have been reviewed.[55,111,112]
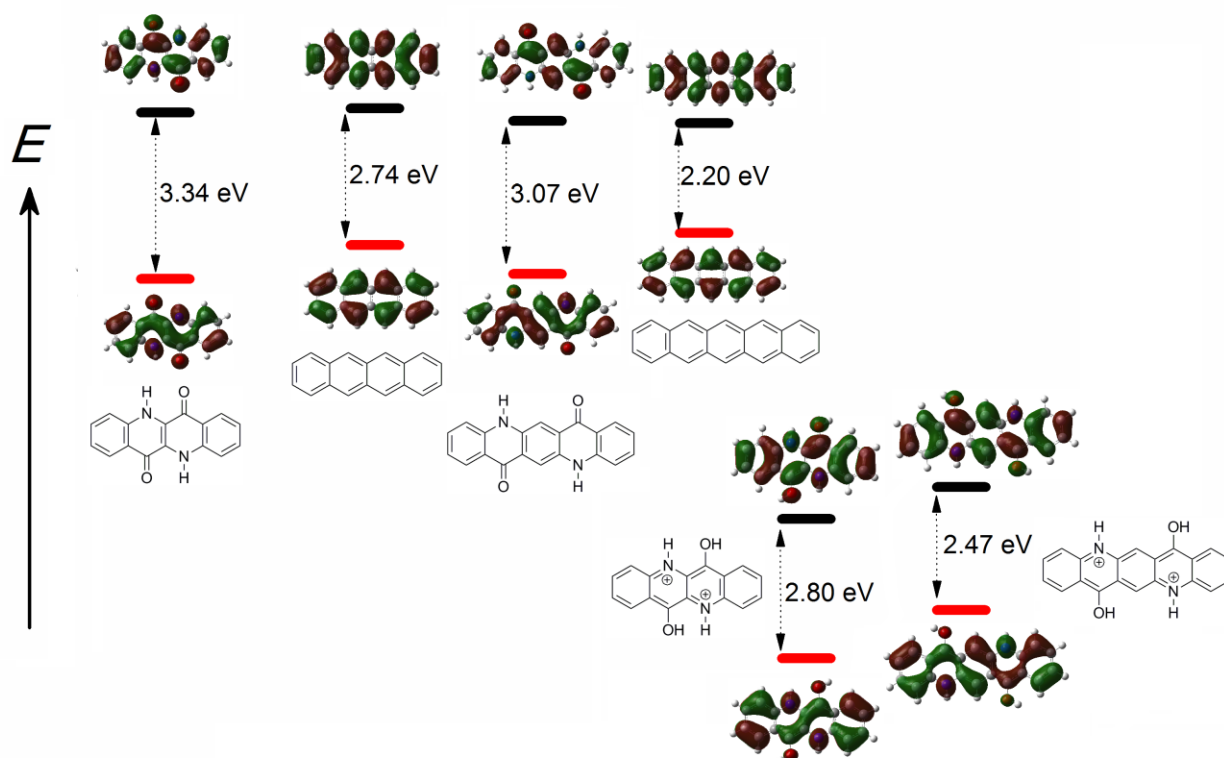
Figure 44. Calculated frontier orbitals and relative energy levels from DFT calculations for tetracene and pentacene compared with epindolidione and quinacridone. Calculations for the protonated epindolidione and quinacridone molecules are shown on the right. Figure originally published in [106].
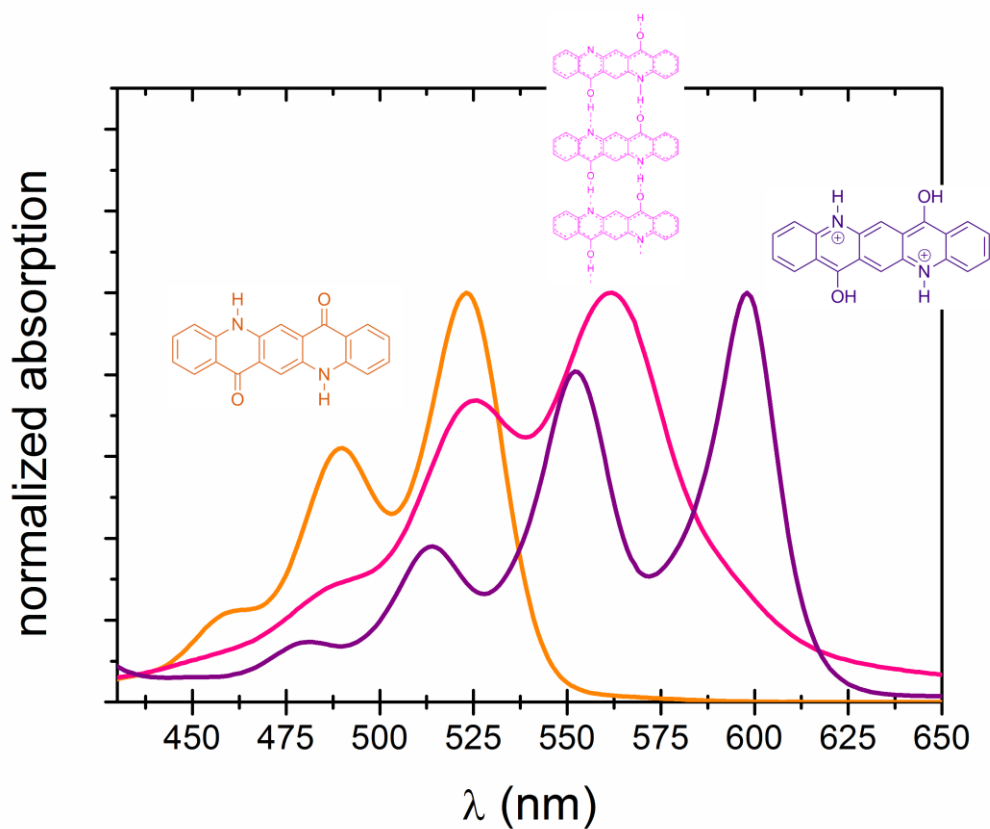
Figure 45. Comparison of quinacridone in DMSO, in its diketo/diamine form, versus the fully-protonated aromatic quinacridone measured in concentrated H_2SO_4 solution. Solid state quinacridone in thin film form demonstrates the same vibrational replica peaks as both solution spectra, suggesting the role of solid state mesomerism in the bathochromic shift from quinacridone in DMSO relative to thin film.
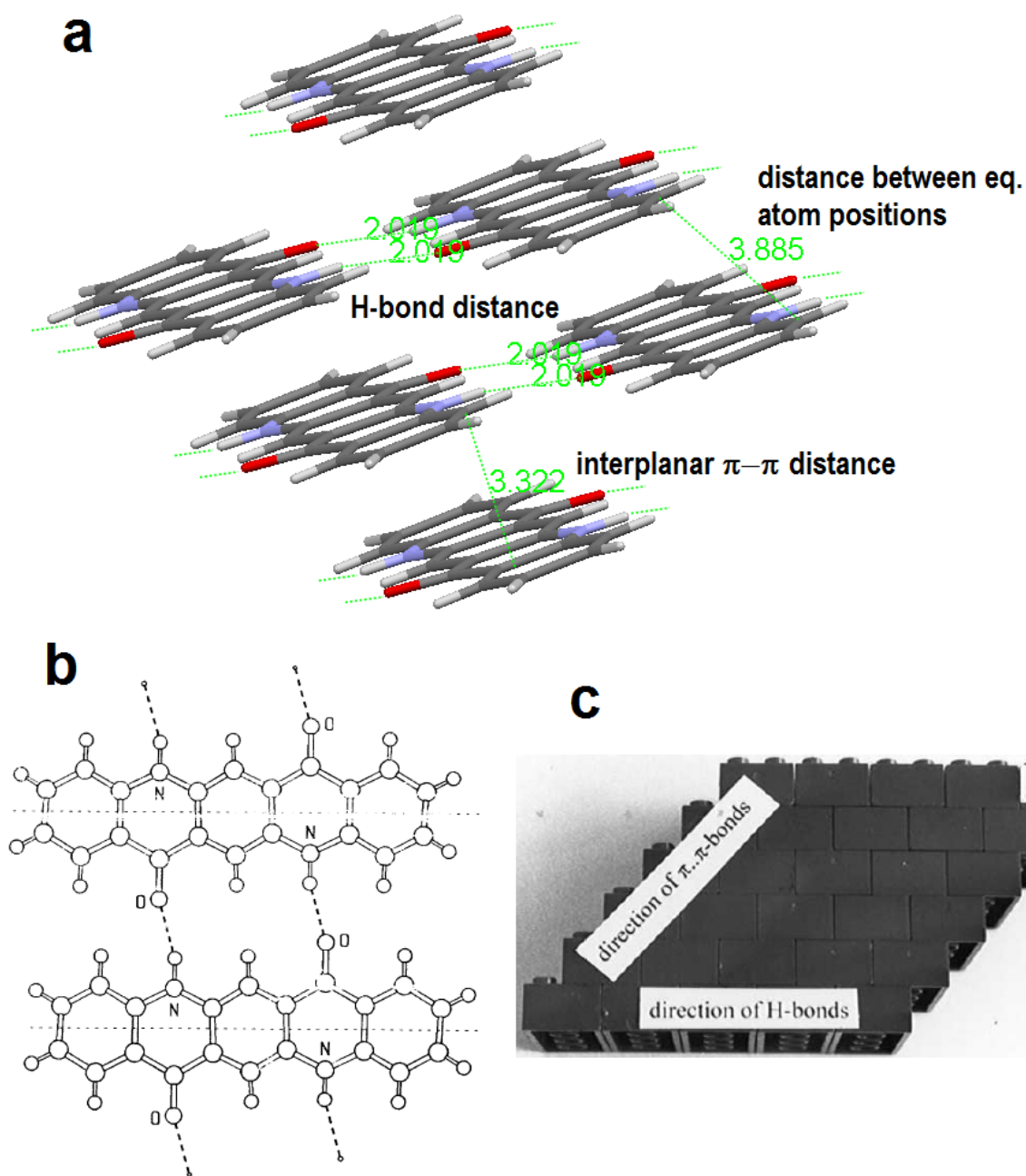
Figure 46. a) Crystal packing in β-quinacridone, which consists of infinite linear chains of H-bonded molecules. This crystal structure was reported by Mizuguchi et al. [107] b) quinacridone H-bonding in the linear-chain polymorphs. c) Schematic illustration of the "bricks-in-a-wall" crystal packing present in many H-bonded pigments, whereby linear chains of H-bonding propagate along one direction, while there is π-π stacking perpendicular to the H-bonding direction. Figure originally published in [113].
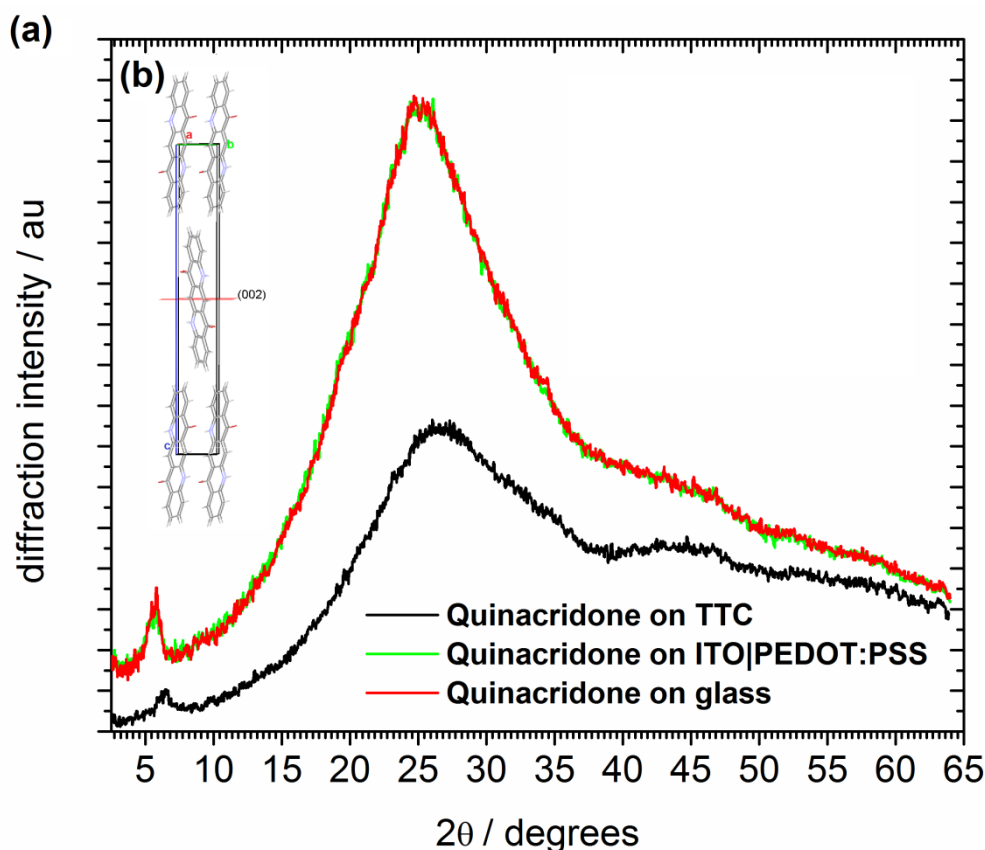
Figure 47. (a) XRD of quinacridone thin films. The broad amorphous peak is originating from the glass substrate. (b) A packing diagram of quinacridone in the β phase with the [002] plane shown, which corresponds to the diffraction peak at $2\theta = 6.5°$. Figure original published in [114].

Extensive π-π stacking and intermolecular H-bonding interplay to afford a high crystal lattive energy in quinacridone-type pigments. To compare the strength of intermolecular interactions in the van der Waals acenes versus the H-bonded analogs we conducted thermogravimetric analysis (TGA). Epindolidione and quinacridone sublimed at 400 °C and 535 °C, respectively, versus 280°C and 370°C for tetracene and pentacene. The difference in molecular weight between the acenes and their analogous H-bonded molecules is insignificant, but the sublimation temperature is much higher for the materials with strong intermolecular interactions. The TGA measurement details and results are shown in Figure 48.
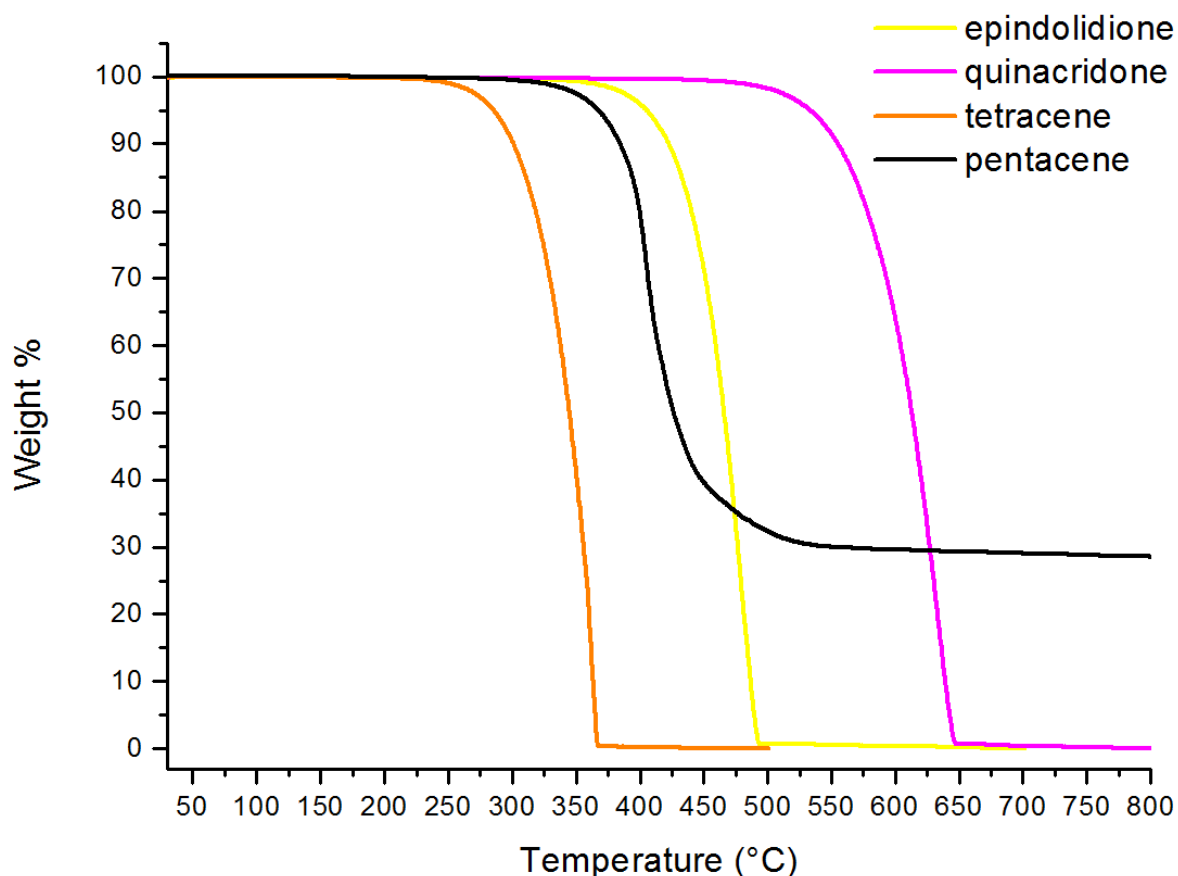
Figure 48. Thermogravimetric analyses (TGA) for the two acenes and their corresponding H-bonded analogs. TGA scans were performed under a nitrogen atmosphere (flow of 40 mL min^{-1}) with a Perkin-Elmer Pyris 6 TGA in the range from 30 to 800 °C with a heating rate of 10 °C min^{-1}. All materials sublimed cleanly without leaving charred residue, with the exception of pentacene, which leaves about 30% charred material. This behaviour has been reported before for pentacene by Bao and coworkers.[115] Figure original published in [106].

4.2 OFET devices and circuits with H-bonded pigments compared with acene semiconductors

In order to compare the acenes, tetracene and pentacene, with their H-bonded analogs: epindolidione and quinacridone, OFETs devices were prepared "side-by-side" using identical processing techniques and device architectures. OFET devices were fabricated using a bottom gate / top contact configuration, with channel dimensions of W/L = 5 mm / 40 μm. Electrochemically-grown Al_2O_3 (32 nm) passivated by vacuum-evaporated tetratetracontane, ($C_{44}H_{90}$, TTC) served as the gate dielectric. Some H-bonded pigments have been previously tested in OFET configurations on SiO_2 gate dielectrics and the resulting mobilities were poor, in the range 1×10^{-7} - 5×10^{-4} cm^2/Vs.[116,117] We have found that the low surface energy of the aliphatic TTC is critical for the growth orientation of the H-bonded molecules, providing π-stacking parallel to the gate electrode and therefore high mobilities. The influence of TTC as a surface energy-lowering passivation layer is discussed in section 2.4. The mobility values are summarized in Table 3. All devices were stored and measured in ambient air under standard laboratory fluorescent lamp lighting unless otherwise noted. With gold source and drain electrodes, pentacene showed characteristic performance with hole mobilities of ~1 cm^2/Vs and electron mobilities of 0.2 cm^2/Vs (the latter measured only in N_2 atmosphere). Tetracene likewise afforded mobilities consistent with literature reports, approx. 0.1 cm^2/Vs

for holes. The transfer and output characteristics of these 'standard' devices are shown in Figure 49. Epindolidione OFET transfer curves measured in air on day 1 and on day 100 are shown in Figure 50a and Figure 50c, respectively. Output characteristics are shown in Figure 51a. This material demonstrated mobilities in the range of $0.9 - 1.5$ cm^2/Vs for holes, and was thus on par with pentacene. With on/off ratio of $\sim10^7$ and negligible hysteresis these devices are superior to the pentacene OFETs that we fabricated.
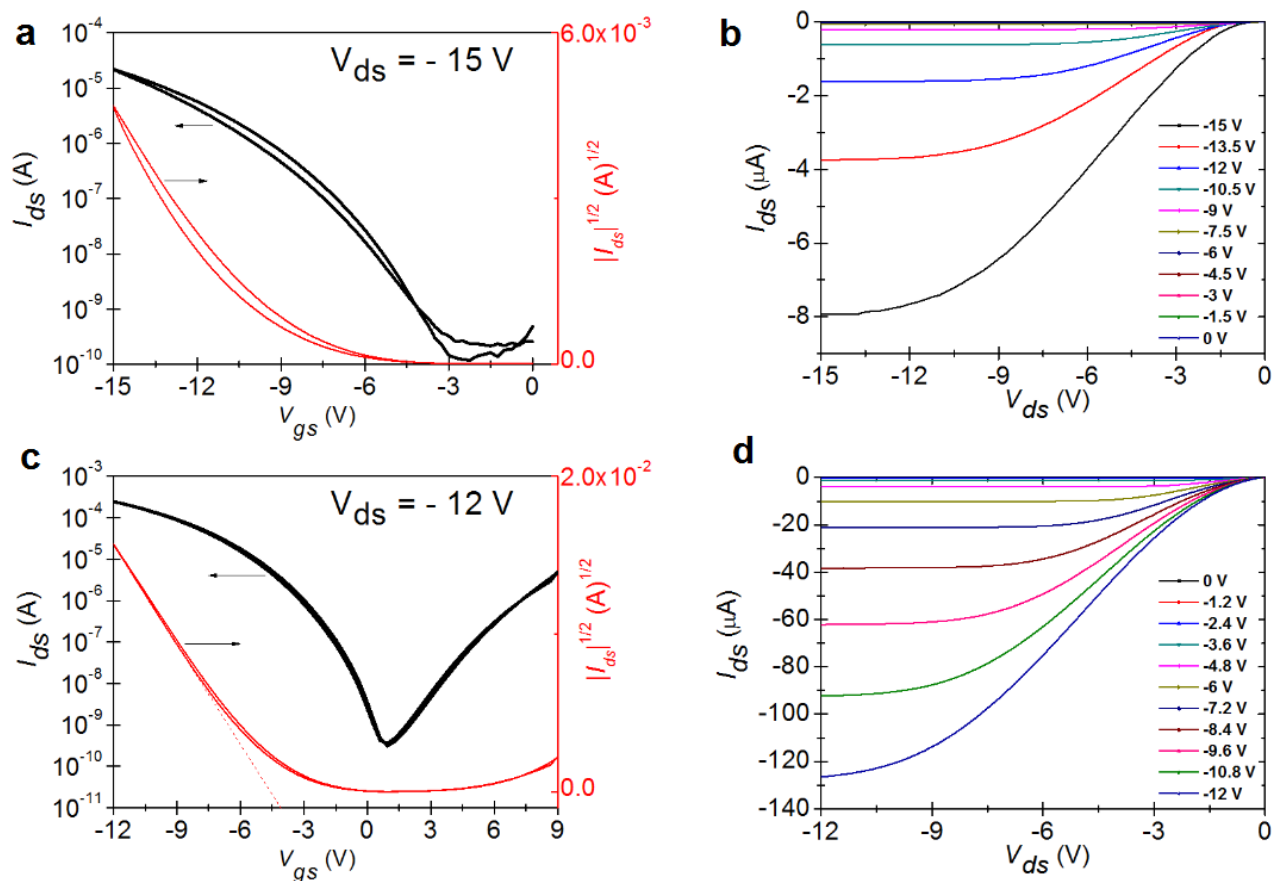

Figure 49. Tetracene and pentacene OFETs. Tetracene and pentacene OFETs were measured alongside the H-bonded pigments as a point of reference. All devices were fabricated using Al_2O_3/TTC composite gate dielectric with a C_{0d} of ~70 nF/cm^2. a) Transfer characteristics for a tetracene OFET. b) Output characteristics for the same device. c) Transfer characteristics for a pentacene OFET measured under N_2 atmosphere, showing ambipolarity. d) p-channel output characteristics for the same device. Figure originally published in [106].

The devices demonstrated air stability with on/off ratio and threshold voltage changing minimally after 100 days. Transfer characteristics for quinacridone OFETs measured in air on day 1 and on day 100 are shown in Figure 50b and Figure 50d, respectively. Output characteristics are shown in Figure 51b. Quinacridone afforded a hole mobility of 0.2 cm^2/Vs. The operational stability in air was comparably impressive, with threshold voltage remaining stable. The devices, however, showed a decline in on/off ratio. The origin of this is not clear, however the photoinduced processes described in more detail in section 5.4 may play a role. The mobility and On/Off ratio values for the OFETs as a function of time are shown in Figure 50e,f. These are the averaged results of a 140-day stability study where a dozen transistors of each material were stored and measured in air. It was found that the H-bonded materials show excellent operational stability relative to their acene counterparts. While both pentacene and tetracene hole mobility and on/off ratio each deteriorate by two orders of magnitude after several days in air, these values for epindolidione and quinacridone degrade by $\sim20\%$ over the time period of 140 days. Epindolidione mobility degrades with a T_{80} lifetime (time to

decay to 80% of the initial value) of ~85 days, whereas quinacridone demonstrates T_{80} of ~115 days. Figure 52 shows a summary of T_{80} values versus mobility for a number of hole-transporting materials in OFET devices reported between 2008-2012 with epindolidione and quinacridone shown for comparison. The H-bonded pigments compare favorably with stability studies of state-of-the-art 'air-stable' p-type devices. We have not conducted stability studies for n-channel operation, which, due to the high-lying LUMO level should not be possible in air for epindolidione and quinacridone. Appropriate synthetic modification of derivatives, according to recent progress in designing air-stable electron-transporting materials, may result in stable ambipolar transport.
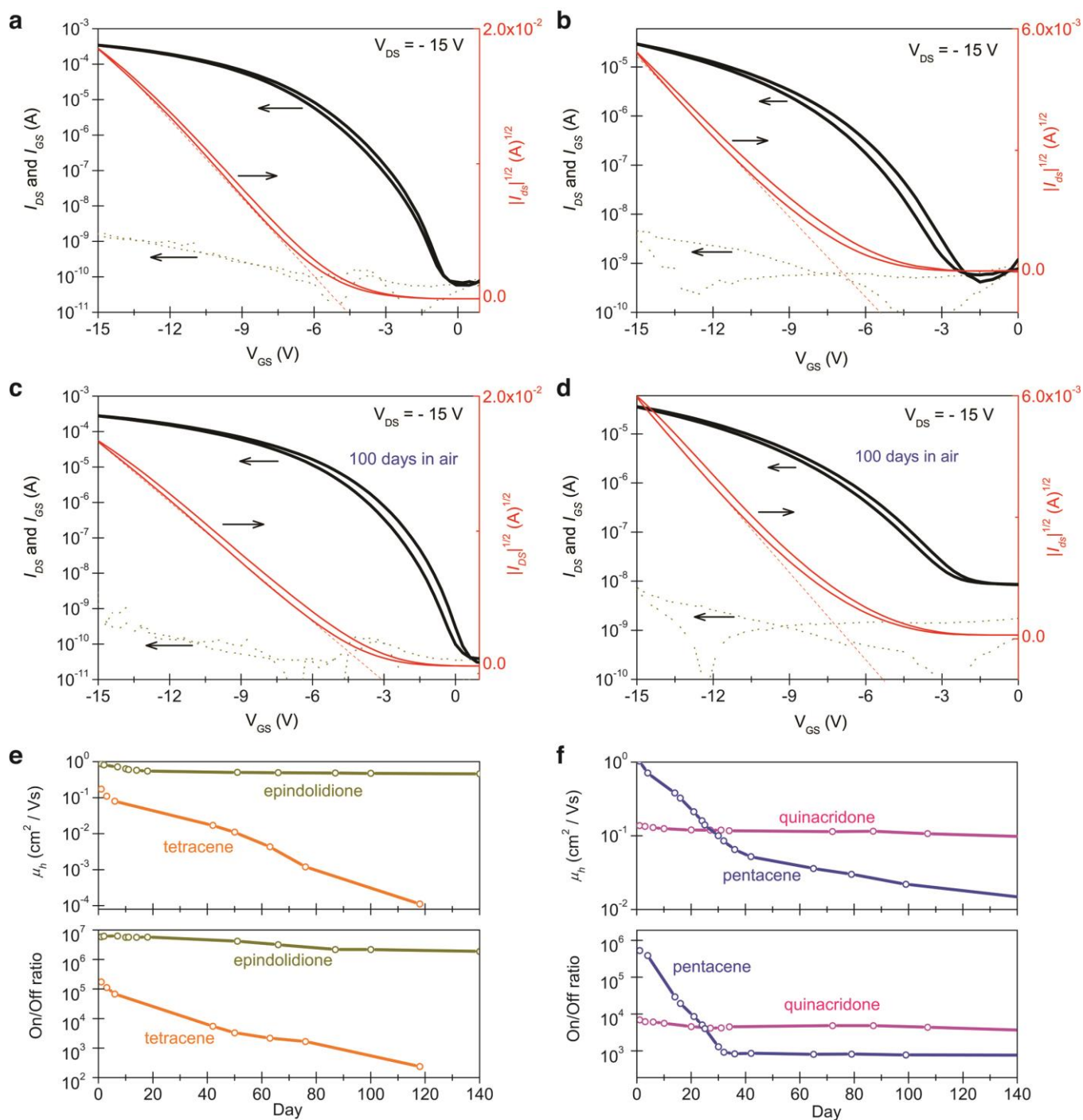
Figure 50. H-bonded pigment organic field-effect transistors. a) transfer characteristics of an epindolidione OFET measured in air, (c) transfer characteristics measured after 100 days in air for the same device. b) transfer characteristics of a quinacridone OFET measured in air, (d) transfer characteristics measured after 100 days in

air for the same device. e) Comparison of mobility and on/off ratio of epindolidione and tetracene OFETs stored and measured in air over 140 days. f) Mobility and on/off ratio of quinacridone and pentacene OFETs measured over the same period.
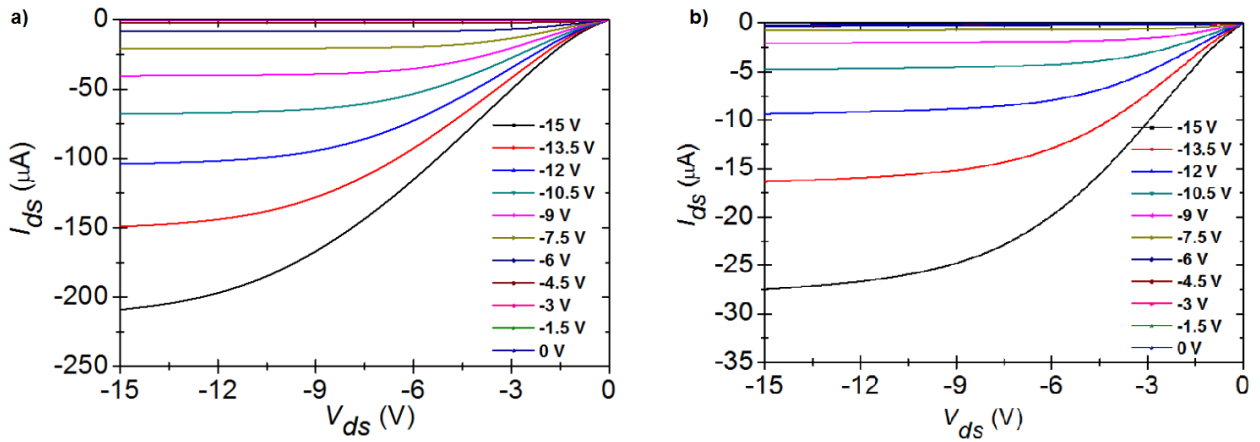
Figure 51. Output characteristics for an epindolidione OFET (a), and a quinacridone OFET (b).
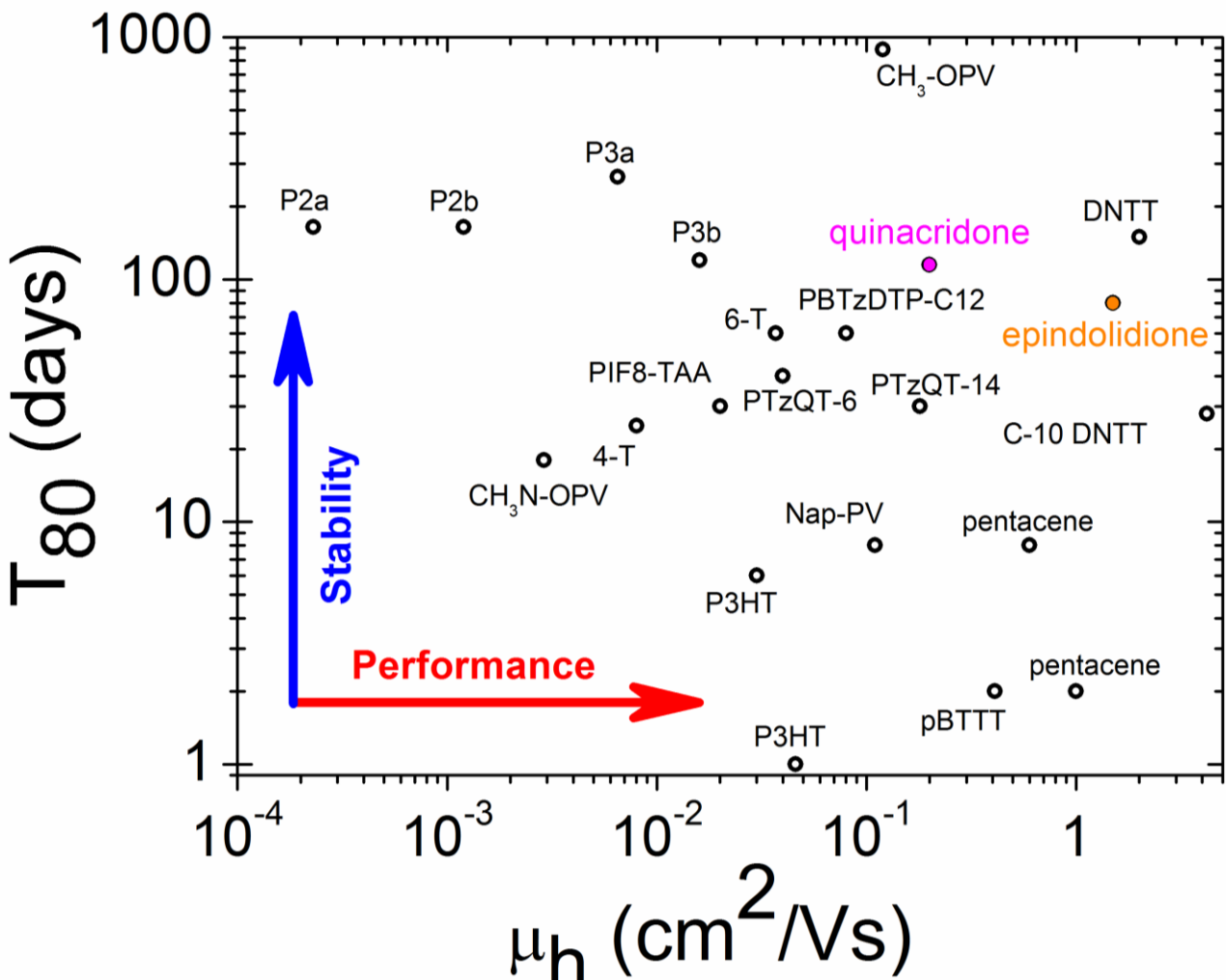
Figure 52. Plot of T_{80} lifetime (time for mobility to degrade to 80% of the initial value) versus initial mobility for a number of reported hole-transporting materials measured in air. Figure original published in [106], where literature references of the materials shown in this plot can also be found.

To rationalize the difference in mobility between epindolidione and quinacridone we speculate that crystallite grain size, *i.e.* intergrain resistance, may play the limiting role. From atomic-force microscopy (AFM), we consistently found that epindolidione films were composed of grains of significantly larger size than quinacridone. AFM scans of both materials deposited on Al_2O_3/TTC are shown in Figure 53a,b. Quinacridone films consisted of rod-shaped crystallites 100-200 nm in size. Epindolidione crystallites, in contrast, were larger, being 400-1000 nm in size. With bigger crystallites, the decrease in the number of grain boundaries may account for the higher observed mobility in epindolidione OFETs. The morphology of the H-bonded pigment crystallites shown here is similar to what was found in the derivatives of indigo (section 3).

We found that quinacridone, like the structurally-related indigoids, supports ambipolar transport. In N_2 environment, with silver source/drain contacts, quinacridone demonstrates ambipolar transport with effective carrier mobility of ~0.01 cm^2/Vs for both carriers. Transfer characteristics of quinacridone OFETs with Ag source-drain contacts is shown in Figure 54. Due to this well-balanced ambipolarity, CMOS-like voltage inverter circuits were measured, demonstrating competitive gains in the 100-200 range (Figure 55).

Figure 53. AFM images for H-bonded pigment films in OFETs. a) 40 nm of epindolidione on Al_2O_3/TTC, and (b) 40 nm of quinacridone on Al_2O_3/TTC. Scale bar = 500 nm.

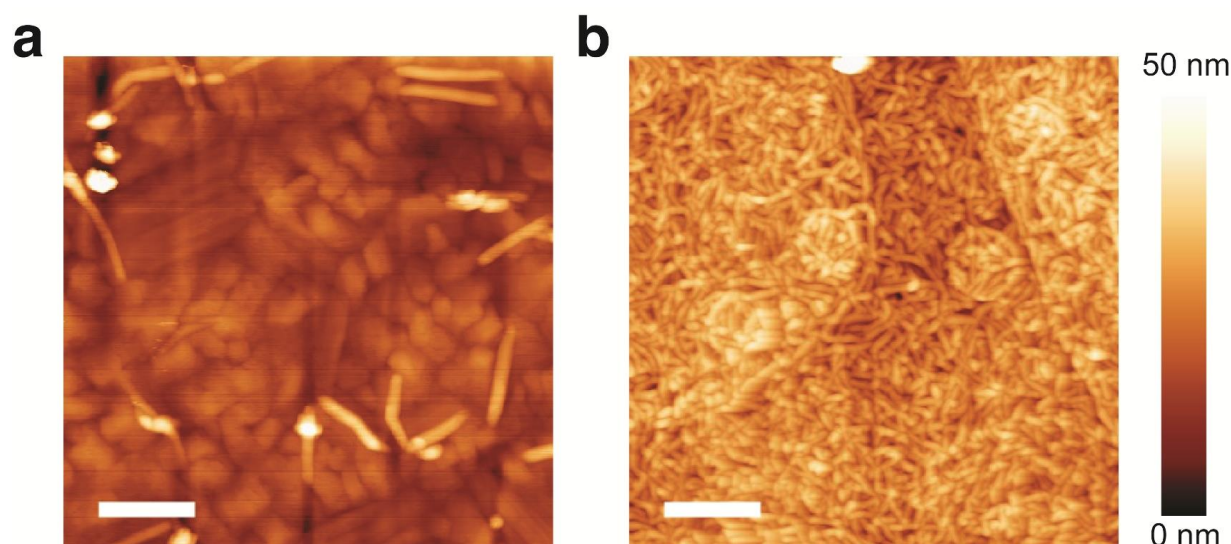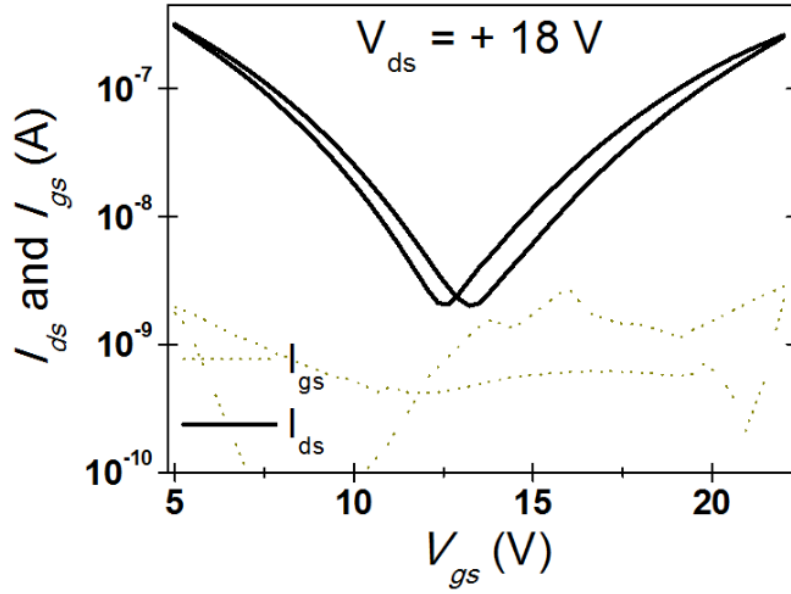**Figure 54.** Transfer characteristics for an ambipolar quinacridone OFET. Silver source/drain electrodes were utilized to support injection of both carriers, the device was measured under N_2.
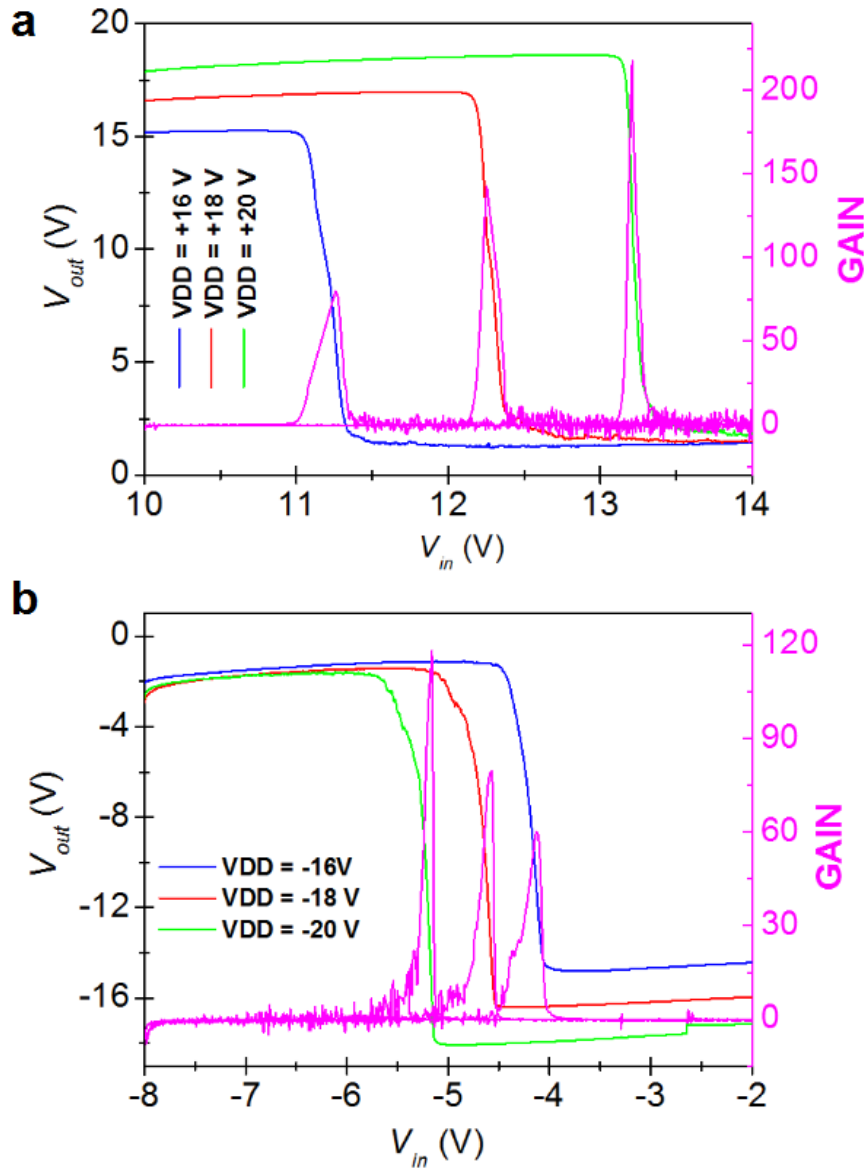
Figure 55. Quinacridone inverter. Quasi steady-state output characteristics for a voltage inverter based on ambipolar quinacridone OFETs shown in the first quadrant, (a) and the third quadrant, (b).

This study compares two of the most well-known organic semiconductors to their H-bonded analogs. The results suggest that intermolecular H-bonded pigments support air stable charge carrier transport with high mobility. The devices initially published in [106] were measured in May 2013 and found to still retain a mobility of 0.7 cm^2/Vs after 325 days in air. As in the case of other indigo derivatives, the polycrystalline nature of the film and intergrain resistance is believed to be the primary limitation in measuring higher mobilities. Nevertheless, epindolidione is currently one of the best OFET materials reported in terms of performance and stability. In terms of molecular design of organic semiconducting materials, epindolidione represents a potentially useful bridge between indigos and linear fused-ring semiconducting materials.

By demonstrating air-stability and good electronic performance, I propose that such H-bonded pigments could be an interesting new paradigm for organic semiconductor design, as these molecules structurally fall outside of what is normally considered for organic semiconductors. Perhaps the same materials used in printer inks and hair-dyes can be used to fabricate future electronic technologies.

5. Photophysics of H-bonded pigments and optoelectronic devices based on them

5.1 Photophysics of indigos

Indigo has always been intriguing due to its brilliant blue color, indeed it is the only naturally-available blue organic dye with sufficient stability for practical applications. This explains the ubiquity of indigo as a dye throughout history. An important consideration about indigo optical properties is that indigo forms H-bonded pigment aggregates. Indigo in the pigment form demonstrates excellent light-fastness and stability, in solution however under the influence of ozone and hydroxyl radicals it will slowly oxidize, into the yellow-colored isatin, anthranilic acid.[118] Both compounds are considered nontoxic and are present in nature as well. These are important considerations when discussing indigo and its derivatives for disposable use-and-throw electronics applications or biointegratable devices.

Indigo undergoes a pronounced bathochromic shift of 50-60 nm in absorbance when going from isolated molecules in dilute solutions to aggregates. Indigo can be dissolved in some solvents such as chloroform and DMSO with a maximum concentration of about 100 μM. In such solutions the absorbance peak occurs at around 600 nm ($\lambda_{\text{max tetrachloroethane}}$ = 605 nm, ε = 16,580).[100] Solvatochromic effects have also been reported. Increasing of solvent dielectric constant leads to bathochromic shift in absorbance, which has been interpreted as resulting from the improved stability of charge-separated resonance forms featuring C$^+$—O$^-$, for example.[100,101,119] Colloidal particles dispersed in water [120] or evaporated thin films [121] show absorbance maxima around 650 nm. Highly-crystalline thin films have even further shifted absorbance around 700 nm.[122] This is consistent with our findings: the UV-Vis absorbance of Indigo in chloroform and in thin-film form is compared in figure 5b. The extent of the bathochromic shift of isolated molecules relative to solid state has been correlated with intermolecular H-bonding. Indigo with substituents in the 4,4' and 7,7' positions, causing steric blocking of intermolecular H-bonding, indeed show no bathochromic shift in absorbance when comparing solid state with solution.[120] Theoretical calculations support that intermolecular H-bonding lowers the energy of the LUMO and is responsible for the bathochromic shifts observed experimentally.[123,124] The key question about the optics of indigo is: Why is it blue? It is surprising that such a small molecule can have a

chromophore absorbing at such low energies. Much experimental and early theoretical work was done by Lüttke and coworkers in the 1960s.[125] They adopted the approach of "stripping down" the indigo molecule, selectively removing the phenyl rings and other components and observing the changes in optical behavior. Their work ultimately concluded that the primary chromophore in indigoids is what they called the "H-chromophore", a cross-conjugated system of two electron-donors, such as NH groups, and acceptors: two carbonyl groups, Figure 56a. Modern DFT calculations confirm this picture, where light absorption results in a transfer of electron density from the donor amines to acceptor carbonyl groups. This transfer of electron density increases the acidity of the NH protons and the basicity of the carbonyl groups.[123,124] One of the most well-known properties of indigos is that they are not luminescent, with fluorescence yield values $\varphi_f \sim 1 \times 10^{-3}$.[126–129] Instead, rapid internal conversion occurs with yields of >0.99, which is thought to be the reason for the exceptional photochemical stability of indigo. There is some controversy concerning the mechanism responsible for this rapid and efficient internal conversion. The theory that is supported by the largest body of experimental evidence is that ultrafast proton transfer occurs in the indigo excited singlet state, leading to a tautomerism of the *keto* form to the *enol* form. The *enol* form then rapidly interconverts back to the more stable keto form, thereby dissipating the energy of the photoexcitation. This process is illustrated in Figure 56. The theory of excited state deactivation via ultrafast proton transfer is supported by several experimental studies.[126,128] Some studies have concluded that single proton transfer occurs, instead of the concerted double-proton transfer leading to *keto-enol* tauromerism.[130,131] In all cases, however, deactiviation of the excited state is attributed to proton transfer. However at least one experimental study concluded that the evidence for proton transfer is lacking.[132] When the –NH protons are eliminated, by attaching substituents like methyl groups, what is found is that fluorescence increases and competes with photochemical *trans-cis* isomerism, with the latter as the dominant mechanism, Figure 56c.[133–136] Photoisomerism is accompanied by a significant change in molecular geometry. This photomechanical effect can be exploited in light crystal optoelectronics as a switch[137] and in light-responsive membranes[138]. Photoisomerism is normally prevented in indigo due to strong intramolecular H-bonding between –NH protons and the carbonyl groups. An interesting consideration, then, is to eliminate the protons responsible for excited state deactivation, but also to "lock" the indigo in the *trans* configuration using a covalently-bound bridge. One such compound is Cibalackrot, a derivative of indigo first reported in 1914.[139] Cibalackrot was reported to have a φ_f of 0.93[136] in methylcyclohexane and 0.76 in dioxane.[140]

We synthesized Cibalackrot via condensation of indigo with phenylacetyl chloride (Figure 56d) according to [139] and fabricated transistors and diodes with the material. The electrochemistry of cibalackrot is very similar to that of indigo, with two-electron reduction and two-electron oxidations present. Transistors are similarly ambipolar, though mobility remained low, in the 1×10^{-3} cm^2/Vs range. Diodes could be fabricated as well, and upon charge injection in forward bias red electroluminescence was observed, in contrast to indigo diodes which emitted no light.[33] The high fluorescence yield, combined with ambipolar transport, recommend cibalackrot as an interesting building block for electroluminescent or light harvesting device applications. Since cibalackrot, as it lacks H-bonding, falls outside of the topic of this dissertation, these results will not be shown here but can be found in the publication [33].
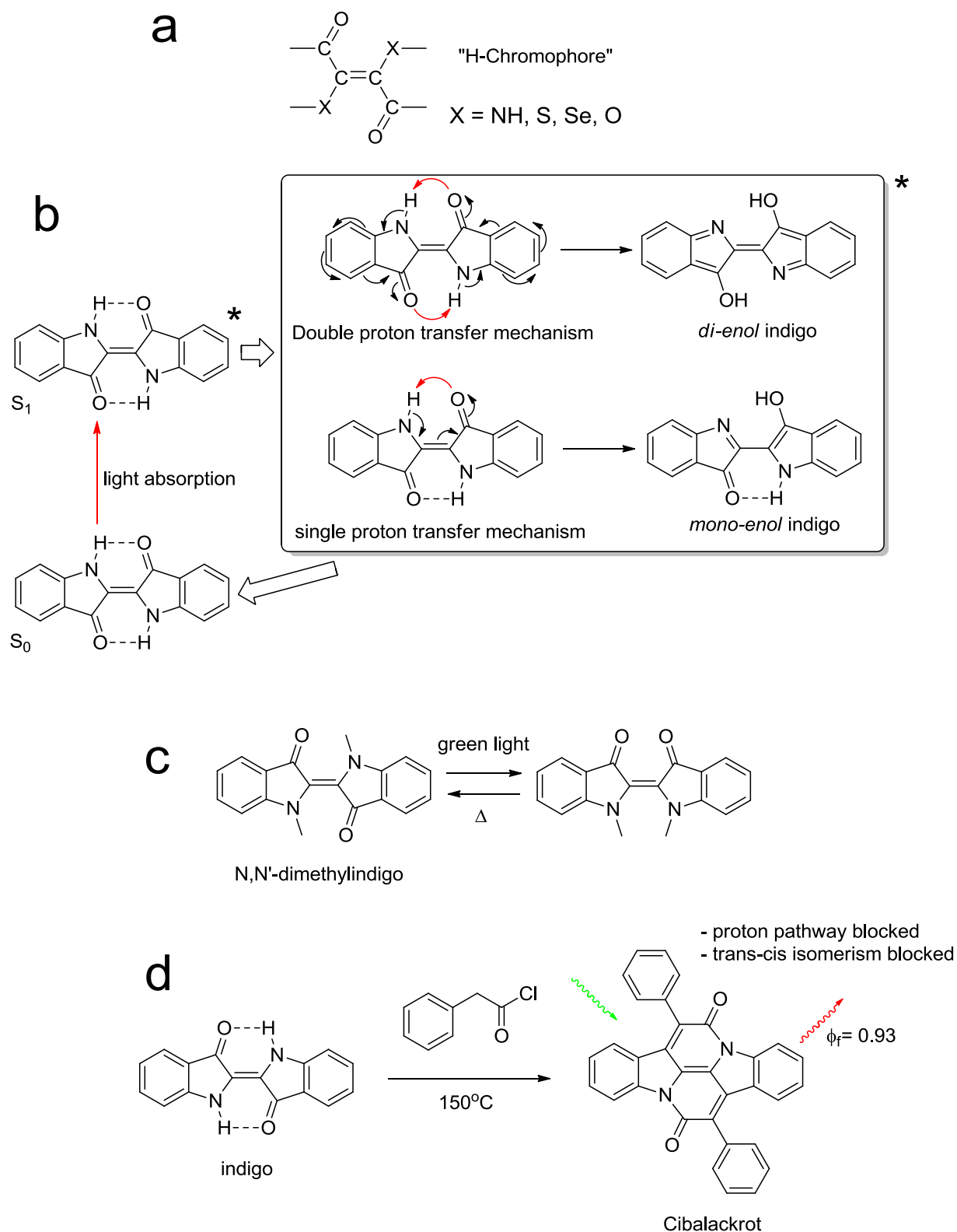
Figure 56. Photophysics of indigos. a) The "H-chromophore", responsible for the low-energy absorption of indigo, consisting of a cross-conjugated system of electron donor units, X, and carbonyl group acceptors. b) Indigo is well-known for its low fluorescence yield and rapid internal conversion. The internal conversion pathway is attributed to ultrafast proton transfer. Two models involving a *keto-enol* tautomerism with one- or two-proton transfer exist. c) exchanging the –NH protons for other substituents, such as methyl groups, yields a molecule which readily undergoes reversible *trans-cis* isomerism as the dominant photophyscal process. d) Removing protons and blocking possible photoisomerization, as in the case of the Cibalackrot molecule, yields in turn a molecule with highly efficient fluorescence.

5.2 Verifying excited state proton transfer in indigo

The high fluorescence yield in the compound cibalackrot is evidence supporting the notion that the proton may play a critical role in the nonradiative processes that deactivate the excited state of indigo. We endeavored to test the hypothesis of excited-state proton transfer that has been proposed in the literature by selectively replacing the N-H protons with deuterons. This isotope exchange technique is a well-known technique for discriminating mechanisms in which protons play a role. If proton transfer is responsible for excited state deactivation in indigo, replacing these protons with heavier deuterons should slow down this process. This should be reflected in the enhanced fluorescence of indigo. The deuterization reaction to produce *N,N'*-dideuteroindigo is shown in Figure 57. To obtain the deuterated indigo, a "deuterated vat" of indigo was produced via reduction of indigo using sodium dithionite in a 1M NaOH/D_2O solution under dry N_2 conditions. The deuterated leuco indigo was then oxidized to the insoluble indigo bubbling dry air through the solution. The suspension was then centrifuged and supernatant poured away. The sediment was washed with D_2O and centrifuged repeatedly until the supernatant was neutral. The product was then collected and dried and finally purified by sublimation. This procedure reliably led to ≈50% deuteration, as calculated from ^{1}H NMR (Figure 58). The stability of deuterated indigo was verified by FT-IR spectroscopy of thin-film evaporated on ZnSe ATR elements. An ATR FT-IR spectrum of an indigo thin-film is shown in Figure 59. In the case of deuterated indigo, the N-D as well as N-H vibrational peaks are clearly visible. Over one week of measurements while the sample was exposed to air the ratio size of the N-D and N-H peaks remained constant, indicating that the deuteration of the sample is relatively stable (Figure 60).

Photoluminescence spectra for indigo and deuterated indigo were collected in various solvents: DMF, DMSO, $CHCl_3$, and $CDCl_3$, using a concentration of 100 μM. In all cases, the photoluminescence intensity of the deuterated indigo sample was 3-4 times higher than the normal indigo sample. Spectra in chloroform are shown in Figure 61. This is strong evidence that the proton transfer mechanism indeed is responsible for excited state deactivation. Time-resolved photobleaching and luminescence experiments comparing normal and deuterated indigo are currently in progress to provide a complete picture of the proton-transfer mechanism.
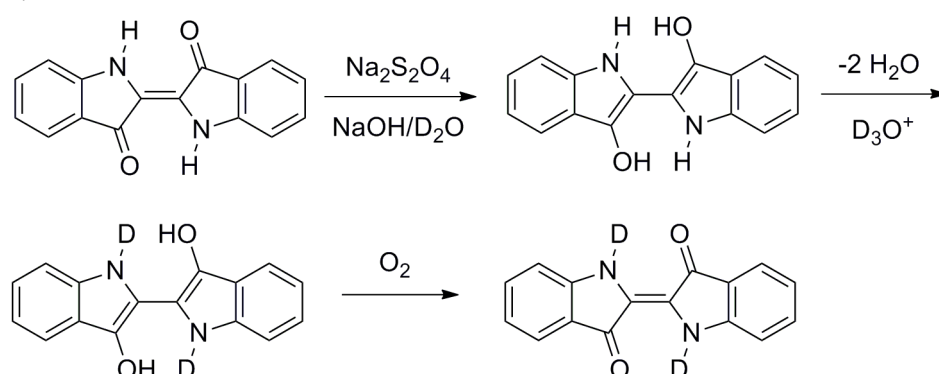
Figure 57. Reaction scheme for the preparation of *N,N'*-dideuteroindigo.
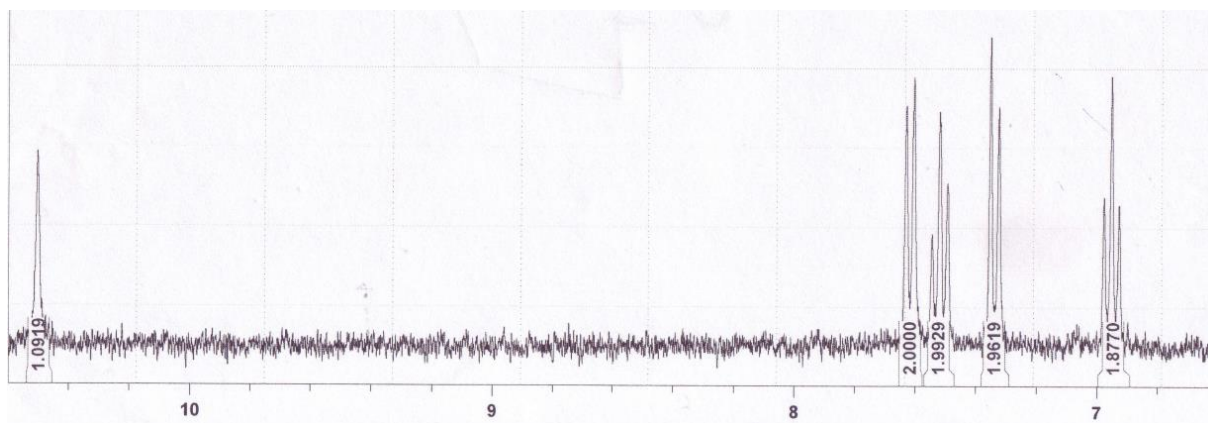
Figure 58. ^{1}H NMR spectrum of indigo following deuterization procedure in D_6-DMSO. X-axis is chemical shift in units of ppm. The N-H proton is found at $\delta = 10.5$ ppm, The sample is about 50% deuterated.
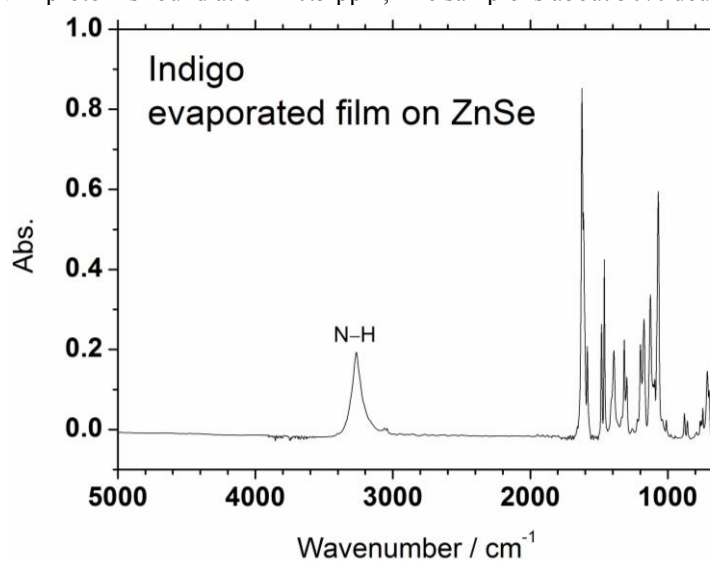
Figure 59. FT-IR spectrum of vacuum-evaporated film on indigo on a ZnSe ATR element
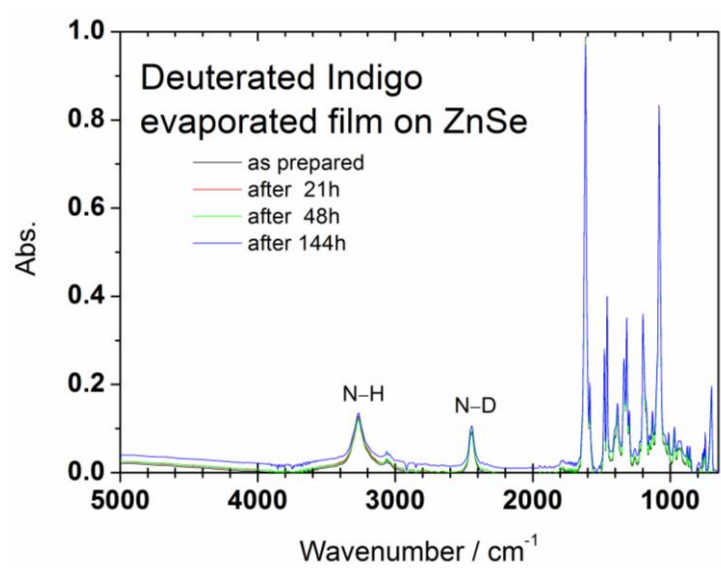
Figure 60. FT-IR spectrum of vacuum-evaporated film on N,N'-dideuteroindigo on a ZnSe ATR element measured over the course of one week showing the stability of the deuterated indigo.
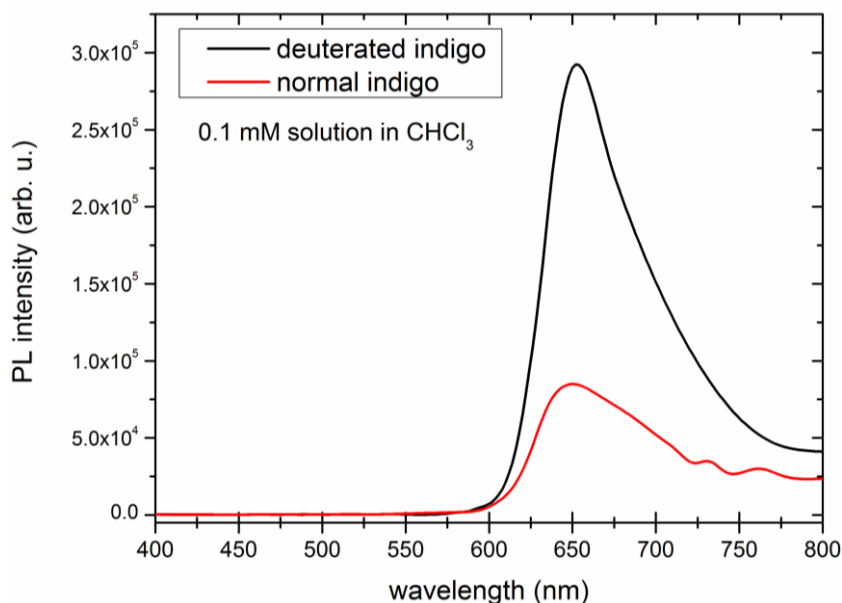
Figure 61. Comparison of photoluminescence of indigo with *N,N'*-dideuteroindigo

5.3 Photoinduced charge transfer with indigos

Photoinduced charge transfer is the fundamental operating principle behind donor-acceptor OPV cells. Despite the ubiquity of indigo, only limited studies concerning some indigo derivative dyes (never NH containing pigment-forming compounds) have been reported in the past on photoinduced charge transfer reactions. In two independent studies, both published in 1986, several *N,N'*-disubstituted indigos were reported to undergo photoreduction in the presence of suitable electron donor molecules, as well as photooxidation in the presence of acceptors.[141,142] This behavior of readily participating in photoinduced electron transfer reactions as a donor and acceptor is rationalized by the low oxidation potential and high electron affinity of *N,N'*-disubstituted indigos, whose electrochemical behavior is very similar to indigo itself. In this work, we have endeavored to establish if similar photoinduced charge transfer reactions occur with the H-bond forming indigo derivatives, with the ultimate application of OPV in mind. Recently we found that H-bonded indigo as well as derivatives such as 5,5'-dibromoindigo undergo photoinduced charge transfer (Figure 62a) to and from the semiconducting polymer P3HT, poly(3-hexylthiophene). Small amounts of indigo in CHCl$_3$ solution quench the photoluminescence of P3HT (Figure 62b). Blends of P3HT and 5,5'-dibromoindigo were prepared using the latent pigment technique described later in section 7. These blends were measured using light-induced electron spin resonance, L-ESR, a useful technique [73,75,143] for establishing the existence of photoinduced charge transfer. Upon photoexcitation using a green laser, which excites the P3HT, a double-signal originating from the radical cation on the P3HT and the radical anion on the 5,5'-dibromoindigo is observed. This is the classic signature of photoinduced charge transfer in donor-acceptor blends. Interestingly, selectively exciting the 5,5'-dibromoindigo by using red excitation (690 nm) also yielded a double-signal, indicating that hole transfer from the photoexcited indigo pigment to P3HT had occurred (Figure 62c). This suggests that in a donor-acceptor blend, absorption from indigo could potentially contribute to photocurrent. This finding is also interesting from the perspective of photophysics of donor/acceptor blends, as the existence of photoinduced charge transfer from the indigo indicates that this process effectively competes with the very rapid internal conversion mechanism. Light-induced ESR measurements are

carried out at low temperatures (60K in this case), thus it is not clear at this point how effectively photoinduced charge transfer might compete with internal conversion at room temperature. Initial attempts to fabricate bulk heterojunction P3HT/indigo solar cells were successful in producing working devices however with low efficiency: this is described in more detail in section 7. A wide range of indigo derivatives electrochemically furnish reductions at relatively low potentials (corresponding to a LUMO level in the -3.6 - 4.0eV range) suggesting that indigos are a promising materials family to explore as acceptor, n-type materials for bulk heterojunction OPV.
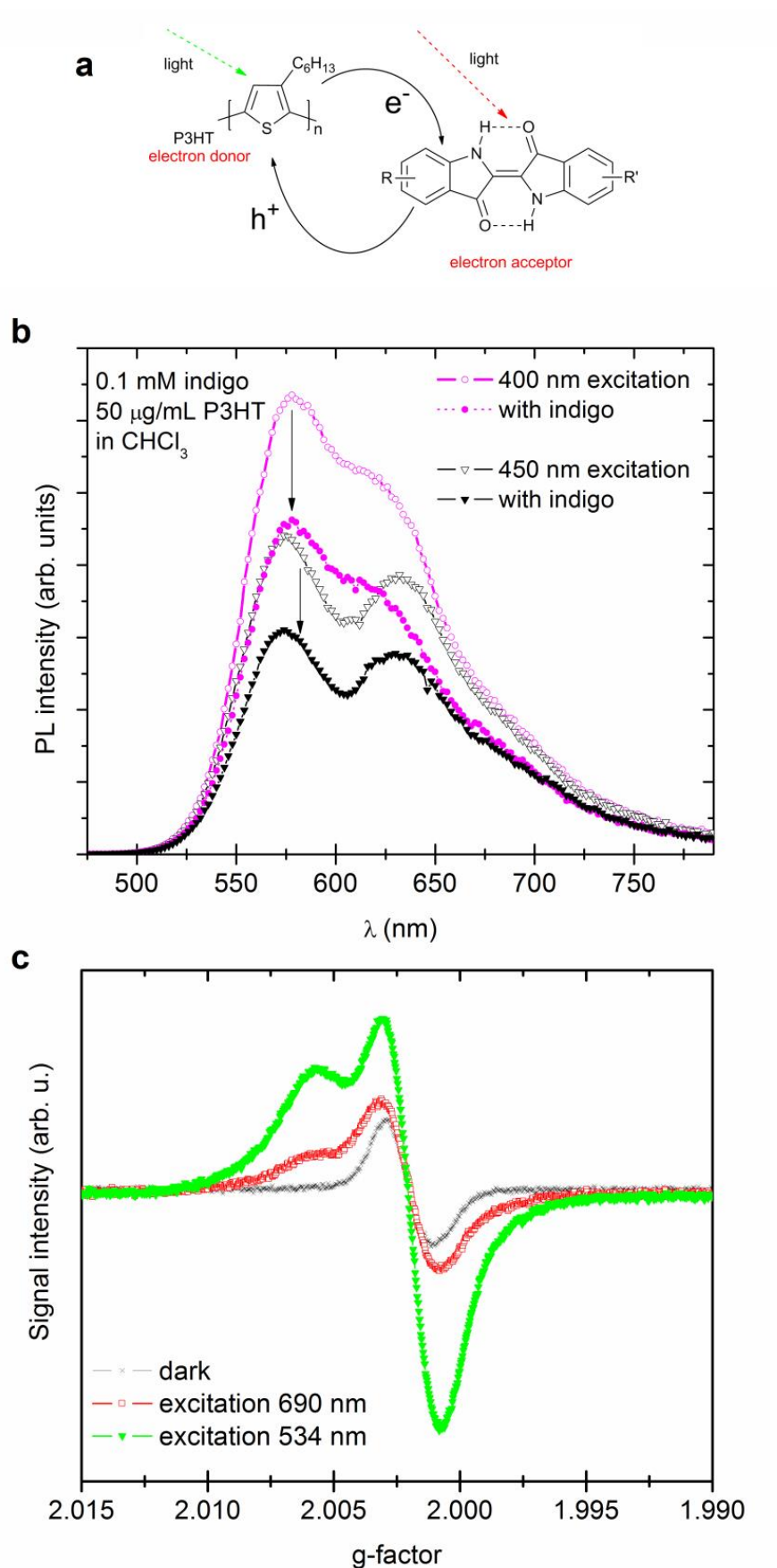
Figure 62. a) Schematic showing photoinduced electron transfer from P3HT to indigo, and photoinduced hole transfer from photoexcited indigo to P3HT. b) Photoluminescence quenching of P3HT with indigo in solution. c) Light-induced electron-spin resonance of a P3HT/5,5'-dibromoindigo blend, excited at wavelengths to selectively excite P3HT or the indigo.

5.4 Quinacridone – single-layer photovoltaic devices

During the comparative studies between pentacene and quinacridone described earlier in Section 4, simple metal/insulator/metal diodes were likewise prepared. We were surprised to find that photoinduced charge generation in single-layer quinacridone metal-insulator-metal diodes is nearly 1000 times more efficient than in pentacene devices. This led to the idea of developing "single-layer" organic solar cells.

Consideration of single-layer photovoltaic devices must be preceded by the introduction of the concept of the exciton – the bound electron/hole pair following photoexcitation of a semiconductor.[144–146]

A photoexcitation in a semiconductor involves promotion of an electron to an unoccupied high energy state, leaving behind a positively-charged vacancy, a hole. This electron-hole pair interacts by Coulombic attraction which is screened by the dielectric constant of the solid, $\varepsilon = \varepsilon_0\varepsilon_r$. The wavefunction describing the relative electron-hole motion, $\Psi(r)$, is analogous to the Schrödinger equation describing the electronic state of a hydrogen atom, however with terms to account for the solid state effects of effective mass and electric field screening:

$$m_0 \rightarrow \mu,\ e^2 \rightarrow \frac{e^2}{\varepsilon}$$

$$-\frac{\hbar^2}{2\mu}\Delta\Psi(r) - \frac{e^2}{\varepsilon r}\Psi(r) = E\Psi(r)$$

Where $\Delta \equiv \dfrac{\partial^2}{\partial x^2} + \dfrac{\partial^2}{\partial y^2} + \dfrac{\partial^2}{\partial z^2}$, the reduced mass term, $\mu = \dfrac{m_e m_h}{m_e + m_h}$, and $r = \sqrt{x^2 + y^2 + z^2}$ is the distance separating the electron and hole.

Thus the binding energy of the ground state of the exciton is given by:

Equation 2: $E_B = \dfrac{\mu e^4}{2\hbar^2\varepsilon^2} = \dfrac{\hbar^2}{2\mu a_B^2}$, where a_B the Bohr radius, $a_B = \dfrac{\hbar^2\varepsilon}{\mu e^2}$

Due to a high value of ε_r, exciton binding energy E_B in inorganic semiconductors is typically lower than 10 meV, well below k_BT. Therefore at room temperature, a photoexcitation can be considered to yield a free electron hole pair. This is, of course, highly relevant for solar energy harvesting applications.

Organic semiconducting materials, in contrast to their inorganic counterparts, have low dielectric constants and thus molecularily-localized tightly-bound Frenkel excitons form following photoexcitation. Frenkel excitons have binding energies greater than k_BT, and binding energy can be considered to be proportional to $1/\varepsilon$ as opposed to $1/\varepsilon^2$, due to small exciton radius. Single-layer organic photovoltaic devices typically show poor performance on account of the high exciton binding energy in organic materials. Such devices yield very low photocurrent densities not exceeding the $\mu A/cm^2$ range under solar illumination, corresponding to monochromatic quantum efficiencies of <1%. The obstacle of high exciton binding energy was overcome in organic materials by using heterojunctions between electron-donor and electron-acceptor materials.[6,7] If the LUMO-LUMO offset of molecular orbital energies of neighboring molecules is greater than the value of the exciton binding energy, efficient polarization of excitons results and photocurrent yields are enhanced by several orders of magnitude. The donor-acceptor concept is at the heart of all organic solar cells at

present, currently achieving efficiencies in excess of 10%. However, the energetic offset between donor and acceptor results in a potential energy loss, decreasing the photovoltage produced by such cells. Also, obtaining optimum nanomorphology between donor and acceptor domains is challenging and often demixing of the two components leads to stability problems in devices. The concept of a single-layer solar cell wherein a different mechanism for exciton dissociation occurs is potentially useful and is the subject of consideration in this section.

Quinacridone single-layer organic metal-insulator-metal (MIM) diodes were found to generate nearly 1000× photocurrent than pentacene MIM diodes under simulated solar irradiation. The external quantum efficiency (EQE) of quinacridone was between 1 and 10% over the range where the pigment absorbs. The EQE action spectra for quinacridone and pentacene are compared in Figure 63. We found that the external quantum efficiency of pentacene devices was 10^{-3} to 10^{-2} %. This is consistent with earlier reports of photogeneration in pentacene diodes. These values are similar to single-layer devices with semiconducting polymers such as poly(phenylene vinylene)[147] and poly(thiophene)[148,149], where quantum efficiencies remain < 1%. The current-voltage (J-V) characteristics of pentacene and quinacridone metal-semiconductor-metal diodes are shown in Figure 64. Devices consisted of ITO|PEDOT:PSS substrates, 100 nm of vacuum-evaporated organic semiconductor, and an evaporated aluminum top electrode. Quinacridone diodes show remarkable photocurrents in the mA/cm^2 range under 1.5 AM illumination, while pentacene produced only ~10 µA/cm^2. Quinacridone diodes afforded an open-circuit voltage (V_{oc}) scaling with the top contact metal work function (inset of Figure 64) and fill factors of 30-35%. These observations are consistent with a dominance of drift current rather than diffusion currents. This is in agreement with reported organic MIM devices, which are considered to be drift-current dominated.[150–153] Importantly, the short circuit current was independent of metal work function. We conclude that the larger photocurrent yield of quinacridone versus pentacene is explained by the more efficient polarization of excitons into free carriers in quinacridone.
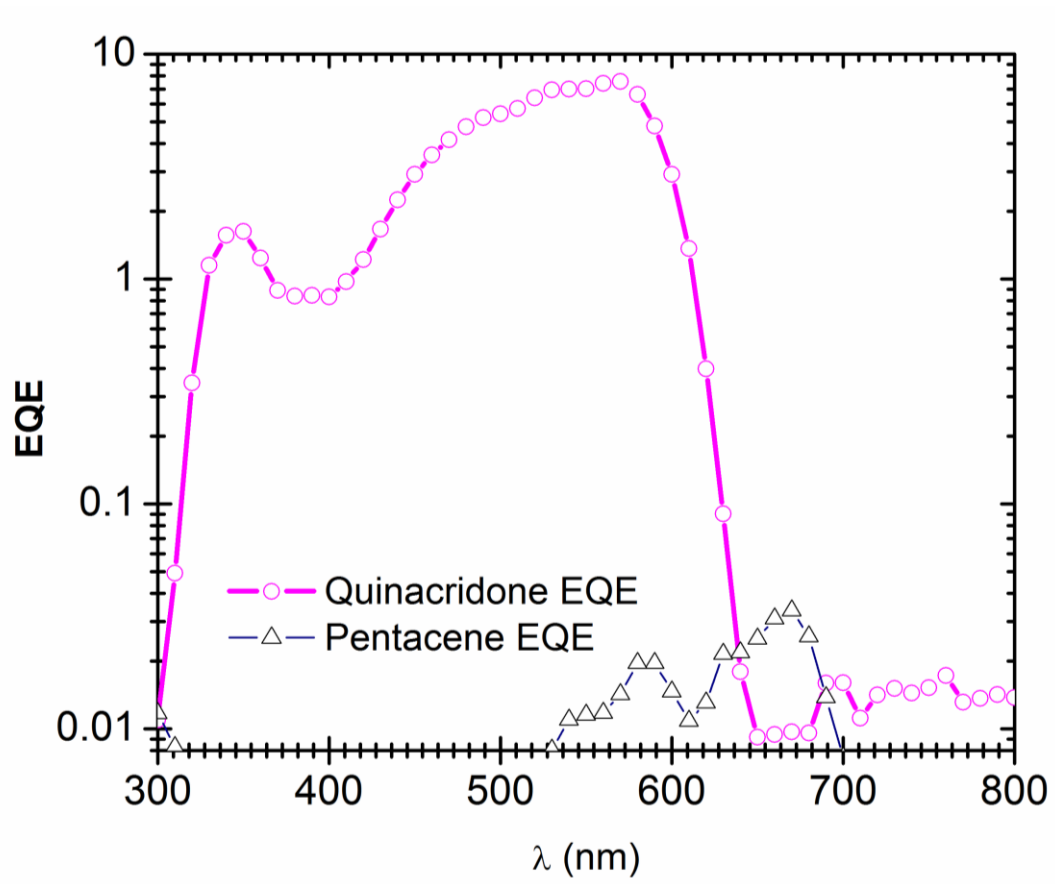
Figure 63. External quantum efficiency as a function of wavelentgh of
ITO|PEDOT:PSS|semiconductor(100nm)|Al diodes quinacridone (circles) and pentacene (triangles).
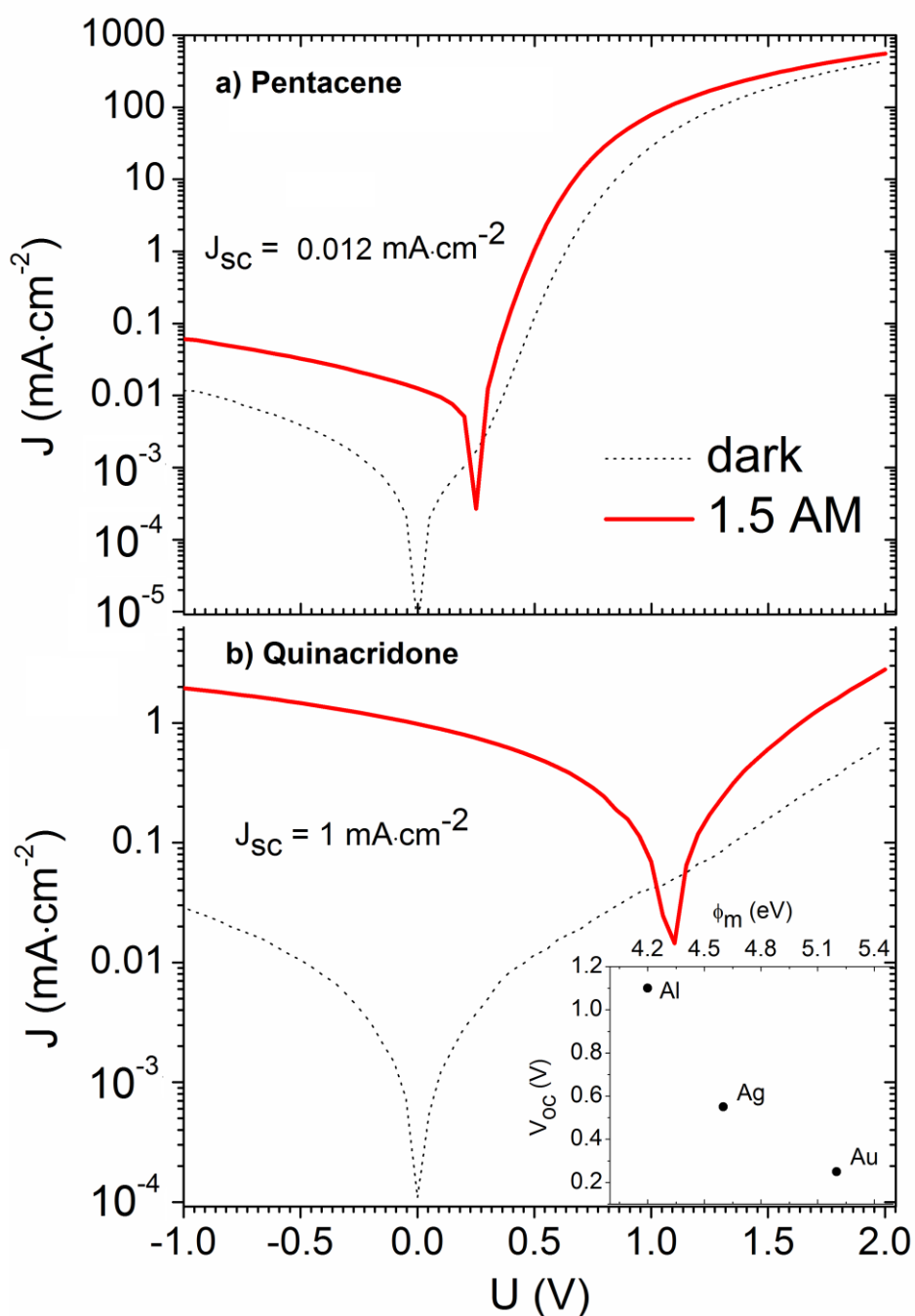
Figure 64. J-V characteristics of ITO|PEDOT:PSS(40nm)|semiconductor (100 nm)|Al (150 nm) diodes (a) pentacene, and (b) quinacridone in the dark and under simulated AM 1.5 illumination. The V_{oc} of quinacridone diodes with different top-contact metals is plotted versus metal work function in the inset.

To provide a preliminary estimate of the effective exciton binding energy in the quinacridone film, we measured the temperature dependence of photocurrent in a lateral geometry. From the thermal activation of photocurrent, we estimate an exciton binding energy of ~12 ± 5 meV (Figure 65). In order to interpret the phenomenon of low effective exciton binding energy in quinacridone, two explanations based on hydrogen bonding were explored. The first explanation is that the presence of strong intermolecular interactions due to H-bonding relative to van der Waals bonds leads a high dielectric constant of quinacridone, and correspondingly lower exciton binding energy. We conducted electrical capacitance-

frequency measurements on MIM structures with different contact metals and averaged results over dozens of devices and found $\varepsilon_r = 4.2$ for quinacridone and $\varepsilon_r = 3.9$ in pentacene (Figure 66). Considering Equation 2, this difference in dielectric constant is far too small to account for a such a large difference in photogeneration efficiency.

Figure 65. Arrhenius plot of the thermally-activated photocurrent ($E_A \equiv E_B$) in quinacridone films measured using a lateral geometry used to estimate the effective exciton binding energy. Figure originally published in [114].

Figure 66. Dielectric constant (ε_r) as a function of probing frequency on the left axis, loss angle on the right axis. Originally published in [114].
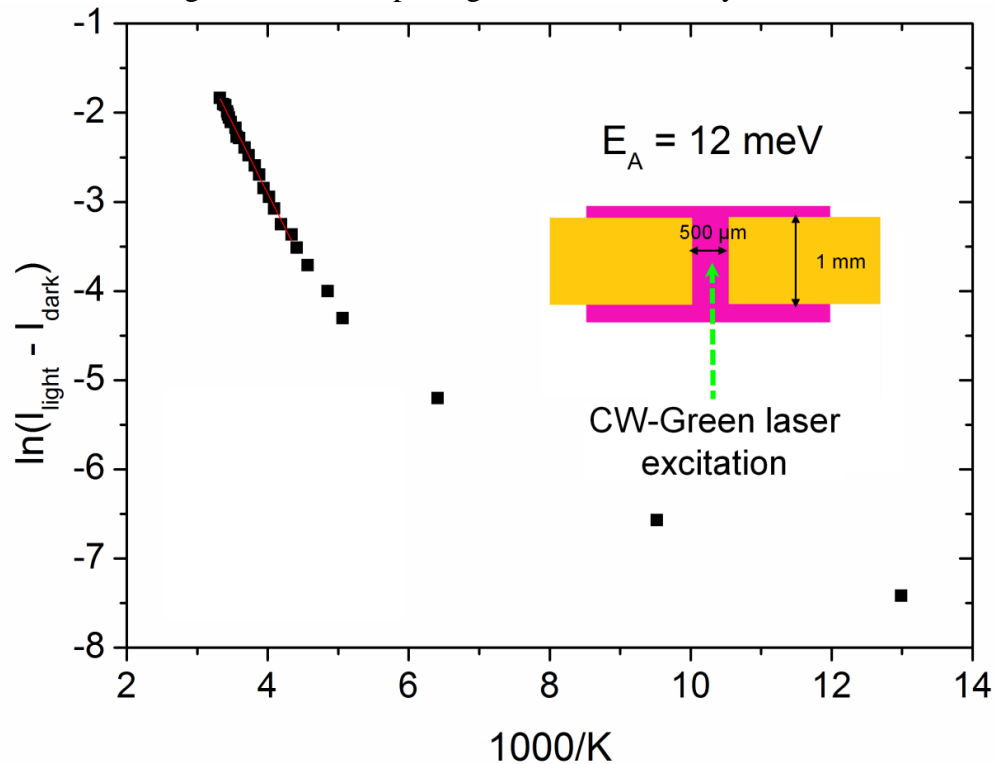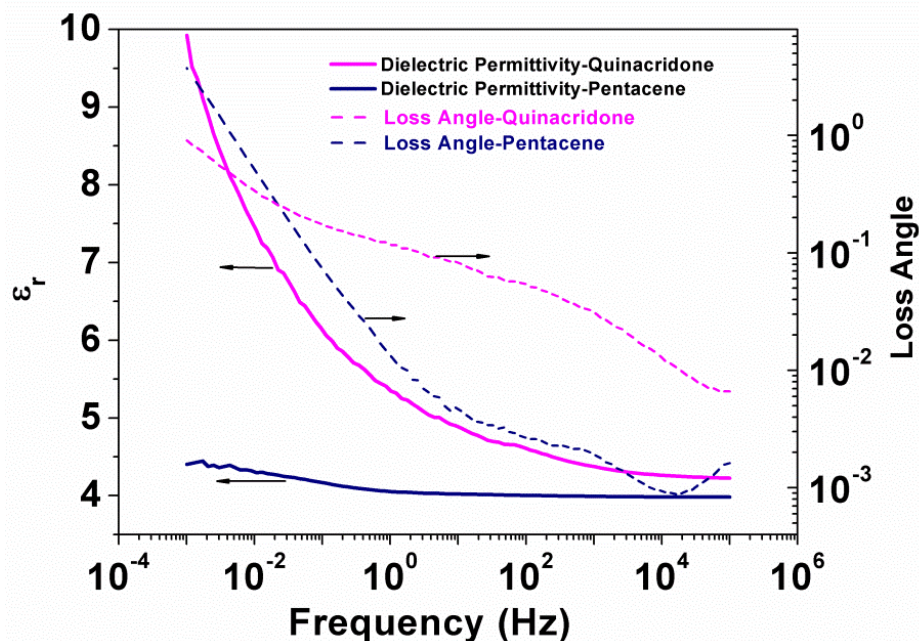
The second explanation is the efficient formation of intermolecular charge transfer (CT) complexes that easily polarize into free-charges. Alternatively, these can be called excimeric states. This can be regarded as an exciton with a larger effective radius and thus decreased Coulombic attraction between the electron and hole. The efficient formation of long-lived (> 10ns) charge-transfer excitons in quinacridone was proposed and supported by several experimental studies carried out by Jan Kalinowski. Time-resolved photoluminescence[154,155] and electroabsorption studies[156] reported by Kalinowski et al. showed that in the solid state of quinacridone, an initially-formed singlet state self-traps into an excimeric CT state within 5 ps. This leads to a pronounced photoconductivity response.[157] Optical studies of quinacridone in solution and solid state [158] show that the transition dipole for the lowest-energy absorption aligns along the hydrogen bonding of neighboring molecules and that blocking the hydrogen bonding chemically will eliminate this absorption, supporting the idea of CT excitons delocalizing effectively between molecules due to hydrogen bonding. The role of such CT excitons has been reported in the H-bonded diketopyrrolopyrrole pigment class as well.[159,160]

We carried out measurements of photoluminescence of quinacridone in dilute solution and compared it with luminescence of quinacridone films (Figure 67). Solution luminescence shows a Stokes shift and typical mirror-image type progression of the vibrational replicas. However, in the case of films there is what appears to be a normal Stokes-shifted fluorescence peak followed by 100-200 nm red-shifted and very broad emission peak. This suggests the role of a CT state in dominating luminescence.
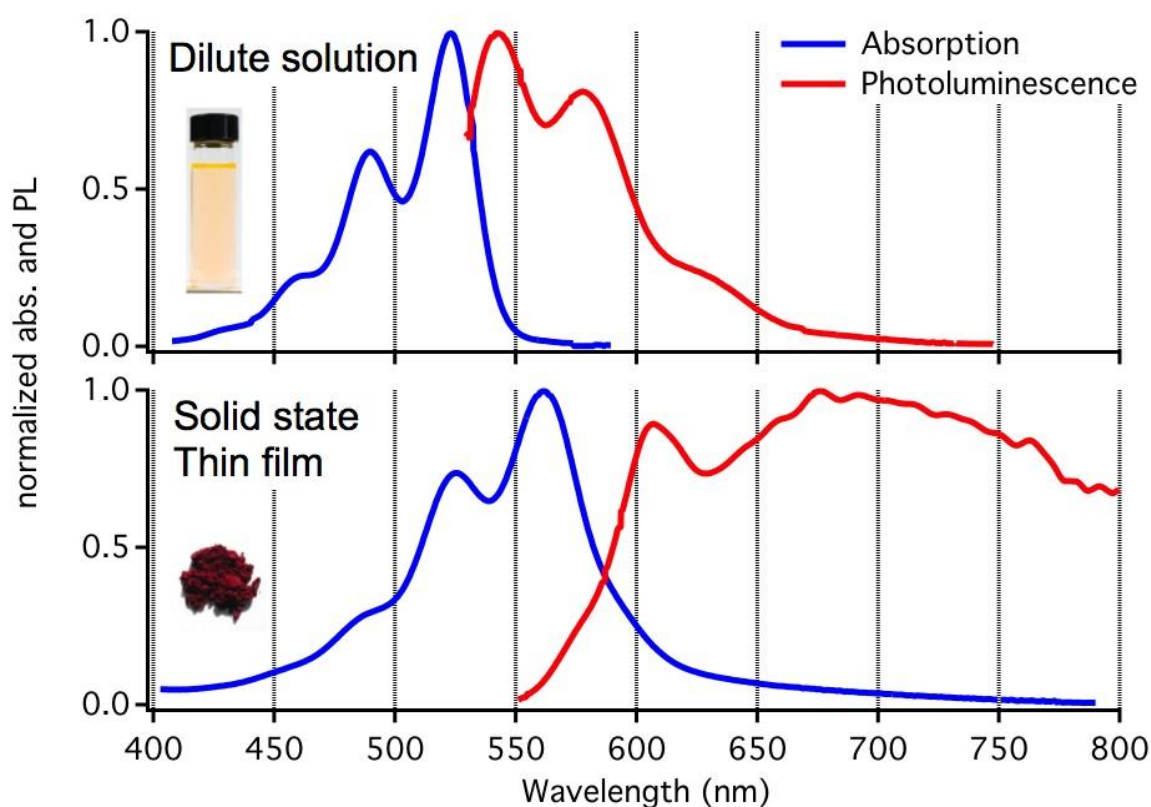

Figure 67. Comparison of absorbance and photoluminescence of a dilute solution (< 0.2 mM) of quinacridone in DMSO versus evaporated thin films.

Based on the evidence from the PL behavior of solutions and quinacridone films, the mechanism for photogeneration in quinacridone is proposed to involve the dissociation of a weakly-bound CT or excimeric state into free carriers. Thus the excimeric energetic states act as a self-acceptor, or self-trap, in quinacridone. This mechanism is illustrated in Figure 68. With the effective generation of free charge carriers, and its demonstrated ambipolarity (section 4.2) to allow transport of both carriers to respective electrodes, quinacridone can act as a "single-layer" organic solar cell material.
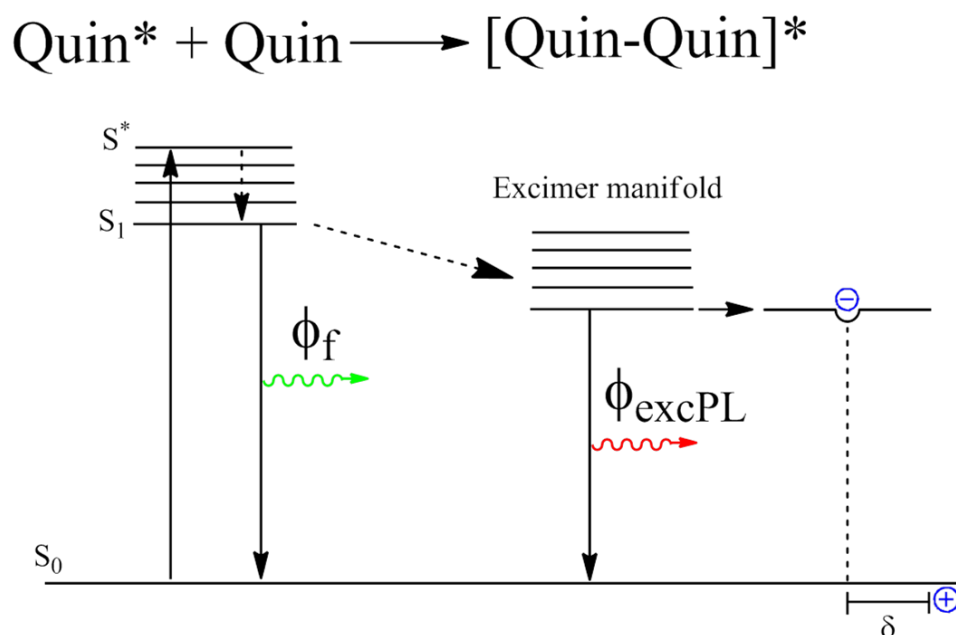
Figure 68. "Self-trapping" excimer model for photogeneration in quinacridone thin films.

Quinacridone, like the other H-bonded pigment molecules used throughout this study, was processed using vacuum evaporation techniques. Alternatively we utilized the "latent pigment" technique of using quinacridone functionalized with thermolabile tert-butoxy carbonyl (tBOC) groups. The latent pigment technique of using a soluble dye that can be thermally regenerated into the parent pigment was developed by Iqbal et al. in the early 1990s.[161,162] We synthesized tBOC quinacridone according to published methods. The chemistry of tBOC substituted compounds is described in more detail in section 6. tBOC quinacridone could be dissolved in organic solvents such as chloroform and chlorobenzene up to concentrations as high as 50 mg/ml. These solutions could be spin-cast to yield films, which when heated to 170 °C or higher rapidly converted into H-bonded quinacridone. The process of solution processing quinacridone diodes using this route is shown in Figure 69. Diodes prepared in this way worked similarly to vacuum-processed ones, however photocurrents were typically lower by a factor of 2. A comparison of vacuum-processed and solution-processed quinacridone diodes is shown in Figure 70. The method requires further optimization and understanding the morphology of thermally-regenerated quinacridone films is a work in progress.
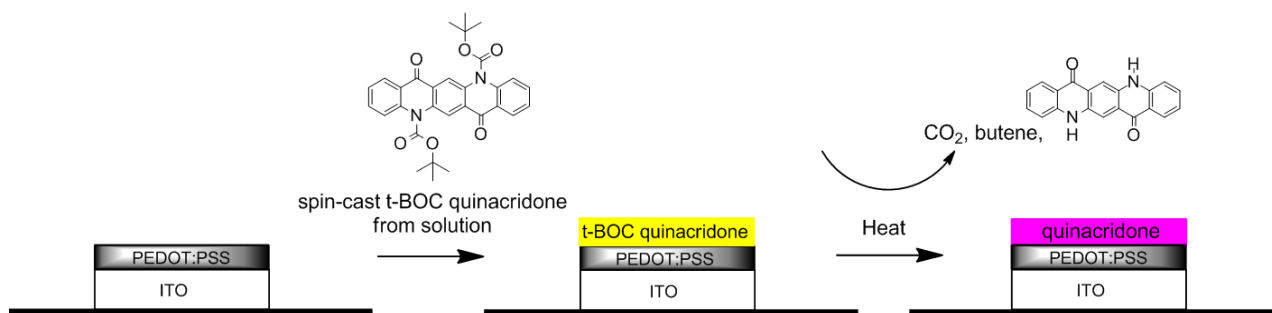
Figure 69. Solution processing of quinacridone thin-films using a latent pigment process.
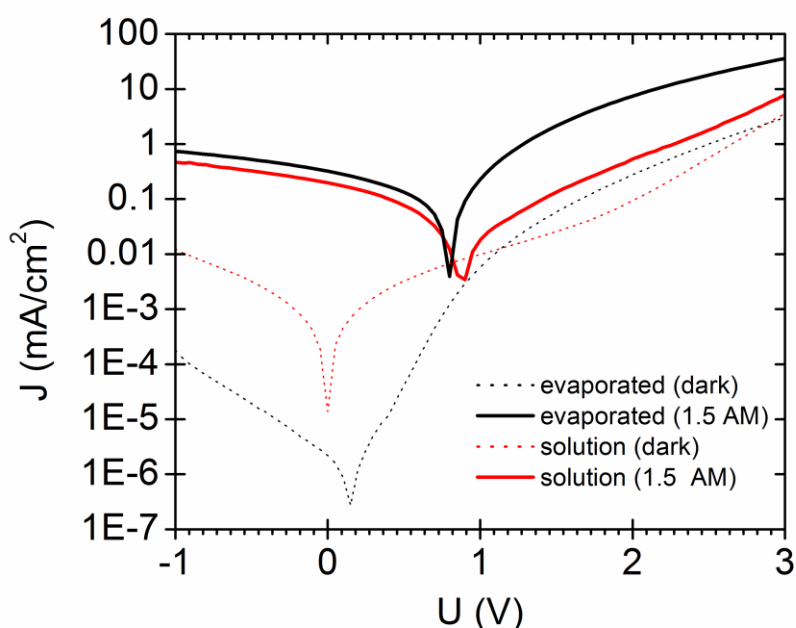
Figure 70. Comparison of diodes of the type ITO|PEDOT:PSS|Quinacridone|Al fabricated via evaporation of the quinacridone and solution processing using the latent pigment route.

Based on these findings about single-layer MIM quinacridone diodes, the author proposes that for a single organic molecular material to be successful for photovoltaic devices, it must fulfil the following conditions:

- broad light absorption
- Low effective exciton binding energy, *i.e.* light absorption must efficiently yield electron/hole pairs
- Ambipolarity, to allow the efficient transport of electrons and holes to the respective electrodes

An avenue for OPV design that is an alternative to the incumbent bulk heterojunction concept offers potential advantages in terms of higher theoretical efficiency due to mitigation of donor-acceptor polarization losses and ease and simplicity of processing. H-bonded pigments, by virtue of their stability and low-cost could be ideal candidates for such devices.

5.5 Epindolidione – single-layer excimer organic light-emitting devices

Single-layer MIM diodes were likewise fabricated using epindolidione thin films. Though not promising as a solar cell absorbing material due to its color, epindolidione demonstrated excimeric effects analogous to quinacridone.

Like quinacridone, epindolidione could be processed using the tBOC latent pigment route. In the case of epindolidione, film fabricated from solution and via vacuum processing yielded diodes that were identical in performance. The latent pigment thin film processing technique for epindolidione is shown in Figure 71. The extinction coefficients and photoluminescence in solution of epindolidione, mono-tBOC, and di-tBOC epindolidione are shown in Figure 73a,b. The absorption coefficient and luminescence of the thin-films is shown in Figure 73c,d. In the case of epindolidione thin films a Stokes-shifted fluorescence peak is visible centered at 532 nm, and to the red of this peak, two bathochromically shifted peaks, one at 632 nm and the next at 690 nm, are visible. These peaks are far too red-shifted to be considered as vibrational replicas and instead are attributed to luminescence of excimeric species.

Single layer MIM diodes fabricated with epindolidione were found to exhibit strong electroluminescence with essentially the same characteristic peaks as those visible in the photoluminescence spectrum, *i.e.* a fluorescence peak at 525 nm and two excimeric peaks, at 632 nm and 692 nm. The absorption of epindolidione is plotted along with the electroluminescence spectrum in Figure 73, and a comparison of photo- and electroluminescence is shown in Figure 74.
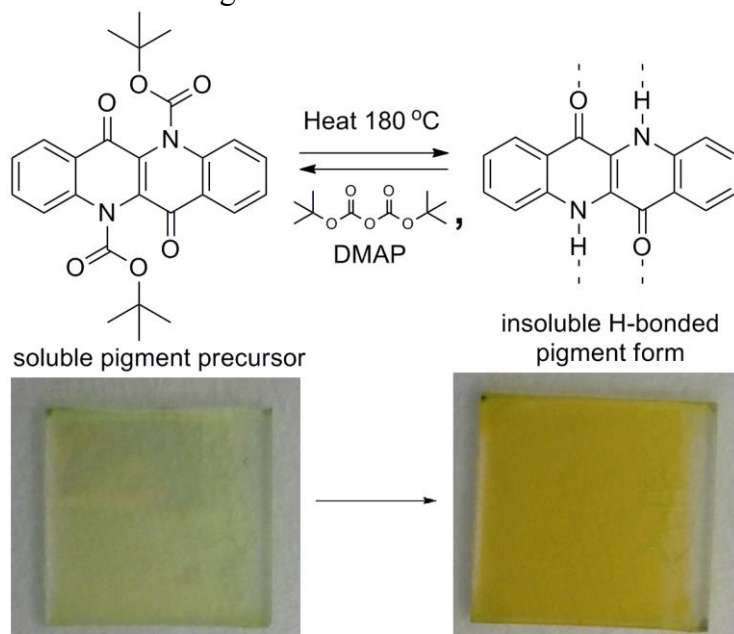
Figure 71. Latent pigment processing technique for epindolidione
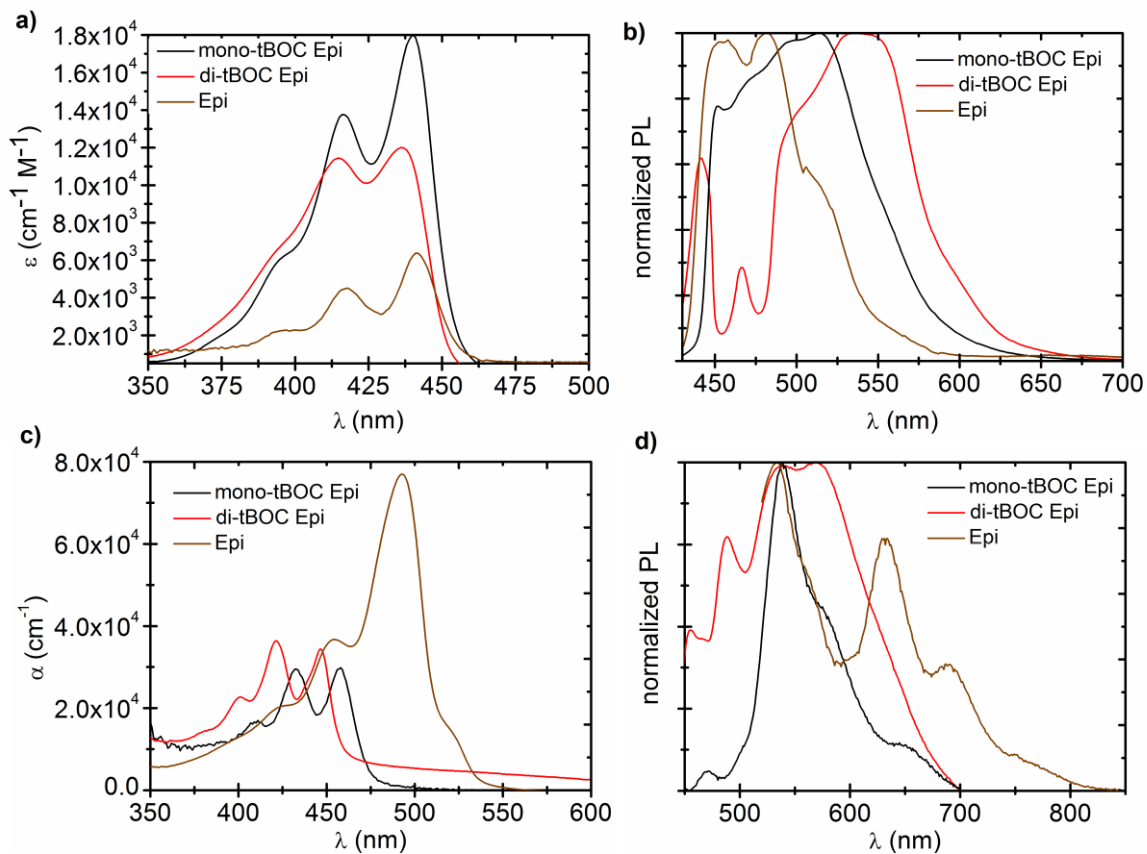
Figure 72. a) Extinction coefficient for epindolidione, N-tBOC epindolidione, and N,N'-ditBOC epindolidione measured in chloroform solution. b) Photoluminescence spectra for the same set of molecules. c) Absorbance coefficient of thin films of the three epindolidiones processed onto quartz substrates. d) photoluminescence of thin films on quartz.
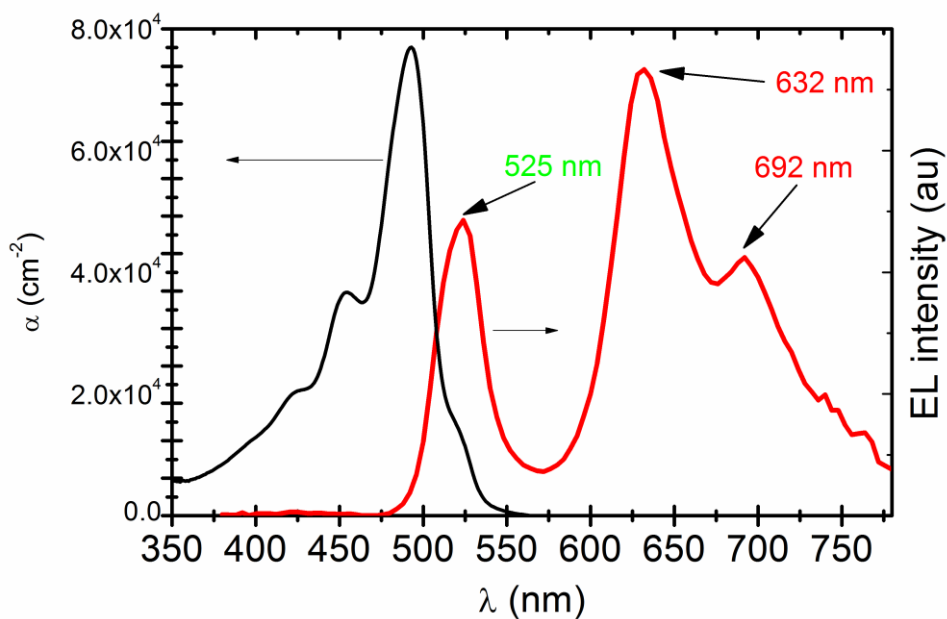
Figure 73. Optical absorption of a evaporated thin film of epindolidione compared with the electroluminescence spectrum of a diode consisting of the same film sandwiched between ITO/PEDOT:PSS and an aluminum top contact.
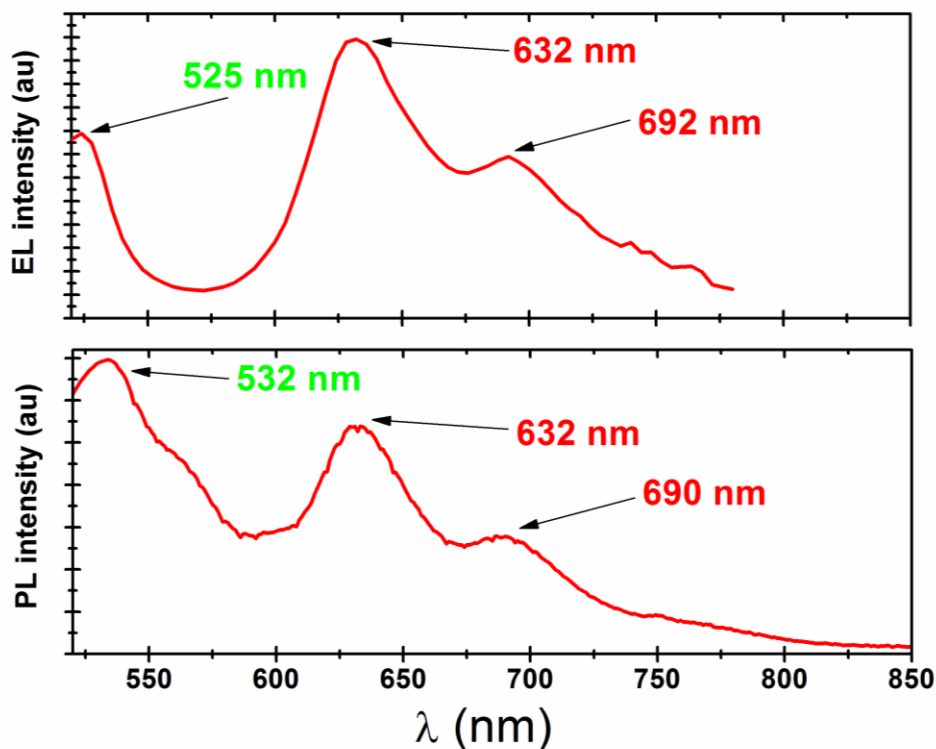
Figure 74. Comparison of the electroluminescence spectrum (top) of epindolidione with the photoluminescence spectrum of the same, excited at 480 nm.

These single-layer excimer organic light-emitting diodes are remarkable for their very broadband emission. The large shift in the excimer emission relative to absorption suggest this material for lasing applications where minimizing self-absorption is desired. A study to measure the dynamics of the fluorescence versus excimer emission in epindolidione is in progress. Single-layer excimer emitting OLEDs are another potential interesting optoelectronic application for H-bonded pigments.

6. Solubilization and functionalization of indigos

Indigos, as all H-bonded pigments, have very poor solubility in organic solvents. This limits their thin-film processability to vacuum-evaporation. Additionally, it seriously hampers any synthetic chemical reactions that might be used to derivatize indigo. To overcome these limitations, we employed the technique of creating a latent pigment of indigo using thermolabile protecting groups to allow solution processing as well as to generate a form of indigo amenable to further chemical modification.[163] The thermolabile protection group chosen is the *tert*-butoxy carbonyl (tBOC) group, well-established in the field of peptide chemistry for protecting the reactive amine function.[164] In 1992, researchers at the *Ciba-Geigy* pigment division in Basel disclosed in a patent on producing soluble precursors, or "latent pigments", using the tBOC group that allowed the solution processing of dyes that could be regenerated into H-bonded pigments. They applied this technique for their diketopyrrolopyrrole class of pigments, as well as quinacridones for industrial coloring applications.[161,162] This method relies on the conversion of the NH group into a carbamate, thereby breaking the intermolecular H-bonding and attaching highly-soluble *tert*-butyl groups – resulting in soluble dye molecules. (Figure 75) The dye can be processed using organic solutions and heat and or acid treatment can remove the tBOC groups when desired. A significant advantage of tBOC groups is that they decompose into gaseous products: CO_2 and isobutene. Upon deprotection, the dyes aggregate via H-bonding, thus regenerating the

pigment. Some interesting, but limited, applications of this technique have also been used in the field of organic electronics, such as making solution-processible and photopatternable polyaniline [165], solution-processed quinacridone/fullerene solar cells [166], and diketopyrrolopyrrole polymers for OFET applications.[116] We applied this tBOC protect-deprotect technique to a range of substituted indigo derivatives, and were able to prepare solution-processed films as well as mixed blends with P3HT.

6.1 Synthesis and characterization of *N,N'*-ditBOC indigos

The reaction for functionalizing indigos with tBOC protecting groups is shown in Figure 75.This reaction was carried out on six different indigo derivatives listed in the table of Figure 75. We prepared pigments **1a-3a** and **5a-6a** from the precursor *o*-nitrobenzaldehydes according to the Baeyer-Drewsen indigo synthesis.[51] Compound **4a** was prepared according to Clark *et al*.[52] **5a** alternatively was prepared via the direct bromination of indigo in nitrobenzene solution at elevated temperatures (> 100°C). **1b-6b** were prepared by stirring the pigments **1a-6a** in dichloromethane at room temperature with ≥ two equivalents of tBOC$_2$O and about one equivalent of dimethyl aminopyridine (DMAP) acting as a catalyst for 1-3 days. Experimental details and analytical data for **1-6** can be found in the supplementary information of the article published on this topic [163]. This method allows the easy separation of indigo mixtures by column chromatography. To underscore the utility of this method, we obtained a historical sample from the early 1900s from the Dyestuff museum at the TU Dresden, courtesy of Prof. Hartmann, consisting of a mixture of unsubstituted indigo, 5-bromoindigo, and 5,5'-dibromoindigo. Separating such a mixture on a preparatory scale would be impossible. The mixture was protected using the tBOC reaction and subsequently separated using column chromatography. Products **1b-6b** could be further purified by recrystallization from ethyl acetate. This procedure yielded crystals suitable for single crystal X-ray diffraction. X-ray crystal structures were determined for compounds **1b** and **5b**, which are very similar. The structures of **1b** and **5b** are shown in Figure 76. The tBOC protected indigos are highly-distorted relative to the planar parent compound. Both tBOC groups arrange on one face of the C$_2$-symmetric molecule, pushing the two indole rings away and resulting in a strained central double bond at C4-C4'. This substantial distortion of the molecule is unlike other reported tBOC compounds, such as tBOC quinacridone, which retains its planarity[167]. The optical absorption of the tBOC indigos exhibited a blue-shift in absorption of 40-60 nm, characteristic of indigoids where the intramolecular H-bonding is broken and the 'H-chromophore' is lost. The tBOC indigo derivatives are red or purple in color, having hypsochromically-shifted absorption by about 50 nm relative to the parent compounds. The *N,N'*-ditBOC indigo has a λ$_{max}$ = 546 nm, ε = 6786. This shift is ostensibly related to the breakdown of the H-chromophore – as turning the NH groups into carbamates significantly decreases their electron-donating character. UV-Vis spectra are shown in Figure 77. We found that like other *N,N'*-disubstituted indigos, compounds **1b-6b** exhibited photochemical *trans-cis* isomerism. Green irradiation of solutions with a laser diode emitting at 532 nm produced a rapid blue-shift in absorption, turning the solution from violet to orange (Figure 78). The existance of isosbestic points at 397 and 494 nm evidences a clean photochemical isomerisation reaction without decomposition. Keeping the sample in the dark for ~125 min resulted in complete restoration of the original violet color. Spectra showing the recovery of irradiated *cis*-rich solution in the dark monitored over time are shown in Figure 79. Photoisomerism in indigoids lacking H-bonding has been reported in *N,N'*-substituted indigos,[133] *leuco* indigo,[168] and the related thioindigo dyes.[135] The behavior observed here resembles closely that of *N,N'*-diacetyl indigo.[135] The parent compounds **1a-6a** did not show photochromic behavior, as reported before for indigos with intramolecular H-bonding.[127,135]

The *t*BOC indigos **1b-6b** could be readily dissolved in chloroform or chlorobenzene with concentrations as high as 100 mg/ml. We spin-cast such solutions onto glass substrates yielding violet-coloured, uniform and extremely smooth films. Atomic-force microscopy (AFM) measurement showed RMS roughness of such films to be between 1-2 nm (see SI). Heating of these films at 200°C afforded blue-coloured deprotected films of **1a-6a**.
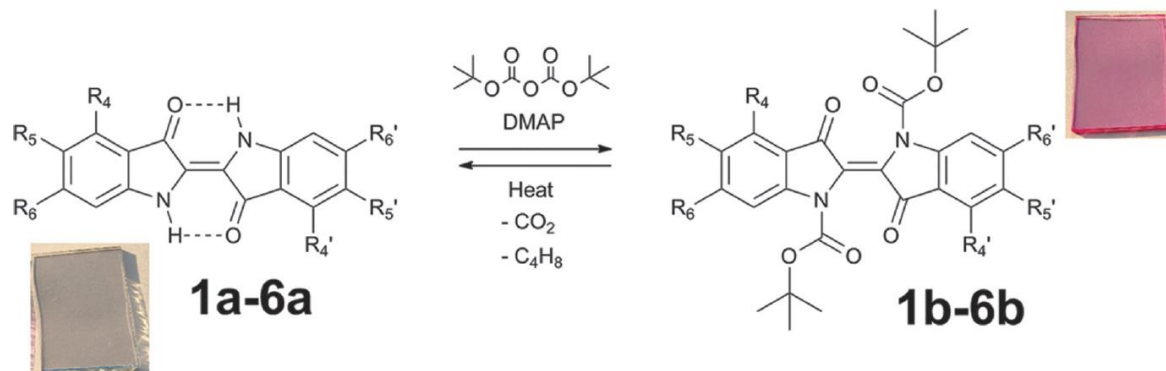
Entry	Substituents [*]	Parent indigo name
1a,b	R=H	Indigo
2a,b	R_4,R_4'=Cl	4,4'-dichloroindigo
3a,b	R_4,R_4'=Br	4,4'-dibromoindigo
4a,b	R_5=Br	5-bromoindigo
5a,b	R_5,R_5'=Br	5,5'-dibromoindigo
6a,b	R_6,R_6'=Br	6,6'-dibromoindigo

Figure 75. Protection and deprotection for indigo pigments (1a-6a) using *t*BOC to yield protected dyes, 1b-6b. The table shows the compounds used in this study. [*]Unless otherwise specified, all R=H. This figure was originally published in [163].
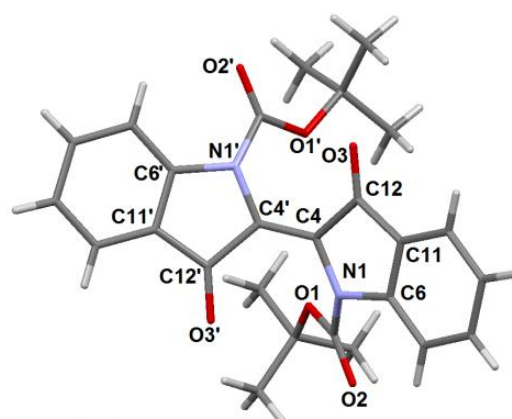
tBOC Indigo
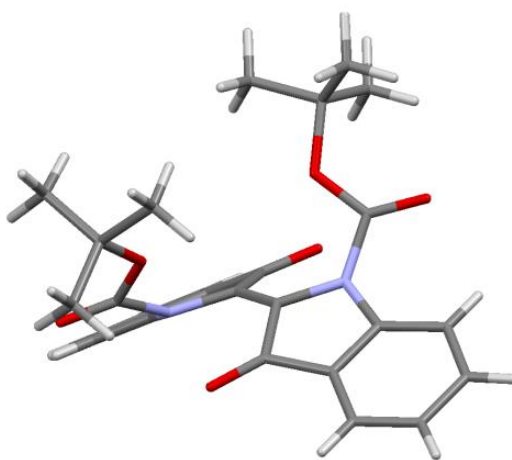
tBOC Indigo, tilted view
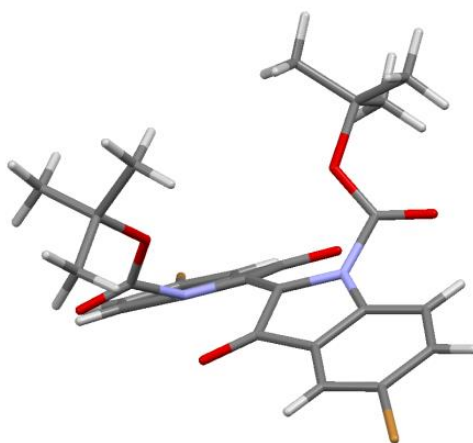
5,5'-dibromo tBOC Indigo

Figure 76. Molecular structures obtained from single crystal X-ray diffraction.
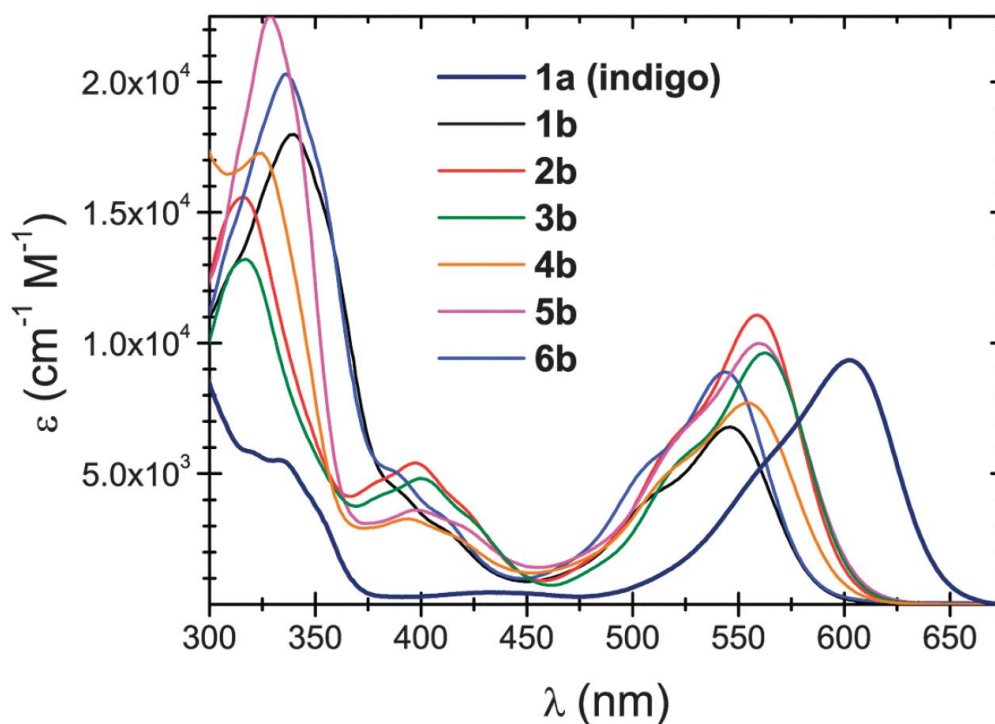
Figure 77. UV-Vis absorbance for indigo and tBOC indigos in chloroform solution. Figure published in [163].
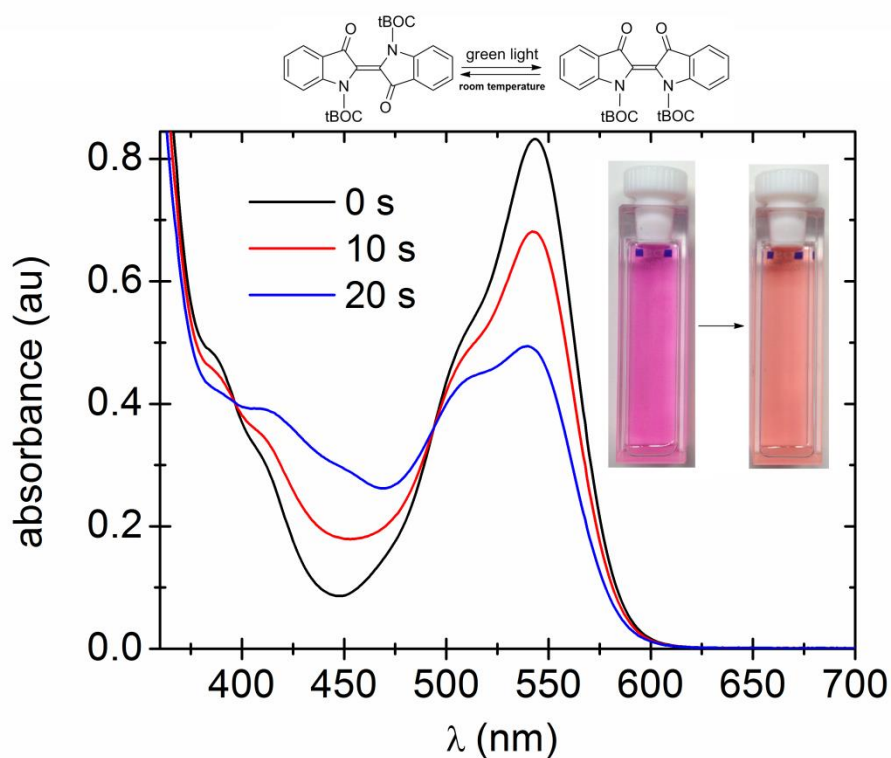
Figure 78. Photochemical *trans-cis* isomerization of N,N'-ditBOC indigo (1b) in acetone solution. The sample UV-Vis spectrum was recorded before and after irradiation (10 and 20s) with a green laser diode (peak 532 nm). A photo of the sample before and after irradiation is shown in the inset. Figure published in [163].
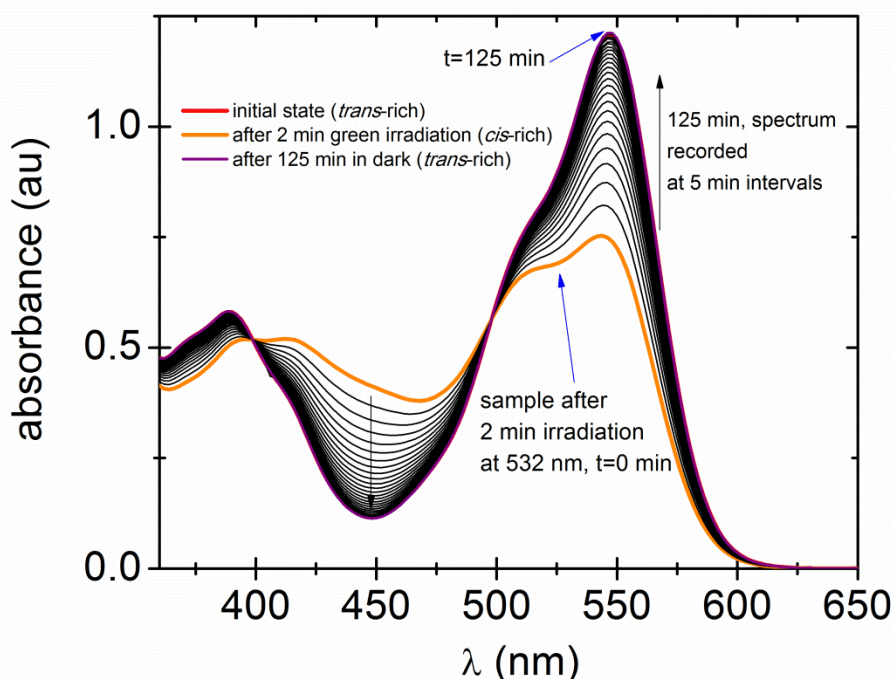
Figure 79. UV-Vis spectra of the reverse *cis-trans* thermal isomerization recorded following illumination with green light. The initial *trans*-rich solution (red trace) was irradiated at 532 nm for 2 min, next a spectrum was measured (orange trace) showing an increased *cis* concentration. The thermal recovery back to the *trans* state is measured over 5 minute intervals. 125 min in dark is sufficient for the system to return back to a UV-Vis spectrum (violet trace) identical with that of the initial state. The red and violet trace overlap completely, demonstrating that the photochemical isomerization reaction appears to be fully reversible. Figure published in [163].

6.2 Thin-film formation using the protect-deprotect route

The deprotection mechanism to yield the pigments **1a-6a** was verified by thermogravimetric analysis (TGA). Heating sample powders to 190-200 °C resulted in a loss corresponding to two equivalents of isobutene and CO_2. A TGA scan for **1b** is shown in Figure 80. We found that while spin-cast films of the protected compounds **1b-6b** were all uniform (Figure 81a), with a rms roughness < 2nm, following deprotection, the films differed significantly from one another depending on the molecular structure of the **1a-6a** parent indigo.

A series of photomicrographs with AFM insets of deprotected films are shown inFigures 82-85. Heating films of **1b** yielded non-contiguous crystallites that were tens of microns in size, with no material in between them (Figure 81b). It was found, by placing a slide above the heated sample during deprotection, that some of the indigo sublimed and created a blue residue on the cover-slide. This behavior is easily rationalized by the fact that the deprotection mechanism from soluble *t*BOC derivatives to the final H-bonded pigment procedes through deprotected but unassociated indigo dye molecules as an intermediate. These small molecules can readily sublime. Thus film formation during deprotection is governed by the process of non-associated indigo molecules evaporating or diffusing to form H-bonded pigment crystals, which are thermally-stable. In the case of all the other substituted indigos **2a-6a**, the individual dye molecules have sufficiently high molecular weight to not sublime during deprotection. In the case of compounds **2a-4a**, we found that films following deprotection featured large micron-sized crystallites. AFM examination revealed that between these large crystallites, a continuous film of much smaller grains of several-hundred nanometers in size existed. In the case of **5a** and **6a**, crystallites in the range of one micron formed, however they are isolated from each other and no continuous film of smaller grains was observed (Figure 85). Compounds **2a** and **4a** clearly demonstrate that at least two distinctly different types of

crystallites exist following deprotection, as can be seen in Figure 82 and Figure 85.
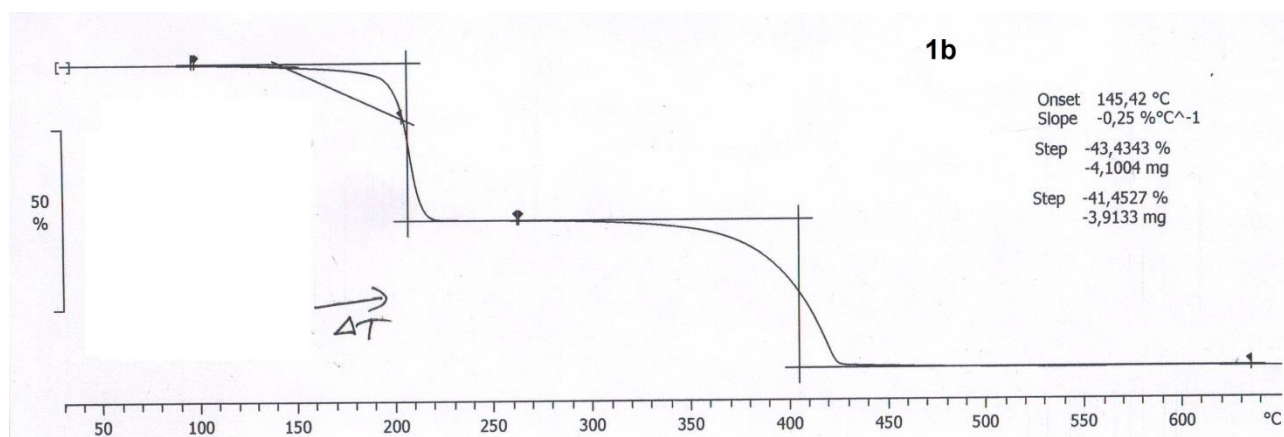
Figure 80. TGA of N,N'-ditBOC indigo (1b) obtained at scan rate of 10 °C/min.
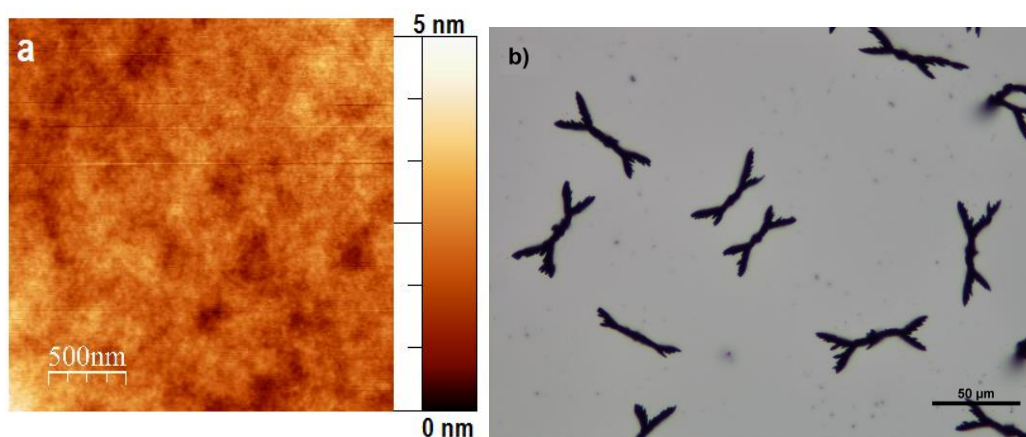
Figure 81. a) AFM image of a spin-cast film of N,N'-ditBOC indigo (1b), film rms roughness = 1.4 nm. b) photomicrograph of indigo crystallites on the surface of glass following the deprotection of a film of 1b.
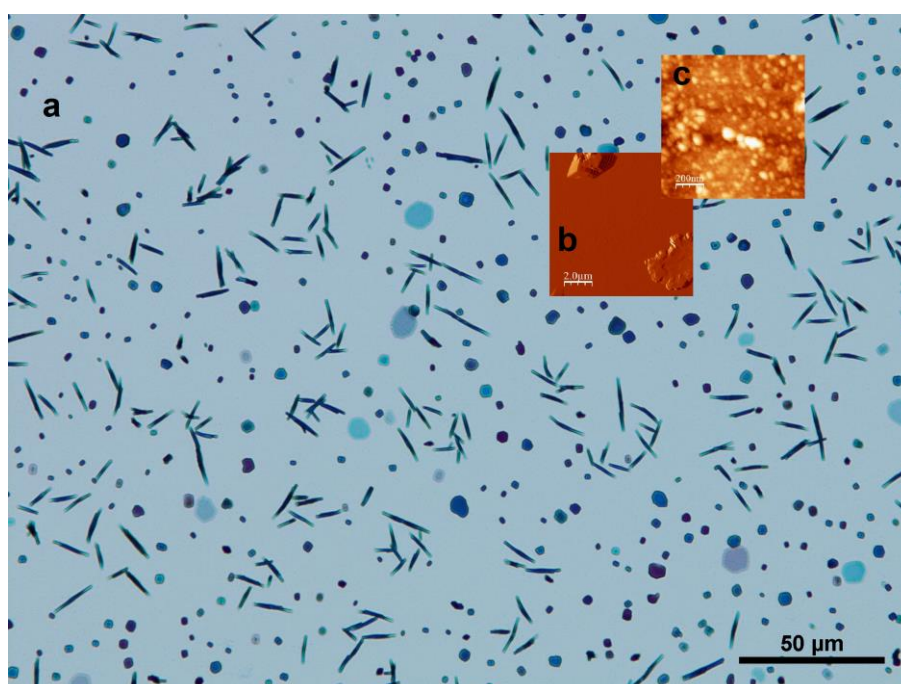
Figure 82. a) optical micrograph of a film of 2a (4,4'-dichloroindigo) processed by spin-casting 2b then heating to 200°C for 5 minutes. b) AFM image showing the large crystallites visible in the optical micrograph. c) AFM zoom-in of the area between the large crystallites, showing a semi-continuous film of nanoscale crystallites.
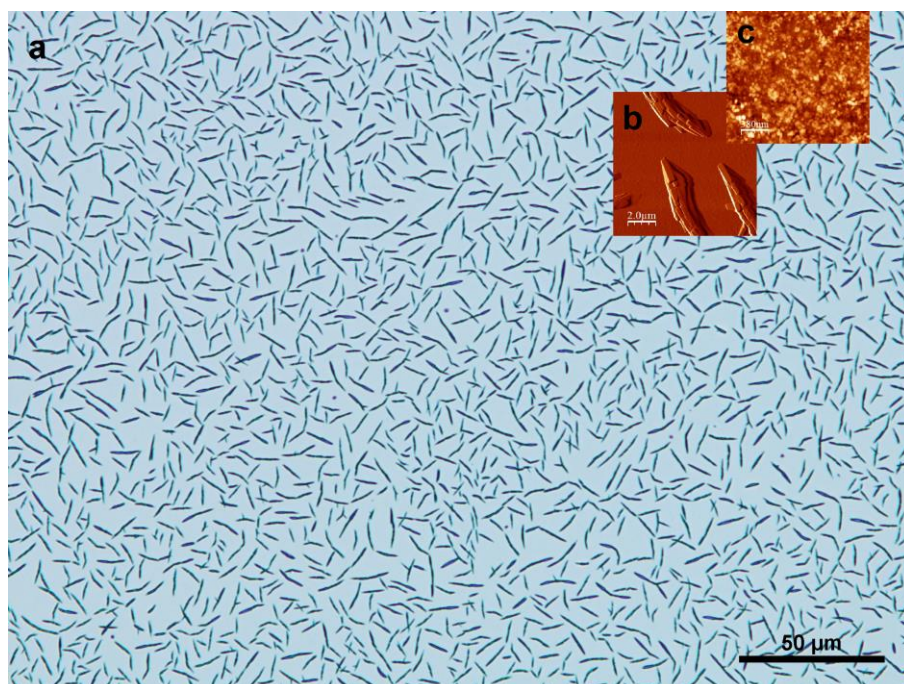
Figure 83. a) optical micrograph of a film of 3a (4,4'-dibromoindigo) processed by spin-casting 3b then heating to 200°C for 5 minutes. b) AFM piezovoltage image showing the large crystallites visible in the optical micrograph. c) AFM zoom-in of the area between the large crystallites, showing a semi-continuous film of nanoscale crystallites.
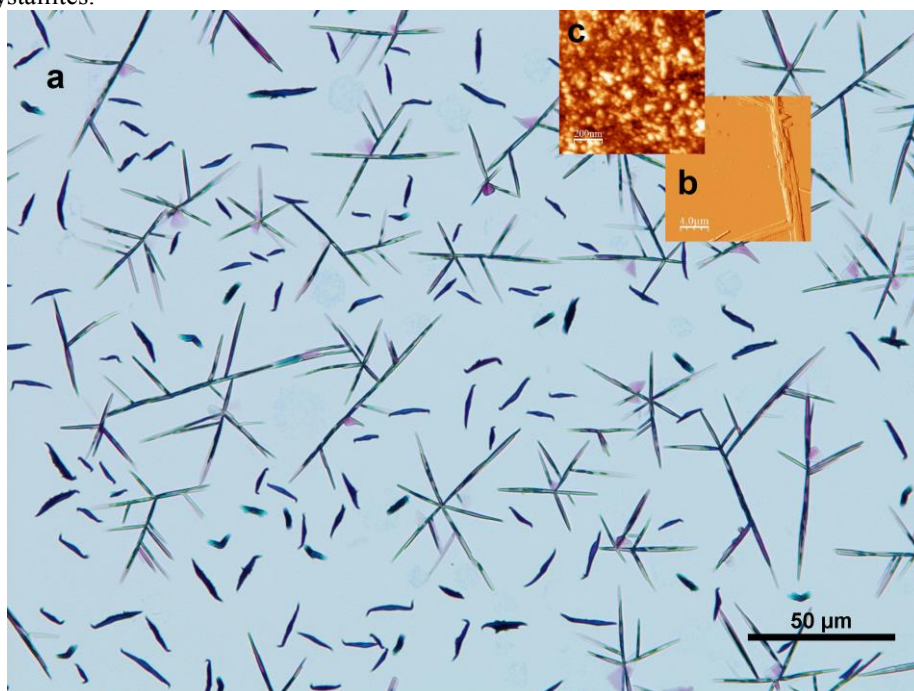
Figure 84. a) optical micrograph of a film of 4a (5-bromoindigo) processed by spin-casting 4b then heating to 200°C for 5 minutes. b) AFM piezovoltage image showing the large crystallites visible in the optical micrograph. c) AFM zoom-in of the area between the large crystallites, showing a semi-continuous film of nanoscale crystallites.
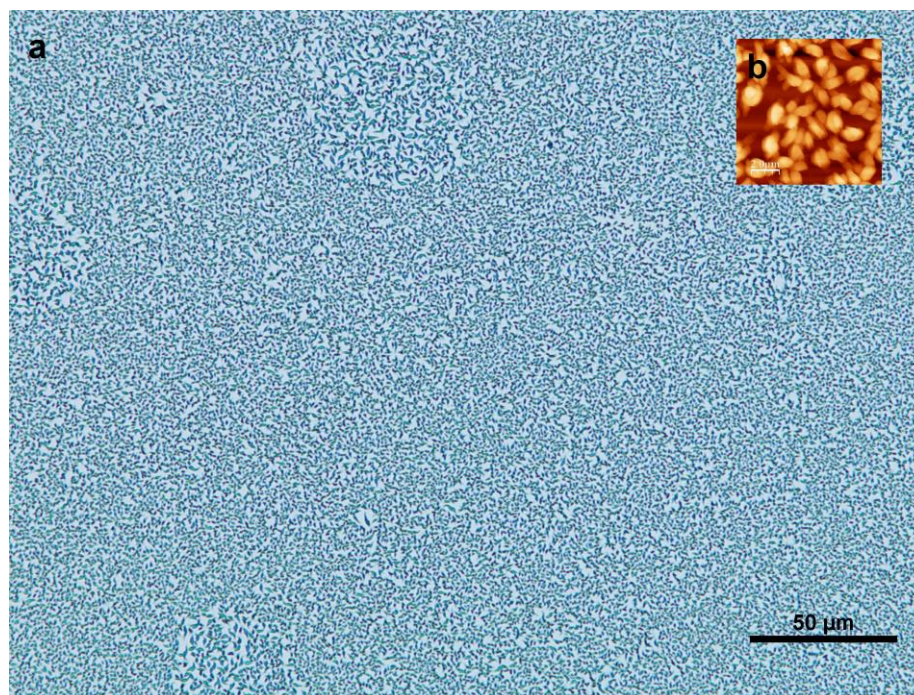
Figure 85. a) optical micrograph of a film of 5a (5,5'-dibromoindigo) processed by spin-casting 5b then heating to 200°C for 5 minutes. b) AFM image showing that the film consists on non-contiguous crystallites.

6.3 Bulk heterojunctions of indigo/poly(3-hexylthiophene)

Organic transistors and organic solar cells using soluble tBOC indigo precursors showed that following deprotection and annealing, the indigo pigments formed very large crystallites, on the size order of tens of microns or even larger. Thus films were very rough and discontinuous, making fabrication of transistor devices difficult and observed mobilities were very low. With blends of tBOC indigos and P3HT spin-cast together to form homogenous thin films, which when heated produced also indigo pigment crystallites within the polymer matrix. Photoinduced charge transfer in such blends was verified by photoluminescence quenching measurements and light-induced electron spin resonance (see section 4). As outlined previously in section 5.3, despite their long history in the chemical literature, H-bonded indigos have not been studied with respect to photoinduced electron transfer reactions. We conducted experiments to verify the existance of photoinduced charge transfer between thermally-regenerated particles of compound **5a** and the semiconducting polymer P3HT. Films were prepared by spin casting mixtures of P3HT:**5b** in $CHCl_3$, followed by heating to 185°C for 5 minutes. Such films were tested using light-induced electron paramagnetic resonance (L-ESR) and also used as the active layer of an organic solar cell. L-ESR is a well-established technique for measuring photoinduced charge transfer in organic donor-acceptor blends.[73] As described in more detail in section 5.3, upon exciting the P3HT polymer with green light at 60K, we observed a double-signal originating from the uncoupled spins of the positive polaron on the P3HT and the radical anion on the indigo (Fig. 5a). The g-value of the radical anion of **5b** was found to be 2.005. P3HT showed a g-value of 2.002, consistent with the literature.[74] Excitation with red light at wavelengths greater than 650 nm where the P3HT does not absorb but **5a** does also yielded a double-signal, indicating that photoinduced hole transfer from **5a** to P3HT occurs. L-ESR experimental details can be found in the SI. The presence of photoinduced charge transfer suggests that donor-acceptor solar cells can be prepared from such a blend. Solar cells fabricated with the structure shown in Figure 86 yielded working devices with good diode characteristics, nevertheless photocurrents remained low, on the order of 200-500 $\mu A/cm^2$ under simulated solar

illumination. This is attributed to the large size of **5a** crystals, which were on the order of 2-3 μm (Figure 86). It is known that domain size of donor-acceptor blends should ideally be on the order of tens of nanometers, and photocurrents on the order we measured for our devices are consistent with bulk heterojunctions with very rough mixing. Additionally, we underline that photocurrents for P3HT-only devices are about two orders of magnitude lower. Therefore we believe that optimizing morphology of the bulk heterojunction during the deprotection reaction is critical for increasing device performance. With the proper substitution on the indigo molecules and optimization of processing conditions we believe that obtaining finer nanomorphology with phase separation on the order of tens of nanometers, which is considered optimal for bulk heterojunctions, can be obtained.

In conclusion, the *t*BOC protect-deprotect procedure allows indigo to be solubilized in organic solvents, and the protected compound can be heated to regenerate the parent pigment. This technique allows simple solution-processing of indigo films. The deprotection behavior of films of *t*BOC protected indigos yields a variety of different H-bonded crystallites. This can be exploited potentially in the synthesis of functional micro- and nanoparticles. Indigo processed in this way together with P3HT yields evidence of photoinduced charge transfer and offers a potential avenue for fabricating donor-acceptor solar cells where indigo pigments function as electron acceptors.
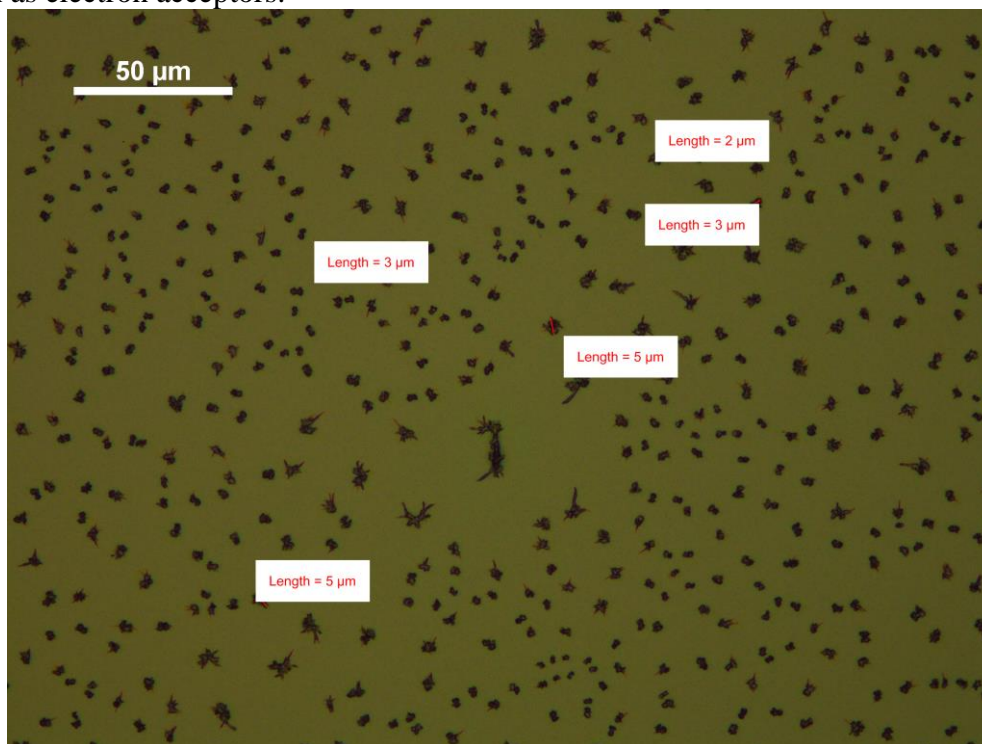
Figure 86. Photomicrograph of 5,5'-dibromoindigo/P3HT blend after deprotection at 185°C for 5 minutes.
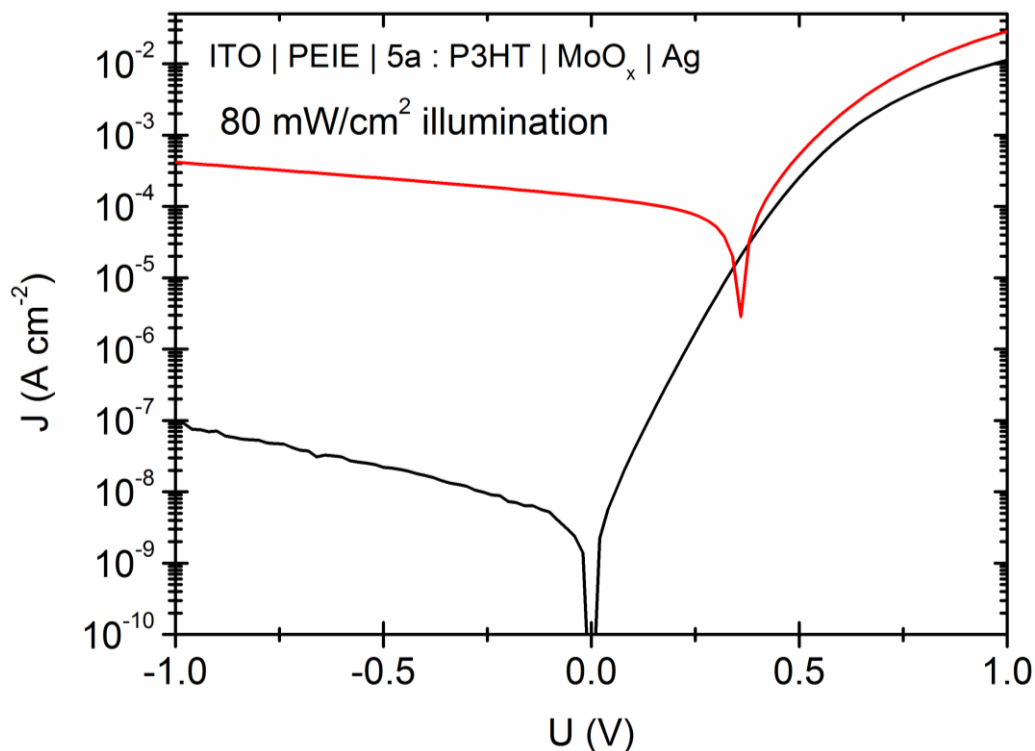
Figure 87. J–V characteristics of a bulk heterojunction diode with 5,5'-dibromoindigo:P3HT as the active layer.

6.4 Extending the indigo molecule – coupling reactions with solubilized indigos

A significant advantage of tBOC-protected indigos is that they can easily be purified by column chromatography.[163] Even mixtures of 5-bromoindigo, 5,5'-dibromoindigo, and indigo – which would be very difficult to separate by other means – can be functionalized with tBOC protecting groups and readily separated chromatographically. More importantly, solubilized N,N'-ditBOC indigos lend themselves well to further synthetic derivation that would be otherwise impossible with the highly-insoluble H-bonded indigos. 5,5'-dibromoindigo, which can be produced by direct bromination of indigo, or 6,6'-dibromoindigo, prepared using [66] can be functionalized by tBOC and then coupled to other synthetic building blocks via Suzuki or Sonogashira chemistry. We were successful in obtaining several "extended" indigos using this chemistry, with some examples shown in Figure 88. Work in applying these derivatives in organic electronics is forthcoming.
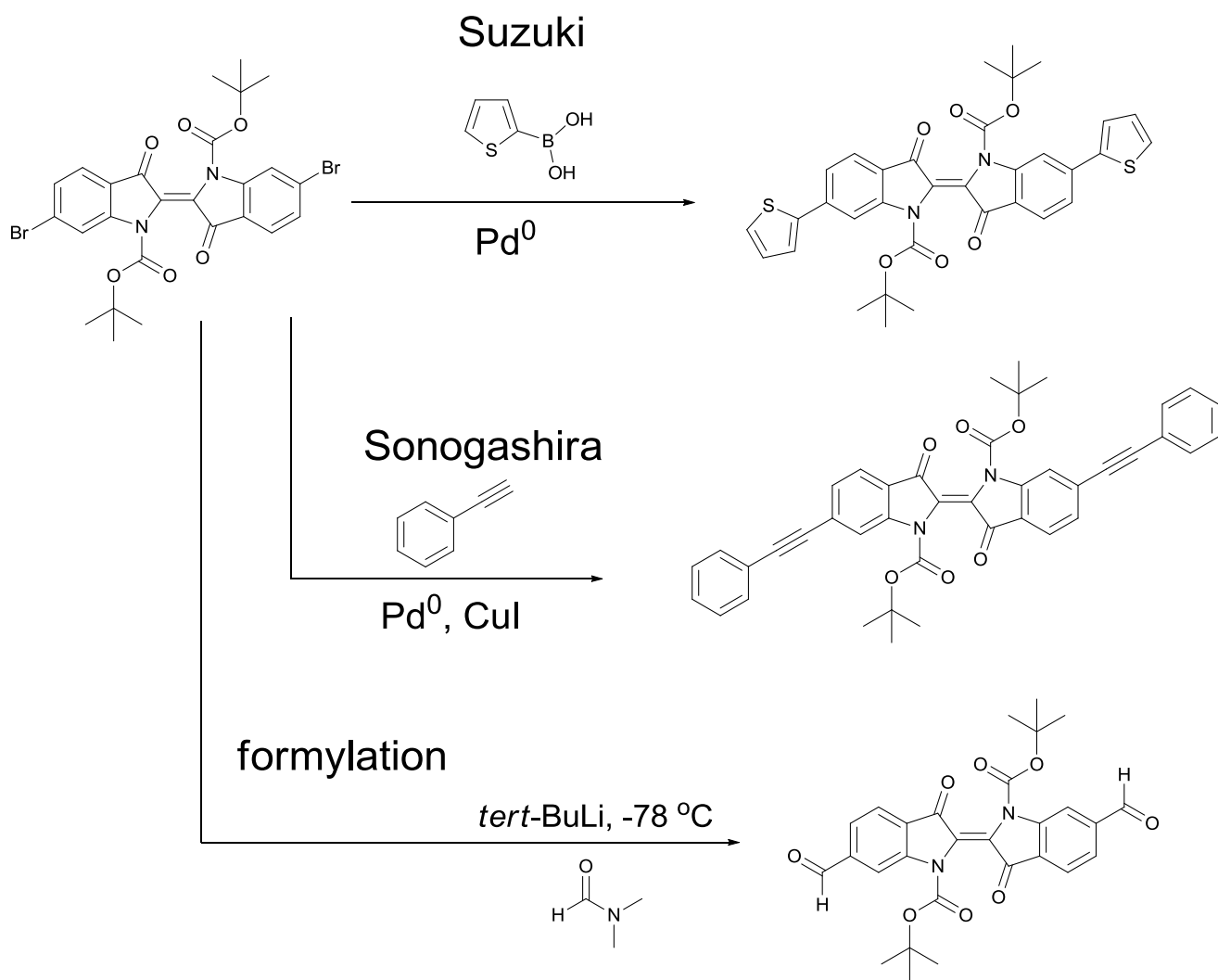
Figure 88. Extended indigos obtained from the tBOC-solubilized dibromoindigo.

7. Conclusions and Outlook

The essential theme of this dissertation was evaluating a class of materials well-known in certain applications and applying them to something new. Indigo and its derivatives are molecules with a long history in chemistry and society. In this dissertation, they return to the attention of science as air-stable, high-mobility organic semiconductor materials. 'Old' dyestuff chemistry, particularly natural-origin dyes, may usher in a new generation of organic semiconducting materials and devices with inherent biocompatibility and sustainability; as well as unique biofunctionality.

Intramolecular π-conjugation has been considered requisite in the designing of organic semiconducting materials since the pioneering work of Nobel laureates Heeger, McDiarmid, and Shirakawa. The manipulation of optical and transport properties has primarily been accomplished through the synthetic modification of individual molecules or macromolecules. This line of research has led to a relatively sophisticated understanding of tailoring molecular structure to achieve a specific set of properties. It is known that mobility along continuous π-conjugated molecules, such as along a polymer chain, is very high.[36,38,39,169,170] Indeed the 2D extrapolation of this concept is the realization of graphene layers, which can support mobility as high as 15,000 cm^2/Vs.[171] However, in typical organic semiconductor devices, it is inter- and not intramolecular conduction that ultimately limits mobility. The studies of H-bonded molecules like indigo and its derivatives underline that, though they are not well-conjugated intramolecularily according to the prevailing design rules for organic semiconductors, they form crystalline solids with a considerable overlap integral between neighboring molecules. Ultimately it is the charge transfer integral between molecules that facilitates conduction.[172] In the case of natural-origin pigments, as well as many synthetic pigments, intermolecular conjugation is driven by interplay of hydrogen-bonding and π-π interactions, leading to organic solids with high lattice energies. This research suggests that ideas from organic H-bond mediated crystal engineering, regularly applied in the pigment industry[54,173–175], might be used to design organic solids with desired properties such as optimal π-π overlap as well as tailor desired optical properties.[114] The concept that a large intermolecular transfer integral within H-bonded organic crystals may be as good a criteria for charge transport as intramolecular conjugation is in conjugated polymers may be an important point arising from the research presented in this dissertation.

Work on this class of H-bonded materials raises many questions and opens up several avenues of future perspectives. Crystal engineering organic semiconductors, where supramolecular effects are relied upon to enhance intermolecular conjugation, is a new concept for organic electronics which has substantial potential to produce materials with high stability. The importance of organic crystal engineering has been recognized in the field of industrial pigment technologies – this body of knowledge is poised to be directly applied to organic semiconductor design. Therefore the first future perspective for this family of H-bonded organic semiconductors is an in-depth understanding of the molecular structure vs. crystalline packing vs. mobility relationship. Preliminary work in this direction has been presented herein. Once certain principles about solid state structure vs. performance are understood, materials chemists must come into play to create novel H-bonded materials, "extended" indigos that utilize crystal engineering principles and molecular structure to achieve target properties. A strategy to overcome the primary obstacle of insolubility in this class of materials has been likewise presented in this thesis – the use of thermolabile solubilizing groups. The final goal of these efforts is organic electronics with high performance, stability, and simple, cheap, and sustainable chemical syntheses routes for the active materials.

Indigos and linear fused-ring compounds like quinacridone and epindolidione were proven herein to be successful in OFETs, however, solar cell materials based on H-bonded

indigos are still lacking. The ultrafast internal conversion of the excited state of H-bonded indigo molecules, however, may make it difficult for them to produce photocurrent with reasonable efficiency. Whether the fast radiationless processes responsible for the stability of this materials class is an obstacle for optoelectronics applications has yet to be determined. The results for indigo blended with a conjugated polymer show, however, that photoinduced charge transfer is possible using indigo.

A major potential idea emerging from this work is single-layer organic solar cells. Using ambipolar light-absorbing H-bonded solids with an intrinsic charge generation mechanism afforded by a dominance of charge-transfer exciton formation and high permittivity is an entirely new design concept for organic photovoltaics. Results with high photocurrent yields in H-bonded quinacridone suggest that such materials could, in fact, be useful in solar cells.[114] The role of dissociative excitonic states also shows promise for light-emitting diode applications, as demonstrated in the case of epindolidione.

Finally, a major future perspective for this class of materials is biointegration. The field of OFET-based bioanalyte detectors and organic semiconductor and conductor *in vivo* biomedical devices is growing at present. Devices utilizing the inherent biocompatibility of many indigo and indigo-like materials combined with the useful chemical handles, *i.e.* amine, carbonyl groups, have yet to be realized.

8. References

[1]   J. M. Allwood, M. F. Ashby, T. G. Gutowski, E. Worrell, *Resources, Conservation and Recycling* **2011**, *55*, 362–381.

[2]   K. Y. Law, *Chemical Reviews* **1993**, *93*, 449–486.

[3]   D. S. Weiss, M. Abkowitz, *Chemical Reviews* **2010**, *110*, 479–526.

[4]   G. M. Farinola, R. Ragni, *Chemical Society reviews* **2011**, *40*, 3467–3482.

[5]   S. Hofmann, M. Thomschke, B. Lüssem, K. Leo, *Optics express* **2011**, *19*, A1258.

[6]   C. W. Tang, *Applied Physics Letters* **1986**, *48*, 183–185.

[7]   C. J. Brabec, N. S. Sariciftci, J. C. Hummelen, *Advanced Functional Materials* **2001**, *11*, 15–26.

[8]   S. E. Shaheen, C. J. Brabec, N. S. Sariciftci, F. Padinger, T. Fromherz, J. C. Hummelen, *Applied Physics Letters* **2001**, *78*, 841.

[9]   C. J. Brabec, S. Gowrisanker, J. J. M. Halls, D. Laird, S. Jia, S. P. Williams, *Advanced Materials* **2010**, *22*, 3839–3856.

[10]   R. A. J. Janssen, J. Nelson, *Advanced Materials* **2013**, *25*, 1847–1858.

[11]   S. Rohr, *Heliatek gmbH press release, January 16th* **2013**.

[12]   H. Sirringhaus, *Advanced Materials* **2005**, *17*, 2411–2425.

[13]   J. Zaumseil, H. Sirringhaus, *Chemical Reviews* **2007**, *107*, 1296–323.

[14]   D. Braga, G. Horowitz, *Advanced Materials* **2009**, *21*, 1473–1486.

[15]   H. Klauk, *Chemical Society reviews* **2010**, *39*, 2643–2666.

[16] M. D. Angione, R. Pilolli, S. Cotrone, M. Magliulo, A. Mallardi, G. Palazzo, L. Sabbatini, D. Fine, A. Dodabalapur, N. Cioffi, L. Torsi, *Materials Today* **2011**, *14*, 424–433.

[17] M. Muskovich, C. J. Bettinger, *Advanced Healthcare Materials* **2012**, *1*, 248–266.

[18] M. Irimia-Vladu, E. D. Głowacki, G. Voss, S. Bauer, N. S. Sariciftci, *Materials Today* **2012**, *15*, 340–346.

[19] P. Meredith, C. J. Bettinger, M. Irimia-Vladu, A. B. Mostert, P. E. Schwenn, *Reports on progress in physics* **2013**, *76*, 034501.

[20] M. Irimia-Vladu, P. A. Troshin, M. Reisinger, L. Shmygleva, Y. Kanbur, G. Schwabegger, M. Bodea, R. Schwödiauer, A. Mumyatov, J. W. Fergus, V. F. Razumov, H. Sitter, N. S. Sariciftci, S. Bauer, *Advanced Functional Materials* **2010**, *20*, 4069–4076.

[21] M. Irimia-Vladu, P. A. Troshin, M. Reisinger, G. Schwabegger, M. Ullah, R. Schwoediauer, A. Mumyatov, M. Bodea, J. W. Fergus, V. F. Razumov, *Organic Electronics* **2010**, *11*, 1974–1990.

[22] M. Irimia-Vladu, N. S. Sariciftci, S. Bauer, *Journal of Materials Chemistry* **2011**, *21*, 1350–1361.

[23] M. Irimia-Vladu, E. D. Głowacki, G. Schwabegger, L. Leonat, H. Z. Akpinar, H. Sitter, S. Bauer, N. S. Sariciftci, *Green Chemistry* **2013**, *15*, 1473–1476.

[24] F. Eder, H. Klauk, M. Halik, U. Zschieschang, G. Schmid, C. Dehm, *Applied Physics Letters* **2004**, *84*, 2673.

[25] U. Zschieschang, T. Yamamoto, K. Takimiya, H. Kuwabara, M. Ikeda, T. Sekitani, T. Someya, H. Klauk, *Advanced Materials* **2011**, *23*, 654–658.

[26] D. Tobjörk, R. Österbacka, *Advanced Materials* **2011**, *23*, 1935–1961.

[27] M. C. Barr, J. A. Rowehl, R. R. Lunt, J. Xu, A. Wang, C. M. Boyce, S. G. Im, V. Bulović, K. K. Gleason, *Advanced Materials* **2011**, *23*, 3499–3505.

[28] A. Hübler, B. Trnovec, T. Zillger, M. Ali, N. Wetzold, M. Mingebach, A. Wagenpfahl, C. Deibel, V. Dyakonov, *Advanced Energy Materials* **2011**, *1*, 1018–1022.

[29] D.-H. Kim, J. Viventi, J. J. Amsden, J. Xiao, L. Vigeland, Y.-S. Kim, J. A. Blanco, B. Panilaitis, E. S. Frechette, D. Contreras, D. L. Kaplan, F. G. Omenetto, Y. Huang, K.-C. Hwang, M. R. Zakin, B. Litt, J. A. Rogers, *Nature Materials* **2010**, *9*, 511–517.

[30] H. Tao, M. A. Brenckle, M. Yang, J. Zhang, M. Liu, S. M. Siebert, R. D. Averitt, M. S. Mannoor, M. C. McAlpine, J. A. Rogers, D. L. Kaplan, F. G. Omenetto, *Advanced Materials* **2012**, *24*, 1067–1072.

[31] V. Benfenati, K. Stahl, C. Gomis-Perez, S. Toffanin, A. Sagnella, R. Torp, D. L. Kaplan, G. Ruani, F. G. Omenetto, R. Zamboni, M. Muccini, *Advanced Functional Materials* **2012**, *22*, 1871–1884.

[32] C.-H. Wang, C.-Y. Hsieh, J.-C. Hwang, *Advanced Materials* **2011**, *23*, 1630–1634.

[33] E. D. Głowacki, L. Leonat, G. Voss, M. Bodea, Z. Bozkurt, M. Irimia-Vladu, S. Bauer, N. S. Sariciftci, *Proceedings of SPIE* **2011**, *8118*, 81180M–81180M–10.

[34] T. Bechtold, R. Mussak, Eds., *Handbook of Natural Colorants*, John Wiley & Sons, Chichester, UK, **2009**.

[35] E. S. B. Ferreira, A. N. Hulme, H. McNab, A. Quye, *Chemical Society reviews* **2004**, *33*, 329–336.

[36] A. J. Heeger, *Polymer* **2001**, *73*, 681–700.

[37] A. Pron, P. Rannou, *Progress in Polymer Science* **2002**, *27*, 135–190.

[38] A. Facchetti, *Chemistry of Materials* **2011**, *23*, 733–758.

[39] J. Mei, Y. Diao, A. L. Appleton, L. Fang, Z. Bao, *Journal of the American Chemical Society* **2013**, *135*, 6724–6746.

[40] K. Tybrandt, K. C. Larsson, A. Richter-Dahlfors, M. Berggren, *PNAS* **2010**, *107*, 9929–9932.

[41] D. Khodagholy, T. Doublet, P. Quilichini, M. Gurfinkel, P. Leleux, A. Ghestem, E. Ismailova, T. Hervé, S. Sanaur, C. Bernard, G. G. Malliaras, *Nature Communications* **2013**, *4*, 1575.

[42] L. Pauling, *The Nature of the Chemical Bond and the Structure of Molecules and Crystals. An Introduction to Modern Structural Chemistry*, Oxford University Press, London, 2nd edn, 1940.

[43] K. Tybrandt, K. C. Larsson, S. Kurup, D. T. Simon, P. Kjäll, J. Isaksson, M. Sandberg, E. W. H. Jager, A. Richter-Dahlfors, M. Berggren, *Advanced Materials* **2009**, *21*, 4442–4446.

[44] M. Seefelder, *Indigo in Culture, Science, and Technology*, Ecomed, Landsberg, Germany, **1994**.

[45] E. Steingruber, *Indigo and Indigo Colorants, Ullmann's Encyclopedia of Industrial Chemistry* **2004**, 1–9.

[46] S. Fantacci, A. Amat, A. Sgamellotti, T. Molecolari, *Accounts of Chemical Research* **2010**, *43*, 802–813.

[47] Z. C. Koren, *Dyes and Pigments* **2012**, *95*, 491–501.

[48] C. J. Cooksey, *Molecules* **2001**, 736–769.

[49] J. L. Wolk, A. A. Frimer, *Molecules* **2010**, *15*, 5473–508.

[50] H. Schmidt, *Chemie in unserer Zeit* **1997**, *31*, 121–128.

[51] A. Baeyer, V. Drewsen, *Chemische Berichte* **1882**, *15*, 2856–2864.

[52] R. J. H. Clark, C. J. Cooksey, *New Journal of Chemistry* **1999**, *23*, 323–328.

[53] M. Zhang, H. Wang, H. Tian, Y. Geng, C. W. Tang, *Advanced Materials* **2011**, *23*, 4960–4964.

[54] E. B. Faulkner, R. J. Schwartz, Eds., *High Performance Pigments*, Wiley-VCH, Weinheim, **2009**.

[55] E. F. Paulus, F. J. J. Leusen, M. U. Schmidt, *CrystEngComm* **2007**, *9*, 131.

[56] S. S. Labana, L. L. Labana, *Chemical Reviews* **1967**, *67*, 1–18.

[57] S. Niementowski, *Chemische Berichte* **1896**, *29*, 76–83.

[58] W. S. Struve, *Process for the Preparation of Linear Quinacridones*, **1958**, U.S. Patent 2821529.

[59] W. S. Struve, *Tetrahalogen Substituted Quinacridones*, **1958**, U.S. Patent 2,821,530.

[60] A. D. Ainley, R. Robinson, *Journal of the Chemical Society* **1934**, 1508–1520.

[61] W. Tuer, PhD Dissertation, Epindolidione , Epindoline Und Lineare Sowie Trigonale Imidazolderivate Neue Materialien Mit Interessanten Fluoreszenzeigenschaften, Ludwig-Maximilians-University Munich, **2001**.

[62] S. VanSlyke, C. W. Tang, *Organic Electroluminescent Devices Having Improved Power Conversion Efficiencies*, **1985**, U.S. Patent US 4539507.

[63] L. B. Kaul, B. Piastra, V. Wolf, F. Prokschy, M. U. Schmidt, *Epindolidione Pigments*, **2007**, U.S. Patent US 7,307,170.

[64] D. Weiss, M. Burberry, *Thin Solid Films* **1988**, *158*, 175–187.

[65] G. Haucke, G. Graness, *Angewandte Chemie* **1995**, *34*, 67–68.

[66] G. Voss, H. Gerlach, *Chemische Berichte* **1989**, *122*, 1199–1201.

[67] G. Voss, *Coloration Technology* **2006**, *122*, 317–323.

[68] J. Mizuguchi, *Crystal Research and Technology* **1981**, *16*, 695–700.

[69] C. Hsiao, *Journal of Materials Science* **1982**, *17*, 2781–2791.

[70] E. F. Paulus, A. Gieren, *Structure Analysis by Diffraction, Ullmann's Encyclopedia of Industrial Chemistry* **2012**, 481–527.

[71] H. Sitter, A. Andreev, G. Matt, N. S. Sariciftci, *Synthetic Metals* **2003**, *138*, 9–13.

[72] T. Singh, N. Marjanović, G. J. Matt, S. Gunes, N. S. Sariciftci, A. Montaigne Ramil, A. Andreev, H. Sitter, R. Schwödiauer, S. Bauer, *Organic Electronics* **2005**, *6*, 105–110.

[73] V. Dyakonov, G. Zoriniants, M. Scharber, C. Brabec, R. Janssen, J. Hummelen, N. Sariciftci, *Physical Review B* **1999**, *59*, 8019–8025.

[74] V. I. Krinichnyi, E. I. Yudanova, *Journal of Renewable and Sustainable Energy* **2009**, *1*, 043110.

[75] N. Schultz, M. Scharber, C. Brabec, N.S. Sariciftci, *Physical Review B* **2001**, *64*, 1–7.

[76] M. C. Scharber, Magnetic Resonance Studies on Conjugated Polymers and Conjugated Polymer Fullerene Mixtures, PhD Dissertation JKU, **2002**.

[77]   C. M. Cardona, W. Li, A. E. Kaifer, D. Stockdale, G. C. Bazan, *Advanced Materials* **2011**, *23*, 2367–2371.

[78]   G. Horowitz, *Advanced Materials* **1998**, *10*, 365–377.

[79]   M. M. Lohrengel, *Materials Science and Engineering: R* **1993**, *11*, 243–294.

[80]   M. Kaltenbrunner, P. Stadler, R. Schwödiauer, A. W. Hassel, N. S. Sariciftci, S. Bauer, *Advanced Materials* **2011**, *23*, 4892–4896.

[81]   R. Ponce Ortiz, A. Facchetti, T. J. Marks, *Chemical reviews* **2010**, *110*, 205–239.

[82]   M. Kraus, S. Haug, W. Brütting, A. Opitz, *Organic Electronics* **2011**, *12*, 731–735.

[83]   M. Horlet, M. Kraus, W. Brütting, A. Opitz, *Applied Physics Letters* **2011**, *98*, 233304.

[84]   A. Opitz, M. Horlet, M. Kiwull, J. Wagner, M. Kraus, W. Brütting, *Organic Electronics* **2012**, *13*, 1614–1622.

[85]   Y. Kanbur, M. Irimia-Vladu, E. D. Głowacki, G. Voss, M. Baumgartner, G. Schwabegger, L. Leonat, M. Ullah, H. Sarica, S. Erten-Ela, R. Schwödiauer, H. Sitter, Z. Küçükyavuz, S. Bauer, N. S. Sariciftci, *Organic Electronics* **2012**, *13*, 919–924.

[86]   J. R. Baker, *CMOS: Circuit Design, Layout, and Simulation*, Wiley-IEEE Press, **2010**.

[87]   E. J. Meijer, D. M. de Leeuw, S. Setayesh, E. van Veenendaal, B. H. Huisman, P. W. M. Blom, J. C. Hummelen, U. Scherf, J. Kadam, T. M. Klapwijk, *Nature materials* **2003**, *2*, 678–82.

[88]   R. W. I. de Boer, A. F. Stassen, M. F. Craciun, C. L. Mulder, A. Molinari, S. Rogge, A. F. Morpurgo, *Applied Physics Letters* **2005**, *86*, 262109.

[89]   T. D. Anthopoulos, S. Setayesh, E. Smits, M. Cölle, E. Cantatore, B. de Boer, P. W. M. Blom, D. M. de Leeuw, *Advanced Materials* **2006**, *18*, 1900–1904.

[90]   P. Sonar, S. P. Singh, Y. Li, M. S. Soh, A. Dodabalapur, *Advanced Materials* **2010**, *22*, 5409–13.

[91]   H. Liu, V. Avrutin, N. Izyumskaya, Ü. Özgür, H. Morkoç, *Superlattices and Microstructures* **2010**, *48*, 458–484.

[92]   A. Stadler, *Materials* **2012**, *5*, 661–683.

[93]   Y. Zhou, C. Fuentes-Hernandez, J. Shim, J. Meyer, A. J. Giordano, H. Li, P. Winget, T. Papadopoulos, H. Cheun, J. Kim, M. Fenoll, A. Dindar, W. Haske, E. Najafabadi, T. M. Khan, H. Sojoudi, S. Barlow, S. Graham, J.-L. Bredas, S. R. Marder, A. Kahn, B. Kippelen, *Science* **2012**, *336*, 327–332.

[94]   M. Zhang, H. Ding, Y. Gao, C. W. Tang, *Applied Physics Letters* **2010**, *96*, 183301.

[95]   S. Günes, H. Neugebauer, N. S. Sariciftci, *Chemical reviews* **2007**, *107*, 1324–38.

[96]   M. Irimia-Vladu, E. D. Głowacki, P. A. Troshin, G. Schwabegger, L. Leonat, D. K. Susarova, O. Krystal, M. Ullah, Y. Kanbur, M. A. Bodea, V. F. Razumov, H. Sitter, S. Bauer, N. S. Sariciftci, *Advanced Materials* **2012**, *24*, 375–380.

[97]   P. Süsse, M. Steins, V. Kupcik, *Zeitschrift für Kristallographie* **1988**, *184*, 269–273.

[98] E. D. Głowacki, L. Leonat, G. Voss, M.-A. Bodea, Z. Bozkurt, A. M. Ramil, M. Irimia-Vladu, S. Bauer, N. S. Sariciftci, *AIP Advances* **2011**, *1*, 042132–042137.

[99] P. Susse, C. Krampe, *Naturwissenschaften* **1979**, *66*, 110.

[100] P. W. Sadler, *Journal of Organic Chemistry* **1955**, *21*, 316–318.

[101] P. W. Sadler, R. L. Warren, *Journal of the American Chemical Society* **1956**, *78*, 1251–1255.

[102] X. Zhan, A. Facchetti, S. Barlow, T. J. Marks, M. A. Ratner, M. R. Wasielewski, S. R. Marder, *Advanced Materials* **2011**, *23*, 268–84.

[103] P. Susse, R. Wasche, *Naturwissenschaften* **1978**, *65*, 157.

[104] E. D. Głowacki, G. Voss, L. Leonat, M. Irimia-Vladu, S. Bauer, N. S. Sariciftci, *Israel Journal of Chemistry* **2012**, *52*, 540–551.

[105] E. D. Głowacki, *unpublished results* **2013**.

[106] E. D. Głowacki, M. Irimia-Vladu, M. Kaltenbrunner, J. Gąsiorowski, M. S. White, U. Monkowius, G. Romanazzi, G. P. Suranna, P. Mastrorilli, T. Sekitani, S. Bauer, T. Someya, L. Torsi, N. S. Sariciftci, *Advanced Materials* **2013**, *25*, 1563–1569.

[107] N. Nishimura, T. Senju, J. Mizuguchi, *Acta Crystallographica Section E Structure Reports Online* **2006**, *62*, o4683–o4685.

[108] D. S. Filho, C. M. F. Oliveira, *Journal of Materials Science* **1992**, *27*, 5101–5107.

[109] G. Lincke, H.-U. Finzel, *Crystal Research and Technology* **1996**, *31*, 441–452.

[110] G. D. Potts, W. Jones, J. F. Bullock, S. J. Andrews, S. J. Maginn, *Journal of the Chemical Society Communications* **1994**, *116*, 2565–2566.

[111] G. Lincke, *Dyes and Pigments* **2000**, *44*, 101–122.

[112] G. Lincke, *Dyes and Pigments* **2002**, *52*, 169–181.

[113] E. D. Głowacki, M. Irimia-Vladu, S. Bauer, N. S. Sariciftci, *Journal of Materials Chemistry B* **2013**, *1*, 3742–3753.

[114] E. D. Głowacki, L. Leonat, M. Irimia-Vladu, R. Schwödiauer, M. Ullah, H. Sitter, S. Bauer, N. Serdar Sariciftci, *Applied Physics Letters* **2012**, *101*, 023305.

[115] T. Okamoto, M. L. Senatore, M.-M. Ling, a. B. Mallik, M. L. Tang, Z. Bao, *Advanced Materials* **2007**, *19*, 3381–3384.

[116] H. Yanagisawa, J. Mizuguchi, S. Aramaki, Y. Sakai, *Japanese Journal of Applied Physics* **2008**, *47*, 4728–4731.

[117] D. Berg, C. Nielinger, W. Mader, M. Sokolowski, *Synthetic Metals* **2009**, *159*, 2599–2602.

[118] C. Iuga, E. Ortiz, J. R. Alvarez-Idaboy, A. Vivier-Bunge, *Journal of Physical Chemistry A* **2012**, *116*, 3643–3651.

[119] E. B. Knott, *Journal of the society of dyers and colourists* **1951**, *67*, 302–306.

[120] M. Wyman, J. Weinstein, *Journal of Organic Chemistry* **1956**, *78*, 2387–2390.

[121] S. E. Sheppard, P. T. Newsome, *Journal of the American Chemical Society* **1942**, *64*, 2937–2946.

[122] A. R. Monahan, J. E. Kuder, *Journal of Organic Chemistry* **1972**, *37*, 4182–4184.

[123] D. Jacquemin, J. Preat, V. Wathelet, E. A. Perpète, *The Journal of Chemical Physics* **2006**, *124*, 74104.

[124] A. Amat, F. Rosi, C. Miliani, A. Sgamellotti, S. Fantacci, *Journal of Molecular Structure* **2011**, *993*, 43–51.

[125] W. Lüttke, H. Hermann, M. Klessinger, *Angewandte Chemie Int Edit* **1966**, *5*, 598–599.

[126] T. Kobayashi, P. M. Rentzepis, *The Journal of Chemical Physics* **1979**, *70*, 886.

[127] J. Seixas de Melo, A. P. Moura, M. J. Melo, *The Journal of Physical Chemistry A* **2004**, *108*, 6975–6981.

[128] J. S. S. de Melo, R. Rondão, H. D. Burrows, M. J. Melo, S. Navaratnam, R. Edge, G. Voss, *Chemphyschem : a European journal of chemical physics and physical chemistry* **2006**, *7*, 2303–2311.

[129] R. Rondão, J. Seixas de Melo, F. A. Schaberle, G. Voss, *Physical chemistry chemical physics : PCCP* **2012**, *14*, 1778–1783.

[130] I. Iwakura, A. Yabushita, T. Kobayashi, *Bulletin of the Chemical Society of Japan* **2011**, *84*, 164–171.

[131] S. Yamazaki, L. Sobolewski, W. Domcke, *Physical Chemistry Chemical Physics* **2011**, *13*, 1618–1628.

[132] T. Elsaesser, W. Kaiser, W. Luttke, *Journal of Physical Chemistry* **1986**, *90*, 2901–2905.

[133] J. Weinstein, G. M. Wyman, *Journal of Organic Chemistry* **1956**, *78*, 4007–4010.

[134] C. R. Giuliano, L. D. Hess, J. D. Margerum, *Journal of the American Chemical Society* **1967**, *90*, 587–594.

[135] G. M. Wyman, *Chemical reviews* **1955**, *55*, 625–657.

[136] G. Haucke, R. Paetzold, *Journal für Praktische Chemie* **1979**, *917*, 978–986.

[137] J. Z. Vlahakis, R. P. Lemieux, *Journal of Materials Chemistry* **2004**, *14*, 1486–1494.

[138] E. Głowacki, K. Horovitz, C. W. Tang, K. L. Marshall, *Advanced Functional Materials* **2010**, *20*, 2778–2785.

[139] G. Engi, *Angewandte Chemie* **1914**, *27*, 144–148.

[140] J. Seixas de Melo, R. Rondão, H. D. Burrows, M. J. Melo, S. Navaratnam, R. Edge, G. Voss, *The journal of physical chemistry. A* **2006**, *110*, 13653–13661.

[141] L. Y. C. Lee, C. Giann, D. G. Whitten, *Journal of the American Chemical Society* **1986**, *108*, 2646–2655.

[142] J. Pouliquen, V. Wintgens, V. Toscanot, *Dyes and Pigments* **1985**, *6*, 163–175.

[143] E. D. Głowacki, K. L. Marshall, C. W. Tang, N. S. Sariciftci, *Applied Physics Letters* **2011**, *99*, 043305.

[144] W. Y. Liang, *Physics Education* **1970**, *5*, 226–228.

[145] V. Bulovid, P. E. Burrows, S. R. Forrest, J. A. Cronin, M. E. T, *Chemical Physics* **1996**, *210*, 1–12.

[146] V. B, S. R. Forrest, **1996**, *210*, 13–25.

[147] R. N. Marks, J. J. M. Halls, D. D. C. Bradley, R. H. Friend, A. B. Holmes, *Journal of Physics: Condensed Matter* **1994**, *6*, 1379–1394.

[148] S. Glenis, G. Horowitz, G. Tourillon, F. Garnier, *Thin Solid Films* **1984**, *111*, 93–103.

[149] E. Kymakis, A. J. Amaratunga, I. Alexandrou, M. Chhowalla, W. I. Mime, **2001**, *4108*, 112–116.

[150] D. L. Morel, E. L. Stogryn, a. K. Ghosh, T. Feng, P. E. Purwin, R. F. Shaw, C. Fishman, G. R. Bird, a. P. Piechowski, *The Journal of Physical Chemistry* **1984**, *88*, 923–933.

[151] B. D. Wohrle, D. Meissner, *Advanced Materials* **1991**, *3*, 129–138.

[152] H. Bottcher, T. Fritz, J. D. Wright, *Journal of Materials Chemistry* **1993**, *3*, 1187–1197.

[153] M. Zhang, H. Ding, Y. Gao, C. W. Tang, *Applied Physics Letters* **2010**, *96*, 183301.

[154] L. Rossi, G. Bongiovanni, J. Kalinowski, G. Lanzani, A. Mura, M. Nisoli, R. Tubino, *Chemical Physics Letters* **1996**, *257*, 545–551.

[155] L. Rossi, G. Bongiovanni, a Borghesi, G. Lanzani, J. Kalinowski, a Mura, R. Tubino, *Synthetic Metals* **1997**, *84*, 873–874.

[156] J. Kalinowski, W. Stampor, P. Di Marco, V. Fattori, *Chemical Physics* **1994**, *182*, 341–352.

[157] P. Marco, V. Fattori, G. Giro, *Molecular Crystals and Liquid Crystals* **1992**, *217*, 223–229.

[158] J. Mizuguchi, T. Senju, *The journal of physical chemistry. B* **2006**, *110*, 19154–19161.

[159] J. Mizuguchi, *The Journal of Physical Chemistry A* **2000**, *104*, 1817–1821.

[160] J. Mizuguchi, S. Homma, *Journal of Applied Physics* **1989**, *66*, 3104.

[161] U. Schaedeli, J. S. Zambounis, A. Iqbal, Z. Hao, H. Dubas, *EP 0654711*, **1993**.

[162] J. S. Zambounis, Z. Hao, A. Iqbal, *Nature* **1997**, *388*, 131–132.

[163] E. D. Głowacki, G. Voss, K. Demirak, M. Havlicek, N. Sunger, A. C. Okur, U. Monkowius, J. Gąsiorowski, L. Leonat, N. S. Sariciftci, *Chemical Communications* **2013**, *49*, 6063–6065.

[164] P. G. M. Wuts, T. W. Greene, in *Greene's Protective Groups in Organic Synthesis*, **2007**, pp. 696–926.

[165] C. Lee, Y. Seo, S. Lee, *Macromolecules* **2004**, *37*, 4070–4074.

[166] T. L. Chen, J. J.-A. Chen, L. Catane, B. Ma, *Organic Electronics* **2011**, *12*, 1126–1131.

[167] J. Mizuguchi, *Acta Crystallographica Section E Structure Reports Online* **2003**, *59*, o474–o475.

[168] R. Rondão, J. Seixas de Melo, M. J. Melo, A. J. Parola, *The Journal of Physical Chemistry. A* **2012**, *116*, 2826–2832.

[169] C. K. Chiang, M. A. Druy, S. C. Gau, A. J. Heeger, E. J. Luis, A. G. Mac Diarmid, Y. W. Park, H. Shirakawa, *Journal of the American Chemical Society* **1978**, *100*, 1013–1015.

[170] W. A. J. Heeger, S. Kivelson, J. R. Schrieffer, W.-P. Su, *Reviews of Modern Physics* **1988**, *60*, 781–850.

[171] A. K. Geim, K. S. Novoselov, *Nature materials* **2007**, *6*, 183–191.

[172] V. Coropceanu, J. Cornil, D. a da Silva Filho, Y. Olivier, R. Silbey, J.-L. Brédas, *Chemical reviews* **2007**, *107*, 926–952.

[173] G. R. Desiraju, *Journal of Molecular Structure* **2003**, *656*, 5–15.

[174] G. R. Desiraju, *Crystal Growth & Design* **2011**, *11*, 896–898.

[175] C. B. Aakeroy, K. R. Seddon, *Chemical Society Reviews* **1993**, *22*, 397–407.

Curriculum Vitae

Personal information

First name(s) / Surname(s)	**Eric Daniel GŁOWACKI**
Mobile	+43 6769611446
E-mail(s)	eric_daniel.glowacki@jku.at
Nationality	Poland and USA
Date of birth	27 October 1986
Gender	Male

Work experience

Dates	01/01/2007 - 15/06/2010
Occupation or position held	Research engineer
Main activities and responsibilities	Optical Materials Department: Passive and active liquid crystal optical components, functional polymeric materials, chemical synthesis of dyes and other functional organic materials
Name and address of employer	Laboratory for Laser Energetics (LLE) 250 East River Rd., 14623 Rochester (United States)
Type of business or sector	US National research lab

Education and training

Dates	01/09/2005 - 01/06/2009
Title of qualification awarded	Bachelor of Science (B.Sc.)
Principal subjects / occupational skills covered	Major: Chemistry Minor: European History Minor: Russian literature
Name and type of organisation providing education and training	University of Rochester Rochester, NY (United States)

Dates	01/09/2009 - 15/06/2010
Title of qualification awarded	Master of Science (M.Sc.)
Principal subjects / occupational skills covered	Chemistry, Chemical Engineering
Name and type of organisation providing education and training	University of Rochester Rochester, NY (United States)

Dates	01/07/2010 - present
Title of qualification awarded	PhD Student
Principal subjects / occupational skills covered	Doctoral study in Technical Chemistry – Department of Physical Chemistry and Linz Institute for Organic Solar Cells (LIOS)
Name and type of organisation providing education and training	Johannes Kepler University Linz (Austria)

Languages

Polish (native), English (native), Russian (fluent), Romanian (conversant), Czech (conversant), French (basic), German (basic)

Publications

ISI H-index: 5
Google Scholar H-index: 6

[1]   M.S. White, M. Kaltenbrunner, E.D. Głowacki, K. Gutnichenko, G. Kettlgruber, I. Graz, et al., Ultrathin, highly flexible and stretchable PLEDs, Nature Photonics. (2013) DOI: 10.1038/nphoton.2013.188.

[2]   E.D. Głowacki, M. Irimia-Vladu, S. Bauer, N.S. Sariciftci, Hydrogen-bonds in molecular solids – from biological systems to organic electronics, Journal of Materials Chemistry B. 1 (2013) 3742–3753.

[3]   E.D. Głowacki, G. Voss, K. Demirak, M. Havlicek, N. Sunger, A.C. Okur, et al., A facile protection–deprotection route for obtaining indigo pigments as thin films and their applications in organic bulk heterojunctions, Chemical Communications. 49 (2013) 6063–6065.

[4]   M. Irimia-Vladu, E.D. Głowacki, G. Schwabegger, L. Leonat, H.Z. Akpinar, H. Sitter, et al., Natural resin shellac as a substrate and a dielectric layer for organic field-effect transistors, Green Chemistry. 15 (2013) 1473–1476.

[5]   M. Bednorz, G.J. Matt, E.D. Głowacki, T. Fromherz, C.J. Brabec, M.C. Scharber, et al., Silicon/organic hybrid heterojunction infrared photodetector operating in the telecom regime, Organic Electronics. 14 (2013) 1344–1350.

[6]   E.D. Głowacki, M. Irimia-Vladu, M. Kaltenbrunner, J. Gąsiorowski, M.S. White, U. Monkowius, et al., Hydrogen-Bonded Semiconducting Pigments for Air-Stable Field-Effect Transistors., Advanced Materials. 25 (2013) 1563–1569.

[7]   J. Gąsiorowski, E.D. Głowacki, B. Hajduk, M. Siwy, M. Chwastek-Ogierman, J. Weszka, et al., Doping-induced immobile charge carriers in polyazomethine: A spectroscopic study, Journal of Physical Chemistry C. 117 (2013) 2584–2589.

[8]   Y. Kanbur, M. Irimia-Vladu, E.D. Głowacki, G. Voss, M. Baumgartner, G. Schwabegger, et al., Vacuum-processed polyethylene as a dielectric for low operating voltage organic field effect transistors, Organic Electronics. 13 (2012) 919–924.

[9]   M. Grucela-Zajac, M. Filapek, L. Skorka, J. Gasiorowski, E.D. Glowacki, H. Neugebauer, et al., Thermal, optical, electrochemical, and electrochromic characteristics of novel polyimides bearing the Acridine Yellow moiety, Materials Chemistry and Physics. 137 (2012) 221–234.

[10] M. Irimia-Vladu, E.D. Głowacki, G. Voss, S. Bauer, N.S. Sariciftci, Green and biodegradable electronics, Materials Today. 15 (2012) 340–346.

[11] E.D. Głowacki, L. Leonat, M. Irimia-Vladu, R. Schwödiauer, M. Ullah, H. Sitter, et al., Intermolecular hydrogen-bonded organic semiconductors—Quinacridone versus pentacene, Applied Physics Letters. 101 (2012) 023305.

[12] E.D. Głowacki, G. Voss, L. Leonat, M. Irimia-Vladu, S. Bauer, N.S. Sariciftci, Indigo and Tyrian Purple - From Ancient Natural Dyes to Modern Organic Semiconductors, Israel Journal of Chemistry. 52 (2012) 540–551.

[13] M. Kaltenbrunner, M.S. White, E.D. Głowacki, T. Sekitani, T. Someya, N.S. Sariciftci, et al., Ultrathin and lightweight organic solar cells with high flexibility, Nature Communications. 3 (2012) 770.

[14] M. Irimia-Vladu, E.D. Głowacki, P.A. Troshin, G. Schwabegger, L. Leonat, D.K. Susarova, et al., Indigo - A Natural Pigment for High Performance Ambipolar Organic Field Effect Transistors and Circuits, Advanced Materials. 24 (2012) 375–380.

[15] E.D. Głowacki, L. Leonat, G. Voss, M.-A. Bodea, Z. Bozkurt, A.M. Ramil, et al., Ambipolar organic field effect transistors and inverters with the natural material Tyrian Purple, AIP Advances. 1 (2011) 042132–042137.

[16] E.D. Głowacki, L. Leonat, G. Voss, M. Bodea, Z. Bozkurt, M. Irimia-Vladu, et al., Natural and nature-inspired semiconductors for organic electronics, Proceedings of SPIE. 8118 (2011) 81180M–81180M–10. (invited)

[17] E.D. Głowacki, K.L. Marshall, C.W. Tang, N.S. Sariciftci, Doping of organic semiconductors induced by lithium fluoride/aluminum electrodes studied by electron spin resonance and infrared reflection-absorption spectroscopy, Applied Physics Letters. 99 (2011) 043305.

[18] E. Głowacki, K. Hunt, D. Abud, K.L. Marshall, Photoswitchable Gas Permeation Membranes Based on Azobenzene- Doped Liquid Crystals . II . Permeation-Switching Characterization Under Variable Volume and Variable Pressure Conditions, Proceedings of SPIE. (2010) 1–10.(invited)

[19] K.L. Marshall, E. Glowacki, C. Sileo, L. Chockalingam, J. Lee, V. Guiliano, et al., Improving the Abrasion Resistance of Organosilane- Modified Sol-Gel Coatings for High-Peak-Power Laser Applications, OSA Technical Digest. (2010) MA4.

[20] E. Głowacki, K. Horovitz, C.W. Tang, K.L. Marshall, Photoswitchable Gas Permeation Membranes Based on Liquid Crystals, Advanced Functional Materials. 20 (2010) 2778–2785.

[21] E. Glowacki, K.L. Marshall, C.W. Tang, Photoswitchable gas permeation membranes based on azobenzene-doped liquid crystals, Proceedings of SPIE. 2 (2009) 74140H–74140H–13. (invited)

Patents

E. D. Glowacki, K. Marshall, *Photo-switchable Membrane and Method*, **2012**, U.S. Patent US20120025136.

Book Chapters

"Organic Solar Cells" E. Głowacki, C. W. Tang, N. S. Sariciftci in *Encyclopedia of Sustainability Science and Technology*, ed. R. A. Meyers, Springer (2012)

"Natural Materials for Organic Electronics" M. Irimia-Vladu, E. Głowacki, N.S. Sariciftci, S. Bauer in *Small Organic Molecules on Surfaces*, H. Sitter et al (eds), Springer Series in Materials Sciences 173, (2013)

Projects (Co)Authored

Co-authored and co-supervised two projects in Austria:

FWF project TRP 294-N19
　　　"Indigo: From ancient dye to modern high-performance organic electronics circuits"

WTZ PL 07/2011
　　　"Auf Imid und/oder Thiayol basierende, nieder- und hochmolekulare neue organische halbleiter: In Richtung effizienter organischer Donor-Acceptor-Photovoltaik"

Awards

SPIE Photonics West 2011, San Francisco: Student Travel Grant Award

MRS Spring Meeting 2012, San Francisco: Best student talk award, symposium OO: Integration of organic electronics with biological applications

Invited Presentations

Polish Academy of Science, Institute of polymer and coal-based materials, Zabrze, Poland. Invited by: Prof. Jan Weszka (16-17.06.2011)

Technische Universitat Dresden, Dresden, Germany. Invited by: Dr. Aleksander Zakhidov (1.-4.11.2011)

Polish Academy of Sciences, Institute of Organic Chemistry, Warsaw, Poland. Invited by: Prof. Daniel Gryko (31.1.2012)

Sabanci University, Department of Materials Science, Istanbul, Turkey. Invited by: Prof. Cleva Ow-Yang (24.4.2012)

Solar Energy Conversion Workshop, Bucharest, Romania. Invited by: Prof. Victor Barsan (23.5.2012)

Graz University of Technology, Solid State Physics Dept., Graz, Austria. Invited by: Prof. Adolf Winkler (25.6.2012)

International Krutyń Summer School on nanomaterials in biomedicine – invited lecturer, (21-27.05.2013)